UNIVERSITY OF ZAGREB
FACULTY OF SCIENCE
DEPARTMENT OF GEOPHYSICS

IVAN GÜTTLER

# SYSTEMATIC ERRORS IN REGIONAL CLIMATE MODELS IN THE LOWER ATMOSPHERE

DOCTORAL DISSERTATION

Zagreb, 2014

SVEUČILIŠTE U ZAGREBU
PRIRODOSLOVNO-MATEMATIČKI FAKULTET
GEOFIZIČKI ODSJEK

IVAN GÜTTLER

# SUSTAVNE POGREŠKE U REGIONALNIM KLIMATSKIM MODELIMA U NIŽOJ ATMOSFERI

DOKTORSKA DISERTACIJA

Mentor:
dr. sc. Čedo Branković

Zagreb, 2014

This dissertation is elaborated on Meteorological and Hydrological Service of Croatia (DHMZ), supervised by dr. sc. Čedo Branković.

This dissertation would not have been possible without the support of many. First of all, I would like to thank to my advisor Čedo Branković. His knowledge, patience and support were crucial in this journey. Also thanks to members of the dissertation committee, Ivana Herceg-Bulić, Filippo Giorgi and Branko Grisogono, for sharing their time and guidance in various stages of my research.

I was happy to have opportunity to work with Lidija Srnec, Mirta Patarčić, Erika Coppola, Laura Mariotti, Csaba Torma and many other colleagues from DHMZ, ICTP and RegCM community. Work with Danijel Belušić and Travis O'Brien was especially inspiring. Many discussions with Marjana Gajić-Čapka, Ksenija Cindrić, Melita Perčec Tadić, Amela Jeričević, Stjepan Ivatek-Šahdan, Graziano Giuliani, Vladimir Malović, Vitomir Puntarec and Marina Kavur were very helpful in solving various computational, technical and administrative challenges.

I wish to thank my mother Ljiljana and brother Željko for taking care and being supportive all these years. Many other family members and friends created pleasant environment and I wish it lasts in years to come. Special thanks to my wife Josipa who followed me through this intense process from the beginning, and to my son Gabriel for keeping me awake in the final moments of this journey.

# Table of contents

# ABSTRACT

Near-surface and surface variables and the surface energy budget components from two simulations of the regional climate model RegCM4.2 over the European/north African domain during the period 1989-1998 are analysed. The simulations differ in selected planetary boundary layer (PBL) schemes: the Holtslag diagnostic non-local PBL scheme and UW prognostic local PBL scheme. Surface radiative and turbulent fluxes are compared against ERA-Interim while systematic errors in surface radiative fluxes are derived with respect to the satellite-based products. Substantial systematic errors and differences between the two simulations are present for some quantities. The most prominent error is an overestimation of the net surface shortwave radiation flux over eastern Europe during summer. This error strongly correlates with errors in the representation of total cloud cover, and less strongly with errors in surface albedo. During winter the amplitude of the surface energy budget components is more in line with reference datasets. Systematic errors may limit the usefulness of RegCM simulations in further applications. However, the use of the UW PBL scheme improves RegCM representation of the total cloudiness and net surface shortwave radiation and reduces near-surface temperature errors over eastern Europe and Russia.

When compared with the default Holtslag scheme, the UW scheme, in the 10-year experiments over the European domain, shows a substantial cooling. It reduces winter warm bias over the north-eastern Europe by 2 °C and reduces summer warm bias over central Europe by 3 °C. A part of the detected cooling is ascribed to a general reduction in lower tropospheric eddy heat diffusivity with the UW scheme. While differences in temperature tendency due to the PBL schemes are mostly localized to the lower troposphere, the schemes show a much higher diversity in how vertical turbulent mixing of the water vapour mixing ratio is governed. Differences in the water vapour mixing ratio tendency due to the PBL scheme are present almost throughout the troposphere. However, they alone cannot explain the overall water vapour mixing ratio profiles, suggesting strong interaction between the PBL and other model parameterisations. An additional 18-member ensemble with the UW scheme is made, where two formulations of the master turbulent length scale in statically unstable conditions are tested and unconstrained parameters associated with (a) the evaporative enhancement of the cloud-top entrainment and (b) the formulation of the master turbulent length scale in statically stable conditions are systematically perturbed. These experiments suggest that the master turbulent length scale in the UW scheme could be further refined in the current implementation in the RegCM model. It was also found that the UW scheme is less sensitive to the variations of the other two selected unconstrained parameters.

Near-surface and surface variables simulated by RegCM4.3 model using the two different PBL schemes under two scenarios of concentrations of the greenhouse gases (RCP4.5 and RCP8.5) and forced by the HadGEM2-ES Earth System Model are also analysed. Over the Mediterranean region, where substantial temperature increase and precipitation decrease are expected in the 21$^{st}$ century, near-surface air temperature *T2m* and total precipitation *R* projections are linked with the climate change of the components in the surface energy budget and total cloud cover, surface albedo and soil moisture. Although for the historical period the two RegCM simulations yield different climatology over the Mediterranean region, the climate change projections for the 21$^{st}$ century are not strongly sensitive to the choice of the PBL scheme.

Keywords: regional climate model, systematic errors, planetary boundary layer, surface energy budget, climate change

# 1. INTRODUCTION

*1.1 Dynamical downscaling and regional climate models*

Atmospheric and oceanic motions and exchange of momentum, mass and energy between different components of the climate system can be mathematically formulated as a numerical climate model. Climate models are broadly divided into global and regional climate models (GCMs and RCMs, respectively). This division is based on domain size over which models simulate climate system: the whole Earth or specific region/continent. RCMs are used to dynamically downscale past, present and possible future climates which were originally simulated either by global climate models, by reanalyses (i.e. estimates of atmospheric state from the measurements and models) or by seasonal forecasts (e.g. Wang et al. 2004). Dynamical downscaling is a method by which simulations at a coarse spatial resolution (e.g. 100-300 km) are regionalized to a finer spatial resolution (e.g. 10-50 km). RCMs can be used to explore various atmospheric processes and interactions between the atmosphere and other components of the Earth climate system (Wang et al. 2004). The state of climate system at a finer spatial resolution can also be estimated by employing various statistical relationships between the processes at the larger and smaller spatial scales; this is the so-called statistical downscaling (Giorgi and Mearns 1991). The two different downscaling methods, dynamical and statistical, have various limitations, theoretical and practical, but they can complement each other when describing the climate system over the region of interest. In this dissertation, climate and its variability as well as climate change over the European region will be investigated using the RegCM RCM (Pal et al. 2007; Giorgi et al. 2012). The increase in spatial resolution to only several tens of kilometres is essential because of substantial variability and complexity of the land surface, topography and coastline over this region (e.g. Branković et al. 2013). Also, spatial resolutions of 10 to 50 km may allow proper treatment of the basic dynamical processes in the coastal and mountainous regions since on this resolution the internal Rossby radius of deformation can be typically resolved (e.g. Hunt et al. 2001).

In terms of physical and mathematical properties, RCMs are similar to numerical models used in weather forecasting. The first successful climate simulations using RCM are described in Dickinson et al. (1989), and the methodology reviews are given in e.g. Giorgi and Mearns (1991), McGregor (1997), Giorgi and Mearns (1999), Wang et al. (2004), Laprise et al. (2008) and Rummukainen (2010). Several international research projects (e.g. PRUDENCE [1], ENSEMBLES[2], CORDEX[3]) focusing on the regional climate and its variability were organized in the past or are currently in progress. One of the goals of the above projects is to compare the results of different RCMs for both present and future climate.

*1.2 Systematic errors and sensitivity to model physics*

The comparison of modelling results against the measurements reveals RCM systematic errors, which in some cases may have large amplitude. Although the amplitude and the sign of systematic errors can differ from one model to the other, and depend on the region and season analysed, some common characteristics emerge. For example, over Europe the errors in the mean seasonal air temperature at 2 m, derived from the PRUDENCE and ENSEMBLES projects, are between ±2.5 °C and the errors in the mean seasonal total precipitation are typically between ±1.5 mm day$^{-1}$ (Jacob et al. 2007; Christensen et al. 2010). These systematic errors could be the genuine RCMs' errors (due to e.g. missing or only partially included processes) or could be due to errors in the boundary conditions which are provided by global models or reanalyses (Noguer et al. 1998). Definitions and details of dynamical downscaling (e.g. domain size, frequency of the boundary conditions, difference in the spatial resolution between forcing and nested models) can also contribute to errors in regional model simulations (Denis et al. 2002). Errors in simulations of the present climate can induce further errors in simulations of future climate i.e. there may be an impact of RCM systematic errors on the simulated climate change signal (e.g. Giorgi and Coppola 2010; Branković et al. 2012; Boberg and Christensen 2012). Although different climate models are based on nearly identical definitions of the atmospheric dynamics (equations of momentum, energy and mass conservation), one source of differences in modelling results is due to different approaches to discretisation of the domain and governing equations of the atmospheric dynamics. The second important source of differences is the formulation of physical processes on spatial scales that are smaller than those directly resolved. For example, at a 50-km grid spacing model cannot resolve clouds, turbulent eddies, various types of atmospheric waves,

[1] Prediction of Regional scenarios and Uncertainties for Defining EuropeaN Climate change and Effects
[2] ENSEMBLE-based Predictions of Climate Changes and their Impacts
[3] COordinated Regional climate Downscaling EXperiment

microphysical processes in clouds, interaction between radiation and atmospheric gases, etc. The lack of any of these processes would degrade the realism of a climate model. However, these unresolved processes are included into models in the form of parameterisations, i.e. empirical or semi-empirical procedures based on direct measurements, laboratory experiments and/or numerical simulations at finer spatial resolutions when these processes are resolved. Due to a variety of possible approaches, there is great diversity of parameterisation schemes in climate models. While climate models can benefit from the increase in horizontal resolution (e.g. Berner et al. 2012), there is need to examine if parameterizations schemes are appropriate at different resolutions since errors compensated at the low resolution experiments may be revealed when the resolution is increased (e.g. Branković and Gregory 2001; Pope and Stratton 2002). An additional source of differences is introduced when selecting specific values for parameters or coefficients in parameterisation schemes; for example, there may be an interval (sometimes unknown) of possible parameter values in a specific parameterisation. Examples of earlier studies with RegCM that explored the impact of different parameterisations or the impact of details in specific parameterisation on systematic errors are as the following: (1) cloud microphysics in Pal et al. (2000); (2) convection in Yang and Arritt (2002); (3) cloud microphysics and convection in Davis et al. (2009); (4) land-surface processes in Steiner et al. (2005, 2009); (5) convection and land-surface processes in Gianotti et al. (2012) and (6) turbulent mixing in the planetary boundary layer (PBL) in O'Brien et al. (2012). The focus of this dissertation is to diagnose systematic errors in the RegCM RCM for the lower atmosphere and at the surface; furthermore, to examine the efficacy and suitability of the two different parameterisation schemes of turbulent mixing in the PBL.

### *1.3 Surface energy balance*

The land surface interacts with the overlaying atmosphere and makes an impact on weather and climate at various spatial and time scales. There is strong evidence that the land surface processes at regional scales may influence climate on continental scale (Schär et al. 1999; Pitman 2003; Seneviratne et al. 2006; Seneviratne et al. 2010). Surface energy and water budgets are the key elements in controlling this influence, and surface energy balance has the critical role on the boundary conditions that in turn affect weather and climate (Betts et al. 1996). The main link between energy and water budgets is evapotranspiration that enters into surface energy budget (SEB) as latent heat flux.

A good knowledge of the components of surface energy budget is a precondition in understanding of how climate and climate change operate and possibly interact with human activities. This knowledge is attained by analysing parameters of the SEB from various observational sources. Although good quality data and improved spatial coverage are becoming increasingly accessible in the satellite era (e.g. Diak et al. 2004; Stephens et al. 2012), the lack of adequate observations is still a major obstacle in analysing the large-scale SEB. Nevertheless, comparing the SEB from different models is useful as it may suggest the exactness of their respective parameterisations (Gutowski et al. 1991). Also, the modelling sensitivity studies, whereby SEB is perturbed at regional scale (see e.g. Branković et al. 2006; Nogherotto et al. 2013 for case of deforestation), indicate large and statistically significant large-scale changes in, for example, temperature and precipitation. Thus, it is important to assess whether the models are able to reproduce the amplitude and regional distribution of the SEB components and to estimate uncertainties.

Most errors, though by no means all, in the modelling radiation budget (which is a part of the SEB) can be linked with the representation of clouds. For example, Jaeger et al. (2008) attributed the underestimation of the net surface shortwave radiation in their regional climate models over Europe to an overestimation of clouds. Markovic et al. (2009) also associated uncertainties in incoming shortwave flux in three RCMs over the USA with imprecision in cloud cover simulations. Explaining the errors in radiation budget over Europe, Kothe et al. (2011) found that, for a proper estimate of the net surface shortwave radiation, uncertainties in surface albedo are less important than uncertainties in total cloud cover and for the net surface longwave radiation they showed that uncertainties in surface temperature are less important than uncertainties in total cloud cover.

In addition to radiative fluxes, the surface and atmosphere exchange heat directly via sensible heat flux and, when evaporation and sublimation take place, they do so via latent heat flux. At the mid-latitude continental scales, heat fluxes can vary considerably in space and with the seasons (e.g. Berbery et al. 1999). In most of the year, both heat fluxes counteract the incoming shortwave flux indicating the heat loss at the surface. The relative contribution of individual fluxes to this heat exchange depends on soil types, soil moisture and vegetation types and coverage (e.g. Betts and Viterbo 2000).

The SEB over different parts of the world is a topic of many studies that used RegCM, version 3 (Pal et al. 2007). For example, various aspects of the RegCM3 radiation budget over land were improved with the introduction of the SUBEX parameterisation scheme for large-scale precipitation, particularly the representation of seasonal and interannual variability (Pal et al. 2000). Shi et al. (2008) found that, in terms of heat fluxes, RegCM3 can simulate reasonably well the major climate features of the east-Asian monsoon. Reboita et al. (2010) claim that, although RegCM3 simulated the sensible heat flux pattern successfully in regions close to South America, its amplitude was too large and associated with the 2 m temperature errors. Similarly, Winter and Eltahir (2010) found that RegCM3 simulates well the sensitivity of latent heat flux to available energy in the summer, but, when compared against the FLUXNET[4] observations, significant differences occurred in seasonal cycles. In a multi-model study over western Africa (Kothe and Ahrens 2010), RegCM3 significantly overestimated net surface shortwave radiation in the region where normally cloudiness is substantial. Over southern Africa, RegCM3 systematically overestimated the observed net surface shortwave radiation and the spatial pattern was consistent with that of cloudiness but the main driver of temperature biases over land with high soil water content was found to be latent heat flux (Sylla et al. 2012). In a model intercomparison study over Europe (PRUDENCE project; Christensen and Christensen 2007), the summer net surface shortwave radiation in RegCM3 is shown to generally exceed the summer net surface shortwave radiation in ERA40 reanalysis (Lenderink et al. 2007).

### *1.4 Planetary boundary layer*

Turbulent eddies in the planetary boundary layer (PBL) strongly influence vertical fluxes of momentum, heat and mass between the surface and the atmosphere. Although the spatial and temporal scales of turbulent eddies are several orders of magnitude smaller than the climatologically relevant scales, sensible and latent heat fluxes due to turbulent eddies are major components of the global energy budget (Andrews et al. 2009; Trenberth et al. 2009; Stephens et al. 2012). The PBL also acts as a sort of interactive buffer zone between the underlying surface

[4] FLUX NETwork, http://fluxnet.ornl.gov/

and free atmosphere, and therefore an understanding of the coupling between the PBL and the land surface is of particular concern. Even though two of the most often analysed variables in climate studies, near-surface temperature and precipitation, are controlled by the PBL processes (e.g. Giorgi et al. 1993; Dethloff et al. 2001; Shin and Ha 2007; Esau and Zilitinkevich 2010; Lesins et al. 2012), climatological aspects of observed and model simulated PBL do not receive much attention in scientific literature.

Substantial differences in spatial resolution of numerical models and spatial scale of atmospheric turbulent eddies (~10-100 km vs. ~10-1000 m) require parameterization of the impact of turbulent eddies on a resolved model flow (e.g. Stewart 1979; Holtslag et al. 2013). Because of strong interactions between PBL processes and surface processes, the fidelity of various feedbacks in models (such as the snow-albedo feedback (Winton 2006) and the methane feedback (Walter et al. 2006)) can be tied to the fidelity of the PBL parameterisation. An analysis of the PBL effects on climatological scales simulated by global or regional climate models typically includes bulk measures of turbulent activity, such as the PBL height and turbulent kinetic energy (*TKE*) and the evaluation of surface fluxes due to turbulent eddies (e.g. Medeiros et al. 2005; Sánchez et al. 2007; Jaeger et al. 2009). From available literature, it appears that none of the currently available PBL parameterisation schemes are generally superior and that the use and design of a specific scheme is often in the function of application (Wyngaard 1985; Grenier and Bretherton 2001; Zhu et al. 2005; Cuxart et al. 2006). Additionally, there is often a substantial time lag between the accepted knowledge of the PBL physics and its implementation in atmospheric and climate models (Baklanov et al. 2011).

Most PBL schemes can be broadly grouped into *non-local* and *local* types of schemes (e.g. Stensrud 2007). The term *non-local* refers to the schemes that use global characteristics of the PBL (e.g. the PBL height) to express turbulent fluxes, and the term *local* refers to the schemes that use local characteristics of the PBL (e.g. vertical gradients of the mean PBL properties). Intercomparison of various PBL schemes in limited area models is a subject of many studies; most of them were conducted for MM5[5] and WRF[6] models in simulations ranging from several hours to several months. Substantial spread in these simulations is found when changing the PBL

[5]PSU/NCAR Mesoscale Model, version 5, Pennsylvania State University and National Center for Atmospheric Research, USA
[6]Weather Research and Forecasting community model (http://www.wrf-model.org)

scheme, often linked with differences in the vertical mixing strength and the entrainment of the above-PBL air (e.g. Hu et al. 2010; Xie et al. 2012; García-Díez et al. 2013; Jerez et al. 2013).

In this dissertation, the impact of the two PBL schemes on simulated climatology over Europe in the regional climate model RegCM4.2 (Giorgi et al. 2012) will be investigated: the non-local diagnostic PBL scheme (the Holtslag scheme; Holtslag et al. 1990; Holtslag and Boville 1993), and the recently implemented local prognostic 1.5-order scheme (the University of Washington or the UW scheme; Grenier and Bretherton 2001). The Holtslag scheme has been a part of the RegCM model since the RegCM2 and its impact on the model one-month "climatology" was explored by Giorgi et al. (1993). The implementation of the UW scheme in RegCM4 is documented in O'Brien et al. (2012) and the initial comparisons between the two PBL schemes are described in O'Brien et al. (2012) and Giorgi et al. (2012).

By exploring the impact of PBL schemes on the RegCM4.2 climatology, a part of the structural uncertainty in RegCM4.2 is addressed. Here, the term "structural uncertainty" refers to uncertainty in the design of climate models that results from the fact that physical process can be represented in numerical models in various ways (e.g. Stainforth et al. 2007; Tebaldi and Knutti 2007; Curry and Webster 2011). The presence of unconstrained and tuneable parameters is a consequence of our incomplete knowledge of physical processes involved or simplifications made in atmospheric models. For example, the range of variation for most parameters in both RegCM PBL schemes is determined from observations and/or idealized high-resolution simulations (e.g. large-eddy simulations in Grenier and Bretherton 2001). The GCM studies that use the perturbed physics ensemble (PPE) approach to systematically analyze model sensitivity to the definitions of parameterisation schemes are fairly common (e.g. Murphy et al. 2004; Stainforth et al. 2005; Zhang et al. 2012), while the PPE studies for RCMs are still performed rarely (e.g. Suklitsch et al. 2011; Bellprat et al. 2012). Although RegCM is a commonly used model, there has not yet been a study of its structural uncertainty by either performing a large ensemble of many various combinations of parameterisations or by varying unconstrained parameters in a large PPE for an extended simulated period. However, there is a growing set of studies analyzing the RegCM structural uncertainty either through changing a subset of parameterisations or through customizing and perturbing the values of a few unconstrained parameters (e.g. Giorgi et al. 1993; Pal et al. 2000; Yang and Arritt 2002; Steiner et al. 2005, 2009; Davis et al. 2009; Winter et al. 2009; Gianotti et al. 2012; O'Brien et al. 2012; Torma and

Giorgi 2014). An overview of representative studies relevant for the RegCM PBL structural uncertainties indicates the lack of a common analysis strategy (e.g. choice of domain, model version or selected variables), thus making it difficult for their results to be generalized. After all, the use of a more advanced parameterisation does not necessarily improve model performance in all variables.

### *1.5 Objective*

The main objectives of this dissertation are (1) to investigate the accuracy of the RegCM climate simulations over Europe carried out specifically for the purpose of this study, (2) to diagnose possible sources of the RegCM systematic errors in those simulations and (3) to investigate possibilities of the reduction of systematic errors for the lower atmosphere in the RegCM model results. The performance of RegCM will be compared with other RCMs and GCMs. The working hypotheses are that the errors in the RegCM originate partly from (1) deficiencies in the representation of cloudiness in the lower atmosphere (which may cause inaccuracies in surface shortwave and longwave radiation fluxes) and from (2) deficiencies in the representation of the turbulent mixing effects in the PBL (particularly in statically stable atmospheric conditions). By testing these hypotheses and by removing some of the above deficiencies, the expected outcome of this research is a reduction of systematic errors in RegCM model in simulations at the longer time scales.

The dissertation is structured as follows. In Chapter 2 data, models and methodology are described. In Chapter 3 the near-surface climatology in the two 10-year RegCM simulations (the Holtslag vs. the UW scheme) and annual cycles of the surface energy budget components are analysed and discussed. In Chapter 4, an intercomparison of vertical profiles for various quantities over selected climatic regions is given, followed by an analysis of the PPE in the UW simulations. In Chapter 5, the impact of the two PBL schemes on the simulated climate change signal is explored. In Chapter 6, conclusions and suggestions for future work are summarized.

# 2. METHODOLOGY

## *2.1 Regional climate model RegCM*

### *2.1.1 Model description and experiments*

The two main sets of RegCM experiments are analysed. In the first set of experiments RegCM is forced by ERA-Interim reanalysis (Dee et al. 2011), in the second set of experiments RegCM is forced by the HadGEM2-ES Earth System Model (Jones et al. 2011). In both sets of experiments, simulations using two different PBL schemes are performed. Additional experiments in both sets are described below.

The RegCM model version used for the first set of experiments is RegCM4.2[7] (Giorgi et al. 2012). The experimental setup included a 50-km horizontal resolution and 23 vertical levels with the model top at 50 hPa. The boundary conditions, provided by ERA-Interim, are used for a) two 10-year experiments from 1989 to 1998, and b) for 18 PPE experiments from 1989 to 1991 (Table 1). In addition to a) and b), further two 3-year experiments from 2008-2010 were carried out. The integration domain included Europe and the northern Africa (Fig. 2.1a). The following parameterisations of the subgrid processes were used: the BATS1e scheme for the land-surface processes (Dickinson et al. 1993), the Pal et al. (2000) parameterisation of large-scale precipitation and clouds, the Emanuel (1991) scheme for deep convection and the scheme for longwave and shortwave radiation transfer from Kiehl et al. (1996). In RegCM4.2 the PBL scheme can be chosen between the Holtslag scheme (Holtslag et al. 1990; Holtslag and Boville 1993) and the UW scheme (Grenier and Bretherton 2001; O'Brien et al. 2012).

The experiments of the first set are referred to as RegCM(HL,EI) and RegCM(UW,EI), indicating the use of the Holtslag PBL scheme (HL) and the University of Washington PBL scheme (UW), respectively, and the use of ERA-Interim boundary conditions (EI). The additional PPE is carried out with the UW scheme (Table 1).

In the second set of the RegCM experiments, the version of the model used was RegCM4.3 and it was forced by the HadGEM2-ES Earth System Model over the domain shown in Fig. 2.1b for the period 1971-2098; for the period 1971 to November 2005, the observed

[7] Available from http://gforge.ictp.it/gf/project/regcm/

concentrations of the greenhouse gases (GHGs) were specified and from December 2005 to 2098 the IPCC RCP4.5 and RCP8.5 scenarios of GHG concentrations were used (Moss et al. 2010). The evaluation of the HadGEM2-ES model is presented in e.g. Martin et al. (2011) and HadGEM2-ES is compared to RegCM in e.g. Güttler et al. (2013b). The choice of the second domain was governed by available computing resources and design of large RegCM ensemble as in Torma and Giorgi (2014). The other differences in RegCM4.3 when compared to RegCM4.2 forced by ERA-Interim are: (1) a mixed scheme for convection consisting of the Emanuel (1991) convection scheme over the sea grid points and the Grell (1993) convection scheme over the land, (2) seasonally variable saturated soil albedo for the desert land-type (Giorgi et al. 2011) and (3) changes in the crop land-type where soil moisture is not allowed to fall below the level of 60% of saturation (Torma and Giorgi 2014). As in the first set of experiments, in RegCM4.3 the impact of the two different PBL schemes (Holstlag vs. UW) is analysed. The experiments of the second set are referred to as RegCM(HL,HA) and RegCM(UW,HA)[8].

In Fig. 2.1a the four selected regions are shown within the model domain, representing various climatic regimes, where the model sensitivity to the different PBL scheme could be distinctly manifested: (1) Russia is characterized by low temperatures with persistent snow cover during winter and early spring with frequent formation of shallow and very stable PBLs; (2) eastern Europe covers a typical European continental region; (3) the Sahara is defined over the desert area in the north Africa, where strong daytime turbulent mixing is present throughout the year; (4) the Mediterranean region is partially overlapping with the Sahara region but the atmospheric processes are largely influenced by the sea. In Chapter 5, annual cycles from RegCM(HL,HA) and RegCM(UW,HA) experiments are analysed only over the Mediterranean region (Fig. 2.1b) which is identical to the Mediterranean region from Chapters 3 and 4 (Medt; Fig. 2.1a).

Statistical significance of the differences (1) between models and observations, (2) between the RegCM simulations with the UW and Holtslag schemes, and (3) between future periods and historical period is determined by the Wilcoxon-Mann-Whitney nonparameteric rank-sum test (WMW; Wilks 2006).

[8] Historical and scenario RegCM(HL,HA) experiments were performed by Csaba Torma (ICTP) and scenario RegCM(UW,HA) experiments were performed by Lidija Srnec and Mirta Patarčić (DHMZ) on the ICTP computing system.

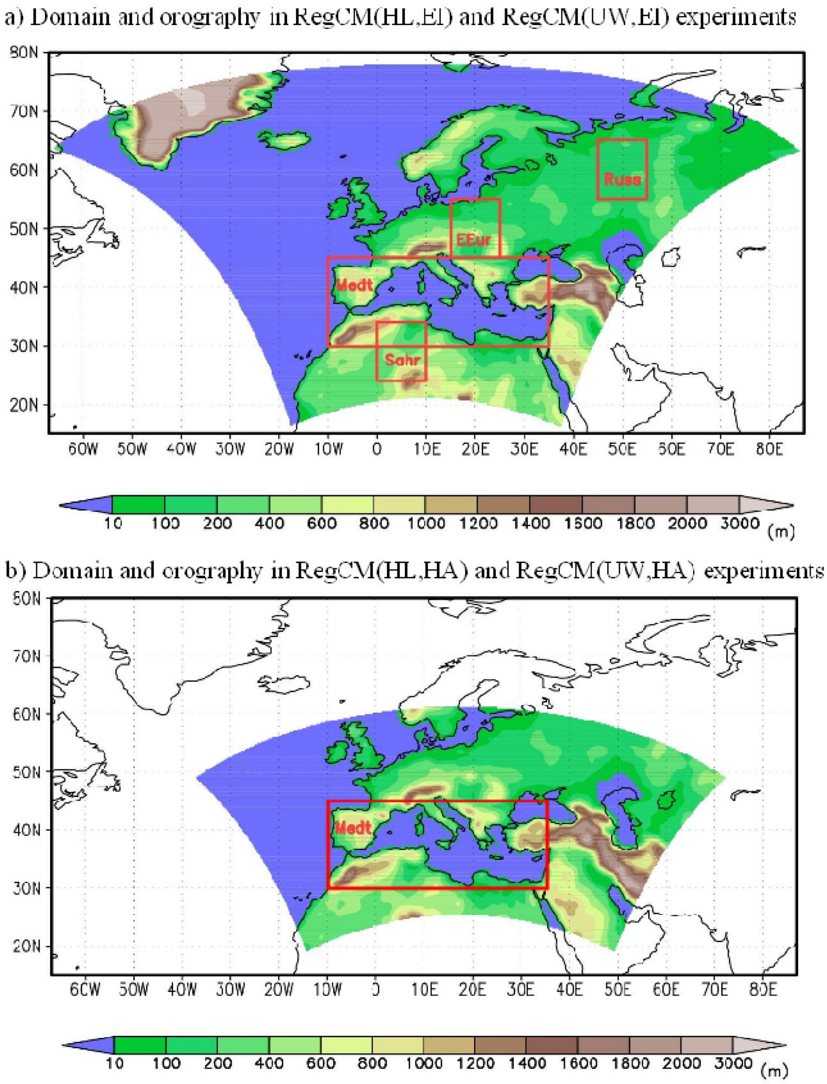


Fig. 2.1 The model domain, orography field (m) and selected regions (Russ: Russia; EEur: Eastern Europe; Sahr: Sahara; Medt: Mediterranean) for which vertical profiles, annual cycle, probability density functions and ensemble sensitivity analyses are calculated in: a) ERA-Interim-forced experiments RegCM(HL,EI) and RegCM(UW,EI) and b) HadGEM2-ES-forced experiments RegCM(HL,HA) and RegCM(UW,HA).

### *2.1.2 The Holtslag PBL scheme*

The temperature tendency due to vertical turbulent mixing is computed in RegCM as:

$$\left(\frac{\partial p^{*}T}{\partial t}\right)_{PBL} = p^{*}\frac{\partial}{\partial z}\left(K_{H}\left(\frac{\partial \theta}{\partial z}-\gamma\right)\frac{\Pi}{c_{p}}\right), \tag{2.1}$$

where $p^*=p_{SURF}-p_{TOP}$ represents the difference between surface pressure and pressure at the model top, $T$ is air temperature, $\theta$ is potential temperature, $K_H$ is eddy heat diffusivity, $\gamma$ is a counter-gradient term that parameterises the dry deep-convection transport, $\Pi=c_p(p/p_o)^{R/c_p}$ is the Exner function, $c_p$ is specific heat capacity of dry air at constant pressure, $p_o$ is pressure at the surface set to 1000 hPa and $R$ is the gas constant for dry air. The counter-gradient term $\gamma$ (see (2.2) below) parameterises the vertical heat transport due to large PBL eddies (e.g. Holtslag et al. 1990; Holtslag and Moeng 1991). The counter-gradient term is applied only in convective PBL layers (not in surface layer and not above PBL) and is determined as:

$$\gamma = C\frac{\left(\overline{w'\theta'}\right)_{SURF}}{w_t h}, \tag{2.2}$$

where $\left(\overline{w'\theta'}\right)_{SURF}$ is the surface heat flux (in kinematic units), $w_t$ is the turbulent velocity scale, $C$=8.5 (Holtslag et al. 1990) and $h$ is the PBL height determined as the height where the gradient Richardson number $Ri$ equals its critical value $Ri_C$ = 0.25. In the Holtslag scheme, it is assumed that the PBL mixing is forced only from the surface fluxes; otherwise, the whole concept of the $Ri_C$ can be questioned (e.g. Mauritsen et al. 2007; Baklanov et al. 2011). There are observational uncertainties related to the value of $C$ in (2.2), for example, in Troen and Mahrt (1986) this parameter is set to $C$=6.5. Similar expressions for tendencies due to turbulent mixing are implemented in the prognostic equations for wind components, and for water vapour and cloud water mixing ratios. However, the counter-gradient contribution is included only in the temperature prognostic equation and is not included in the calculation of tendencies in the prognostic equation for water vapour mixing ratio. This is a variation from the original Holtslag et al. (1990) formulation and was implemented in RegCM by Giorgi et al. (2012) in order to reduce too dry conditions in the lower atmosphere. The Holtslag scheme is written in terms of potential air temperature, so the Exner function must be included in order to reconstruct air temperature.

In the Holtslag scheme, eddy heat diffusivity $K_H$ inside the PBL is determined as:

$$K_H = k w_t z\left(1-\frac{z}{h}\right)^2, \tag{2.3}$$

where $k$=0.4 is the von Kármán constant, and $z$ is the height inside PBL.

Above the PBL, $K_H$ is determined as a function of $Ri$, wind shear and the asymptotic turbulent length scale is set to $l_\infty$=40 m (e.g. Pielke 2002):

$$K_H = K_{HO} + \left[Ri(\sigma) - Ri_C(\sigma)\right] \cdot l_\infty^2 \cdot \sqrt{\left(\frac{\Delta u}{\Delta z}\right)^2 + \left(\frac{\Delta v}{\Delta z}\right)^2}, \tag{2.4}$$

where $\sigma$ is the model sigma vertical coordinate and $K_{HO}$ is the background minimum vertical mixing coefficient. There is no unique formulation or value for the asymptotic length scale $l_\infty$ in (2.4) for vertical mixing above the PBL (e.g. Pielke 2002) which makes this parameter a candidate for sensitivity tests. However, since the focus here is on the new PBL scheme in the RegCM model (the UW scheme), sensitivity experiments (Table 1) are primarily designed to examine the impact of the unconstrained parameters in the UW scheme.

In the Holtslag scheme, the maximum eddy diffusivity and viscosity are not constrained inside PBL and above PBL are set to $0.8\Delta z^2/\Delta t$, where $\Delta z$ is the layer depth and $\Delta t$ is the model time step. At the same time, the minimum eddy diffusivity and viscosity are set to a relatively high value of 1 $m^2$ $s^{-1}$ inside and above the PBL. However, for very stable conditions, eddy heat diffusivity and viscosity are set to zero; this was shown to reduce a part of the warm bias during the winter in the high latitude regions (Güttler 2011).

*2.1.3 The UW PBL scheme*

While the Holtslag scheme is used only inside the PBL with a different approach to vertical mixing applied above the PBL, the UW scheme utilizes a consistent mixing approach for all turbulent layers across the whole atmospheric column. Whereas the origin of turbulent mixing in the Holtslag scheme is the surface heating due to incoming solar radiation and the related static instability, the UW scheme also includes a second region of the increased turbulent activity and mixing which is associated with the buoyancy perturbations due to the cloud-top entrainment instability and long-wave cooling present at the stratocumulus-topped PBLs (e.g. Stull 1988). Of course, both schemes "sense" turbulent mixing due to surface friction and wind shear. The UW scheme is developed in terms of liquid water potential temperature and total water mixing ratio and a separate iterative reconstruction determines the PBL tendencies for air temperature and for water vapour and cloud water mixing ratios. In the UW scheme, the eddy heat diffusivity $K_H$ is related to the $TKE$ following Mellor and Yamada (1982):

$$K_H = l\sqrt{2 \cdot TKE} \cdot S_H \,, \tag{2.5}$$

where $S_H$ is the stability function (e.g. Galperin et al. 1988) and $l$ is the master turbulent length scale with two options implemented in RegCM. In convective boundary layers, one of the two following formulations for $l$ can be chosen in initial model setup:

$$l_1 = \frac{\min(kz, 0.1\Delta z)}{1 + \frac{\min(kz, 0.1\Delta z)}{\lambda}}, \tag{2.6}$$

$$l_2 = \min(kz,\ 0.1\ \Delta z), \tag{2.7}$$

where $l_1$ is based on Blackadar (1962) and $l_2$ is consistent with the fact that in layers close to the surface, the distance from surface limits the size of turbulent eddies (e.g. Stull 1988); $\lambda$ is the asymptotic master turbulent length scale set to $0.085 z_c$, where $z_c$ is the depth of convective sublayer (Grenier and Bretherton 2001). For the same $z$ and $\Delta z$, $l_2$ is larger than $l_1$ and the use of $l_2$ increases $K_H$ (cf. (2.5)). In stably stratified conditions, there is no difference in the formulation of the master length, i.e.

$$l_1 = l_2 = \min\left( R_{STBL}\sqrt{\frac{TKE}{N^2}}, kz \right), \tag{2.8}$$

where $N$ is buoyancy (or the Brunt-Väisälä) frequency and $R_{STBL}$ is a scaling factor (e.g. Nieuwstadt 1984; see Mahrt and Vickers (2003) and Grisogono (2010) for the discussion). Only at the top of the cloud-topped PBL the following closure for the eddy heat diffusivity is assumed (Nicholls and Turton 1986):

$$K_H = w_e \Delta_i z, \tag{2.9}$$

where $w_e$ is the entrainment rate determined as

$$w_e = A\frac{TKE^{3/2}}{l\Delta_i b}, \tag{2.10}$$

where $\Delta_i b$ is the buoyancy difference across $\Delta_i z$ (the depth of the entrainment layer). $A$ is the entrainment efficiency defined as

$$A = a_1(1 + a_2 E), \qquad (2.11)$$

where $a_1$ is based on observations and set to 0.19, $E$ parameterises the evaporative enhancement of entrainment efficiency (e.g. Grenier and Bretherton 2001; their Appendix B) and $a_2$ is largely unconstrained parameter ranging from 10 to 100 (see e.g. Bretherton and Park (2009) for the discussion of the range of $a_2$ parameter).

As a part of the UW scheme, an additional prognostic equation for $TKE$ is implemented where local change of $TKE$ is governed by the buoyancy production and destruction, shear production, turbulent vertical transport and turbulent dissipation (e.g. Grenier and Bretherton 2001). Additionally, in the RegCM dynamical core the horizontal and vertical advection of $TKE$ and horizontal diffusion are computed (the second, third and the last terms in the following equation):

$$\frac{\partial TKE}{\partial t} + \vec{u} \cdot \vec{\nabla} TKE + w\frac{\partial TKE}{\partial z} = -K_H N^2 + K_M S_f^2 + \frac{\partial}{\partial z}\left(K_{TKE}\frac{\partial TKE}{\partial z}\right) - B_1 \frac{TKE^{3/2}}{l} + D \qquad (2.12)$$

where $K_M$ and $K_{TKE}$ are the momentum and $TKE$ turbulent diffusivities respectively, $S^2_f$ is the wind shear squared, $B_1$ is a constant in the turbulent dissipation term and $D$ is the horizontal diffusion term. In the RegCM implementation of (2.12), vertical gradient and vertical velocity are transformed to the $\sigma$ vertical coordinate system. The inclusion of the $TKE$ prognostic equation increases the RegCM computational requirements, where simulations with the UW scheme take approximately 30% more computer time when compared to simulations with the Holtslag scheme.

*2.2 Perturbed physics ensemble method*

Sensitivity of model climatology to several important aspects of the UW scheme is tested by an ensemble of RegCM simulations, each simulation is of a 3-year duration, 1989-1991. Different formulations of the master turbulent scale $l$ (in (2.6) and (2.7)) and the values of $a_2$ (in (2.11)) and $R_{STBL}$ (in (2.8)) are systematically varied (Table 1) making in total an 18-member ensemble. The parameter $a_2$ can be interpreted as the efficiency of evaporative enhancement of the cloud-top entrainment. In the region of mixing of the cloud-top air and the above-inversion air, evaporative cooling may force further sinking of the mixed air thus resulting in enhanced entrainment (Bretherton and Park 2009). A reduced $a_2$ means that "for a given *TKE*, higher cloud-top liquid water content (a thicker cloud) is needed to generate a given entrainment rate" (Grenier and Bretherton 2001). As a consequence, the reduction of $a_2$ can locally reduce the magnitude of eddy diffusivity (cf. (2.9)-(2.11)) and modify the vertical slope of the eddy diffusivity profile thus directly impacting temperature tendency from the PBL scheme (cf. (2.1)). Knight et al. (2007) emphasized the importance of the cloud entrainment rate which was associated with a 30% variability of climate sensitivity in their large PPE. Both, the importance of entrainment in large PPE and limitations in measuring its effects, make the parameter $a_2$ a prime candidate to test in a model environment.

Within the context of the present formulation of $l$ in the UW scheme, the experiments in Table 1 are broadly divided in two subsets: one when $l$ is formulated as in (2.6), and one when $l$ is formulated as in (2.7). For each definition, $l_1$ or $l_2$, in addition to the default value ($a_2$=15.0), the parameter $a_2$ is varied so as to acquire a value larger than the default and a value smaller than the default ($a_2$=20.0 and $a_2$=12.0, respectively). Similarly, for each value of $a_2$, the parameter $R_{STBL}$ is varied around its default value ($R_{STBL}$=1.5) with smaller and larger values relative to the default ($R_{STBL}$=1.0 and $R_{STBL}$=2.0, respectively). In such a way, the changes in the UW parameters considered are nearly "symmetrical" relative to their default values; the aim is to assess their possible impacts when it is not *a priori* clear what might be the ultimate model response to such changes.

Table 1: Experiments, values of perturbed parameters $a_2$ (in (2.11)) and $R_{STBL}$ (in (2.8)) and the choice of the formulation for the master turbulent length scale (in (2.6) and (2.7)). EXP001 is the default RegCM(HL,EI) and EXP002 is the default RegCM(UW,EI).

| EXP | PBL scheme | Master turbulent length scale (m) | Efficiency of evaporative enhancement of cloud-top entrainment $a_2$ (dimensionless) | Scaling parameter in stable boundary layer turbulent length scale $R_{STBL}$ (dimensionless) |
|---|---|---|---|---|
| 001 | Holtslag | - | - | - |
| 002 | UW | $l_1$ | 15.0 | 1.50 |
| 003 | UW | $l_1$ | 15.0 | 1.00 |
| 004 | UW | $l_1$ | 15.0 | 2.00 |
| 005 | UW | $l_1$ | 12.0 | 1.50 |
| 006 | UW | $l_1$ | 12.0 | 1.00 |
| 007 | UW | $l_1$ | 12.0 | 2.00 |
| 008 | UW | $l_1$ | 20.0 | 1.50 |
| 009 | UW | $l_1$ | 20.0 | 1.00 |
| 010 | UW | $l_1$ | 20.0 | 2.00 |
| 011 | UW | $l_2$ | 15.0 | 1.50 |
| 012 | UW | $l_2$ | 15.0 | 1.00 |
| 013 | UW | $l_2$ | 15.0 | 2.00 |
| 014 | UW | $l_2$ | 12.0 | 1.50 |
| 015 | UW | $l_2$ | 12.0 | 1.00 |
| 016 | UW | $l_2$ | 12.0 | 2.00 |
| 017 | UW | $l_2$ | 20.0 | 1.50 |
| 018 | UW | $l_2$ | 20.0 | 1.00 |
| 019 | UW | $l_2$ | 20.0 | 2.00 |

### *2.3 Diagnostic model of surface energy budget*

The following surface energy budget (SEB) components are analysed in Chapters 3 and 5: net surface shortwave flux *SWR*, net surface longwave flux *LWR*, sensible heat flux *SHF* and latent heat flux *LHF*. In models, *SWR* and *LWR* are the products of radiation and land-surface parameterisations, and *SHF* and *LHF* are determined by land-surface parameterisation and by interaction with the lowest atmospheric levels. For $SWR = SWR_{SFC}\downarrow - SWR_{SFC}\uparrow$ and $LWR =$

$LWR_{SFC}\downarrow$ - $LWR_{SFC}\uparrow$, i.e. the net surface fluxes are the differences between the downward (↓) and upward (↑) fluxes, we base our discussion on a conceptual model defined by Kothe et al. (2011; their Appendix 2):

$$SWR = (1 - ALB)(1 - CLD)SWR_{TOA} \downarrow, \tag{2.13}$$

$$LWR = \sigma TS^4 (0.165CLD^2 - 0.25), \tag{2.14}$$

where surface albedo $ALB$ and total cloud cover $CLD$ range from 0.0 to 1.0, $SWR_{TOA}\downarrow$ is incoming shortwave radiation at the top of the atmosphere, $\sigma$ is the Stefan-Boltzmann constant. The rationale for (2.14) and the choice of specific numerical values of two constants can be found in e.g. Kondratyev (1969). The total cloud cover $CLD$ refers to the effective cloud fraction; in ERA-Interim it is computed by using the maximum-random overlap algorithm, and in RegCM as the mean between maximum and random overlap. In satellite estimations used to evaluate model experiments (see the next subsection), $CLD$ is determined as a fraction of cloud-covered pixels over region including both cloud-covered and cloud-free pixels.

Following Dickinson et al. (1993) heat fluxes can be parameterised as:

$$SHF = \rho_{AIR} C_D V_{AIR} (T_{AIR} - TS) c_p, \tag{2.15}$$

$$LHF = \rho_{AIR} C_D V_{AIR} (q_{AIR} - q_{SAT}) L_v f_g, \tag{2.16}$$

where $\rho_{AIR}$ is the air density, $C_D$ is aerodynamic drag coefficient, $V_{AIR}$, $T_{AIR}$ and $q_{AIR}$ are wind speed, temperature and specific humidity respectively at the lowest model level, $c_p$ is specific heat capacity at the constant pressure, $q_{SAT}$ is saturated specific humidity at surface temperature $TS$, $L_V$ is latent heat of evaporation and $f_g$ is wetness factor. The following sign convention is applied in the rest of analysis: if a process adds energy to the surface, the associated flux is positive; if a process removes energy from the surface, the associated flux is negative.

At the Earth-atmosphere boundary, the following surface energy balance generally holds (e.g. Berbery et al. 1999; Stensrud 2007; Lesins et al. 2012):

$$SWR + LWR + SHF + LHF + GHF + SMF = 0, \tag{2.17}$$

where $GHF$ is the ground heat flux and $SMF$ is heat flux due to snowmelt. Under the assumption of the interface with no heat capacity and infinitesimal thickness, (2.17) does not include a storage term (e.g. Lesins et al. 2012). Only the first four terms in (2.17) were at disposal, but since they are the largest contributors to SEB it is possible to ascertain its main characteristics. The sum of *GHF* and *SMF*, termed residual in this study, is equal (in absolute terms) to the sum of the radiative (*SWR* and *LWR*) and turbulent heat (*SHF* and *LHF*) fluxes.

### *2.4 Data*

#### *2.4.1 Gridded temperature and precipitation data*

Mean monthly near-surface temperature (i.e. air temperature at 2 m) *T2m* and total precipitation from the CRU[9] TS 3.0 dataset (Mitchell and Jones 2005) available at a 0.5° × 0.5° latitude/longitude grid are used to evaluate RegCM temperature and precipitation. Evaluation of the RegCM simulations is made on the CRU grid, and the CRU land-sea mask is used when computing the area averaged quantities over land. CRU is used to examine model errors of the mean seasonal fields and errors in the mean annual cycles over selected regions in RegCM(HL,EI) and RegCM(UW,EI). Additionally, E-OBS 7.0 dataset (Haylock et al. 2008), available at a 0.25° × 0.25° grid, is also used for evaluating the RegCM mean monthly near-surface temperature and total precipitation.

#### *2.4.2 Satellite data*

Evaluation of the RegCM net surface shortwave and longwave fluxes, surface albedo and total cloud cover is made by the estimates of the same quantities from the NASA GEWEX/SRB[10] project. GEWEX/SRB is a global satellite-based dataset on a 1°×1° resolution (Gupta et al. 2006; Stackhouse et al. 2011). The GEWEX/SRB version 3.0 used here contains monthly mean products based on the algorithms from Pinker and Laszlo (1992) for shortwave fluxes and Fu et al. (1997) for longwave fluxes (here denoted as ALG1) and the products based on alternative, or quality-check, algorithms from Gupta et al. (2001) for shortwave fluxes and Gupta et al. (1992) for longwave fluxes (denoted as ALG2). Surface albedo in ALG1 was estimated as ratio of the

[9] Climatic Research Unit, University of East Anglia, Norwich, UK
[10] Global Energy and Water Cycle Experiment (GEWEX) Surface Radiation Budget (SRB) program

mean monthly surface upward and downward shortwave fluxes, while surface albedo in ALG2 was available at monthly frequency. The total cloud cover data is part of GEWEX/SRB as well. The GEWEX/SRB data were used for model evaluation in various regional climate studies (Pal et al. 2000; Winter et al. 2009; Kothe and Ahrens 2010; Winter and Eltahir 2010; Kothe et al. 2011; Sylla et al. 2012).

Estimates of the net surface longwave fluxes and the total cloud cover from the EUMETSAT CM SAF[11] CLARA-A1[12] dataset (Karlsson et al. 2013) are also used as an alternative evaluation dataset. These products are derived from the AVHRR[13] sensor carried on polar-orbiting satellites, but also use information from ERA-Interim reanalysis for some variables such as surface downward longwave radiation. The CLARA-A1 dataset is available at a 0.25° × 0.25° grid.

*2.4.3 Turbulent flux measurements and analysis*

For the period 2008-2010, observed sensible and latent heat fluxes were acquired from the C-SRNWP Programme (http://www.cosmo-model.org/srnwp/content/) for four locations in Europe: Sodankylä (Finland), Cabauw (the Netherlands), Lindenberg (Germany) and Fauga-Mauzac (France). From the 3-hourly time-series of the above turbulent heat fluxes probability density functions (PDFs) are calculated for all seasons by binning the values into the 5 W $m^{-2}$ bins. In this way, observed and simulated turbulent fluxes are compared over a wide range of values. For the same period (2008-2010), additional RegCM experiments with the identical setup as in RegCM(UW,EI) and RegCM(HL,EI) were made and the RegCM simulated as well as ERA-Interim PDFs of heat fluxes were estimated at grid points nearest to the above C-SRNWP stations. The Perkins skill score (PSS; Perkins et al. 2007) is computed to determine how close (or similar) are the PDFs. The PSS measures the common area below two PDF curves and if they overlap exactly, the PSS equals to 1.

ERA-Interim is used as a basic reference to evaluate RegCM simulations over large land areas when flux measurements are not available. However, since ERA-Interim was also used to force RegCM, it cannot be considered as a fully independent validation dataset.

[11] Climate Monitoring Satellite Application Facility (CM SAF)
[12] CM SAF cLoud, Albedo and RAdiation dataset from AVHRR data (CLARA-A1)
[13] Advanced Very High Resolution Radiometer

# 3. SYSTEMATIC ERRORS IN SURFACE AND NEAR-SURFACE VARIABLES

In this chapter, the mean seasonal and monthly near-surface temperature, *T2m*, and total precipitation errors in RegCM simulations are analysed and will be linked with the model systematic errors in the surface energy budget components. Next, an analysis of the surface radiative and turbulent heat fluxes is presented. Additionally, other important quantities, such as total cloud cover *CLD* and surface albedo *ALB*, are linked with simulated and observed components of surface energy budget. We explore below whether the systematic errors in RegCM with the Holtslag scheme are reduced when the UW scheme is implemented in the RegCM version used here. Work presented in this chapter is based on Güttler et al. (2013a,b).

### *3.1 Near-surface temperature and precipitation errors*

The reference simulation RegCM(HL,EI) reveals an underestimation of *T2m* relative to CRU data over the northern Africa during winter, with errors ranging between -2 °C and -4 °C (Fig. 3.1a). In the central parts of the domain, *T2m* is simulated well with the mean errors between -1 °C and 1 °C. In the northern and north-eastern parts of the domain RegCM(HL,EI) overestimates *T2m*, typically between 2 °C and 4 °C. Even larger overestimation of *T2m* over the same region was found in the previous versions of RegCM (i.e. RegCM3) and was linked with model deficiencies in simulating very cold and stable conditions associated with increased cloudiness (Güttler 2011). The winter warm bias in the RegCM simulations is also seen over other domains, e.g. North America (Mearns et al. 2012) and Central Asia (Ozturk et al. 2012). During JJA, large *T2m* systematic errors are, on the other hand, found in the central part of the European domain, ranging between 2 °C and 4 °C (Fig. 3.1c). Over the northern Africa, cold bias prevails during DJF, while warm bias can be detected over north-eastern Africa during JJA.

First, we ascertain that the spatial distribution of the *T2m* errors in JJA differs from that in DJF, pointing to a possibly different origin of these errors in the two contrasting seasons. Coppola et al. (2012; their Fig. 8) detected similar spatial structure of the *T2m* errors over the northern Africa in the tropical-band version of RegCM (where RegCM encompassed the tropical belt and was limited only with southern and northern boundaries). They reported the cold bias over the Sahara and generally over the north Africa during DJF, but the cold bias also dominated in JJA over the western Sahara whilst the warm bias prevailed over the eastern Sahara. This error pattern suggests that some local processes are possible sources of *T2m* errors over the northern Africa, because in Coppola et al. (2012) the upper-air flow over northern Africa was not influenced either by the nesting or by domain size.

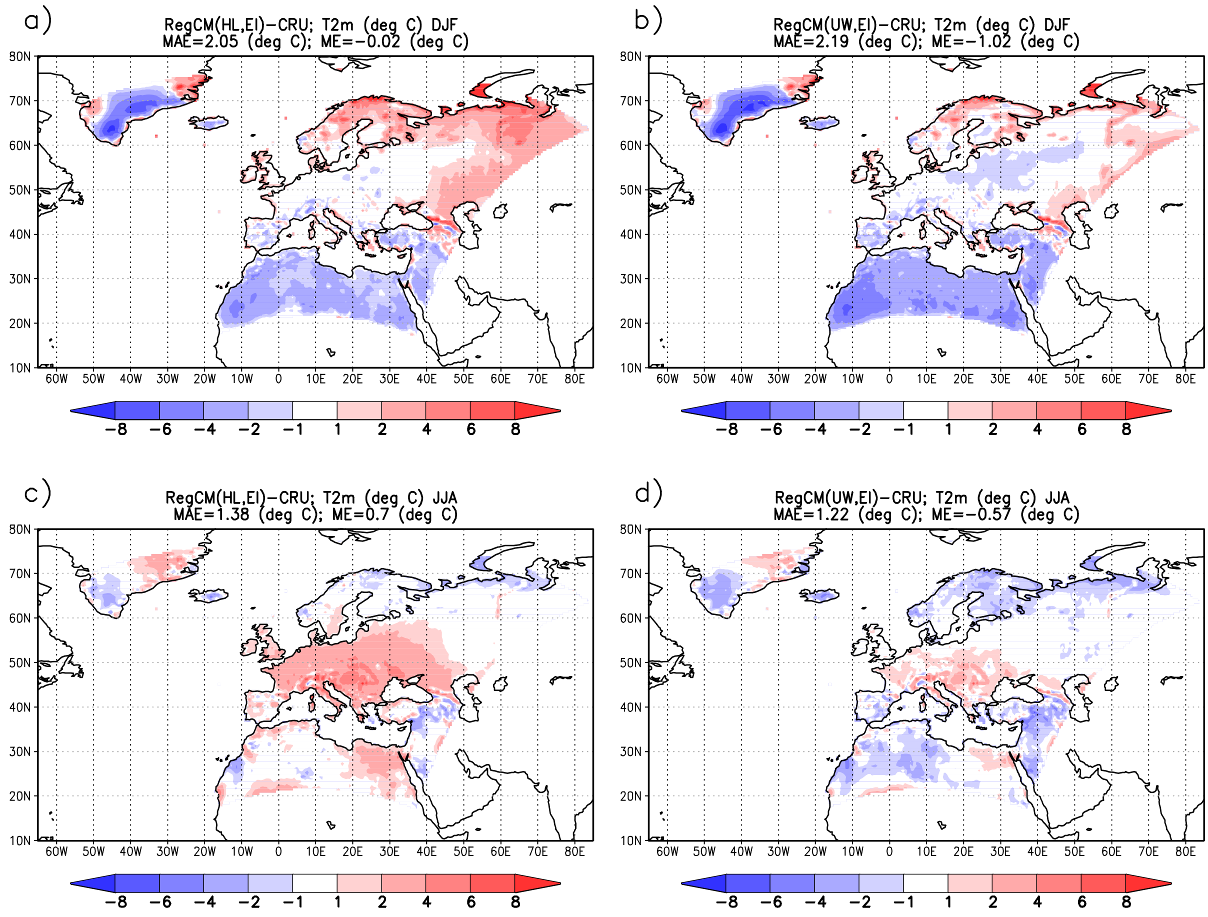


Fig. 3.1 Systematic errors in near-surface temperature *T2m* in RegCM(HL,EI) (left) and RegCM(UW,EI) (right) when compared against CRU TS 3.0 for winter (top) and summer (bottom). The period simulated is 1989–1998. *MAE* (mean absolute error) and *ME* (mean error) are computed over the entire domain. Units are °C. See Güttler et al. (2013a) for more details.

The *T2m* response in the RegCM(UW,EI) experiment (i.e. RegCM using the UW scheme while keeping all other aspects of the model parameterisations unchanged), is shown in Fig. 3.1b,d. The summer positive *T2m* errors are now generally reduced with the magnitude between 1 °C and 2 °C, as are the winter positive errors in the north-eastern part of the domain. However, the winter cold bias over the northern Africa is enhanced with the UW scheme, thus contributing to an increase of the overall mean error from -0.02 °C in RegCM(HL,EI) to -1.02 °C in RegCM(UW,EI). A similar model response was also documented by O'Brien et al. (2012) in their simulations over the North American region. In spite of the drawback in the winter cold bias over the northern Africa, we can nevertheless judge that, in terms of the *T2m* climatology, the use of the UW scheme in RegCM is overall beneficial over the domain considered. A possible origin of cooling induced by the UW scheme will be explored in the next chapter by analyzing vertical profiles of eddy heat diffusivity and temperature tendency. In this chapter, however, systematic errors in *T2m* will be linked with systematic errors in other relevant surface variables in RegCM(HL,EI) and RegCM(UW,EI). Potential sources of the near-surface temperature bias over the northern Africa can include limitations and deficiencies that are related to very specific geophysical properties over this region, like, for example: the albedo specification in the land-surface scheme (Sylla et al. 2010), the overestimation of the total cloud cover during DJF (Güttler et al. 2013b) and the need to include the aerosol-related processes in RegCM simulations (Solmon et al. 2012). However, the RegCM simulations of surface and near-surface climatology over the whole Africa is comparable to other regional climate models (e.g. Kothe and Ahrens 2010; Kim et al. 2013).

A closer inspection of the *T2m* mean monthly errors over the four selected regions (Fig. 3.2) supports the previous discussion. Generally, the near-surface temperature is lower in RegCM(UW,EI) when compared to RegCM(HL,EI). The largest positive impact of the UW scheme is seen over the central parts of the domain during summer where the mean seasonal error is reduced from 3.5 °C in RegCM(HL,EI) to 1.4 °C in RegCM(UW,EI) (Fig. 3.2b). Another positive impact of the UW scheme is seen over Russia during winter when the mean seasonal error is reduced from 1.3 °C down to -0.7 °C (Fig. 3.2a). The largest negative impact of the UW scheme is most clearly present over the Sahara during winter (Fig. 3.2d), but in other regions additional cooling from the UW scheme also often increases negative errors already present in the RegCM(HL,EI). However, even when such additional cooling is taken into account, the range of seasonally averaged temperature errors in the RegCM(UW,EI) is typically from -1.5 °C to 1.5 °C.

The above modelling errors should be viewed in the context of *T2m* values from ERA-Interim and E-OBS. Whereas the mean differences between CRU and E-OBS, amounting over

Russia and Eastern Europe to between -0.5 °C and 0.5 °C, indicate observational uncertainties, ERA-Interim shows a general tendency to slightly or moderately overestimate CRU *T2m* over all four regions. While winter warm bias over Russia is present in both RegCM(HL,EI) and ERA-Interim, large summer warm bias over Eastern Europe is unique to RegCM simulations.

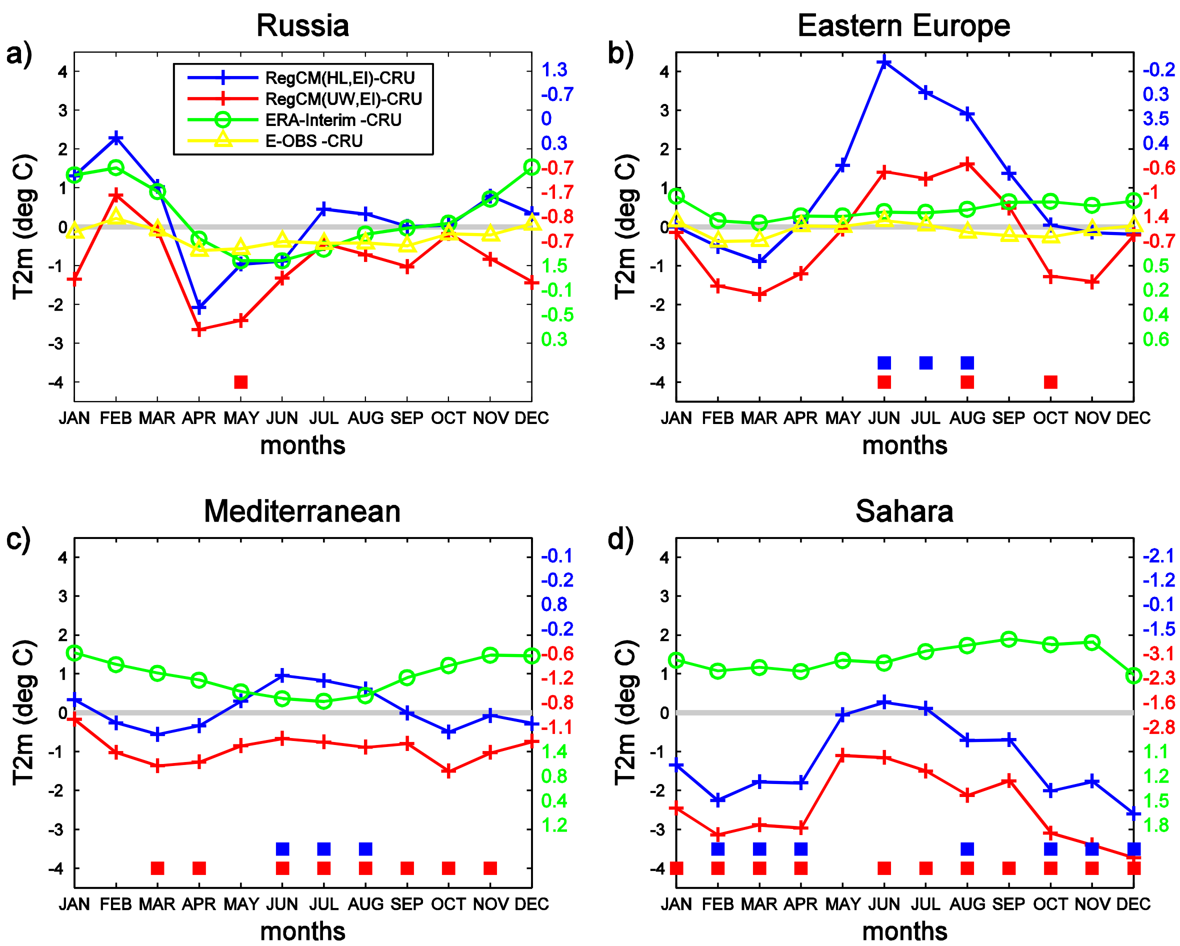


Fig. 3.2 Annual cycle of near-surface temperature *T2m* errors relative to the CRU TS 3.0 for RegCM(HL,EI) (blue plus mark), RegCM(UW,EI) (red plus mark), ERA-Interim (green circles) and E-OBS (yellow triangles) datasets over four (or two for the case of E-OBS) selected regions. The period analysed is January 1989 - December 1998. Units are °C. Blue (red) solid squares at the bottom of each panel mark the months when the difference between the medians of RegCM(HL,EI) (RegCM(UW,EI)) and CRU monthly area averages are statistically significant at the 95% confidence level. The coloured numbers on the right side of the y-axes are the mean seasonal values (DJF, MAM, JJA and SON) corresponding to identically coloured graphs in each panel (e.g. blue values correspond to the seasonal means of the RegCM(HL,EI)-CRU anomalies).

The RegCM(UW,EI) experiment is wetter than the default RegCM(HL,EI); this is seen in the mean seasonal precipitation when compared against CRU (Fig. 3.3). The winter wet bias in RegCM(HL,EI), with the magnitude between 0.5 and 1 mm day$^{-1}$ over large parts of Europe (Fig. 3.3a), is slightly increased in RegCM(UW,EI) which is seen in the mean area error increase from 0.67 mm day$^{-1}$ to 0.75 mm day$^{-1}$ (Fig. 3.3b). However, a general precipitation increase in RegCM(UW,EI) has a positive impact on model's summer climatology. Here, the dominant dry bias over central Europe in RegCM(HL,EI) is much reduced in RegCM(UW,EI) (cf. Fig. 3.3 bottom panels), but the drying still persists in the south-eastern Europe.

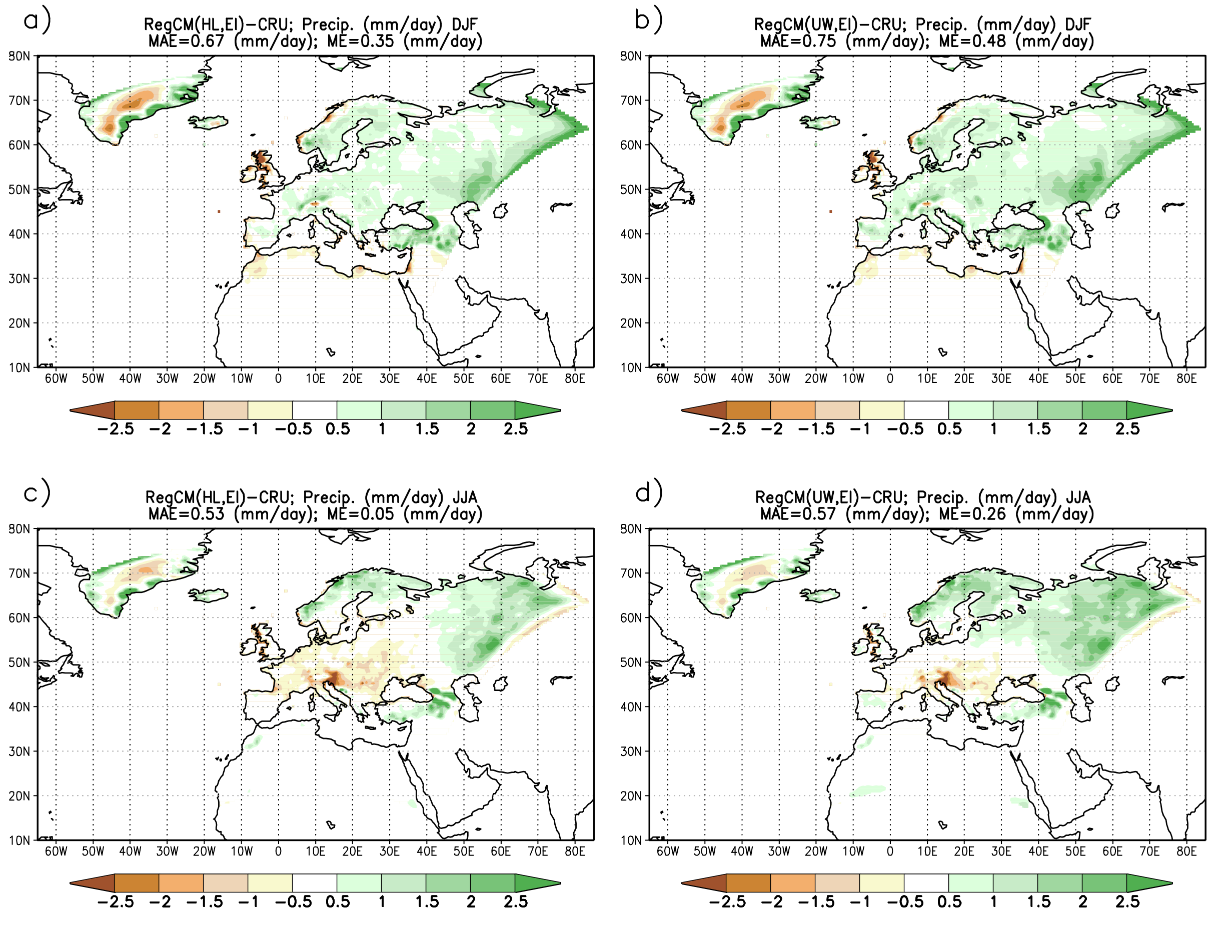


Fig. 3.3 Same as Fig. 3.1 but for total precipitation amount $R$. Units are mm day$^{-1}$. See Güttler et al. (2013a) for details.

The dominant wet bias in RegCM(UW,EI) relative to RegCM(HL,EI) is clearly seen in Fig. 3.4 (cf. the red and blue graphs). The exception is the Sahara region where the precipitation biases are negligible throughout the annual cycle. The overall impact of the wetter

RegCM(UW,EI) on the sign and amplitude of systematic errors varies over different regions and in different seasons. From Fig. 3.4 it could be, however, inferred that the UW scheme generally has a beneficial impact in the regions and seasons where the dry bias in RegCM(HL,EI) prevails, but where the wet bias in RegCM(HL,EI) is dominant, the UW schemes tends to increase it further. For example, the overestimation of the winter precipitation over Russia is from 0.59 mm day$^{-1}$ in RegCM(HL,EI) increased to 0.78 mm day$^{-1}$ in RegCM(UW,EI) while the mean summer error is increased from 0.87 mm day$^{-1}$ up to 1.4 mm day$^{-1}$. On the other hand, the mean summer error over eastern Europe is reduced from -0.86 mm day$^{-1}$ in RegCM(HL,EI) to -0.52 mm day$^{-1}$ in RegCM(UW,EI).

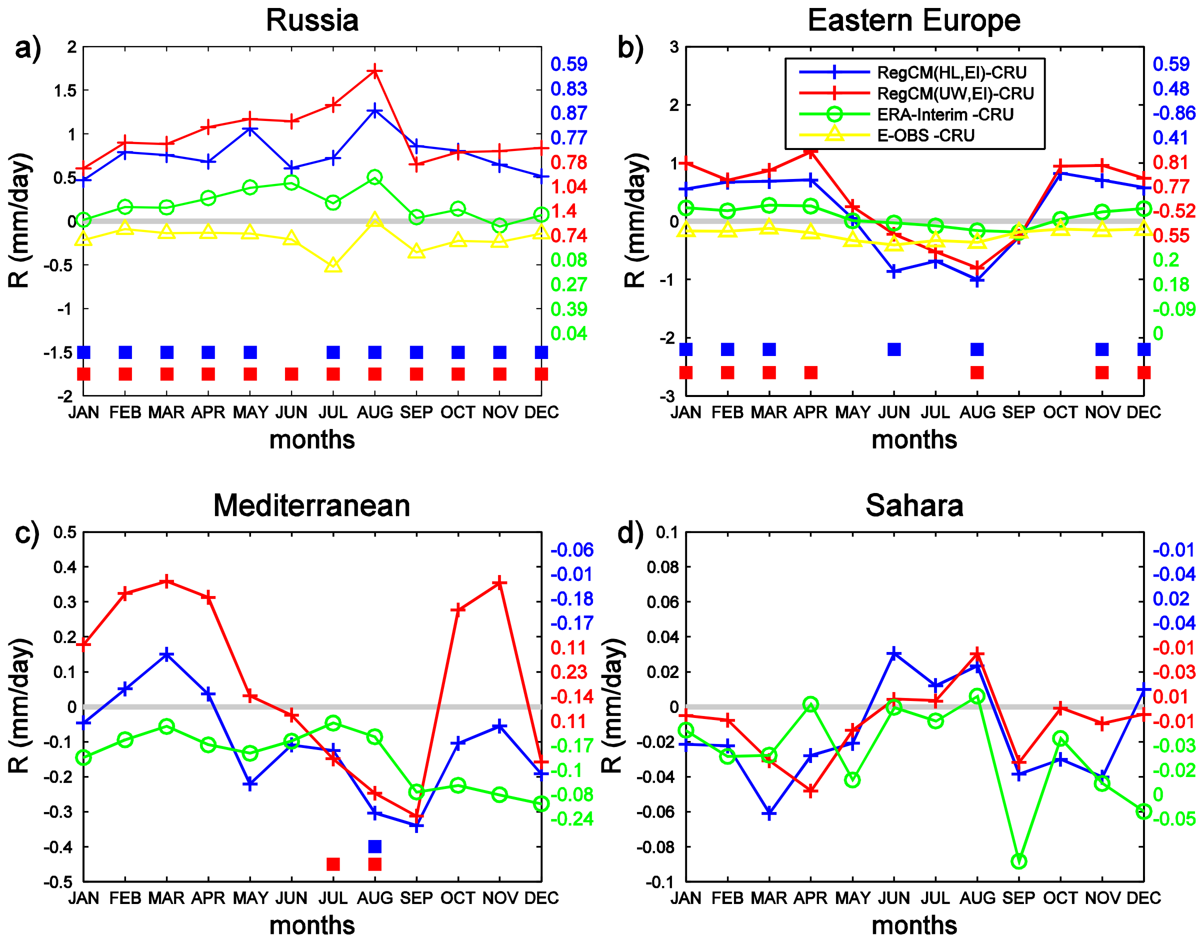

Fig. 3.4 Same as Fig. 3.2 but for total precipitation amount $R$. Units are mm day$^{-1}$.

*3.2 Net surface shortwave radiation SWR*

In this and subsequent subsections, an analysis of the surface energy budget components is presented and associated with the systematic errors in *T2m*. The largest discrepancy in the net surface shortwave radiation *SWR* between various sources is seen during the warm half-year in the eastern Europe (Fig. 3.5b), where both RegCM simulations substantially overestimate the GEWEX/SRB data and they are also larger than in ERA-Interim. While in ERA-Interim the mean summer *SWR* amounts to 195.2 W $m^{-2}$, in RegCM(HL,EI) and RegCM(UW,EI) is 236.3 W $m^{-2}$ and 229.5 W $m^{-2}$ respectively, an overestimation of approximately 21% and 18%. Although during the summer RegCM(UW,EI) is slightly closer to reanalysis and the satellite-based products than RegCM(HL,EI), the differences between the two RegCM experiments are not statistically significant. In other regions, the largest overestimations by the model are also in the warm part of the year, but they are smaller than over the Eastern Europe (Fig. 3.5 a,c,d). During the cold half of the year, when the amplitude of *SWR* is relatively low, the errors are much smaller in comparison with the warm period, amounting to less than 10 W $m^{-2}$. These errors are comparable to those found by e.g. Jaeger et al. (2008), Kothe et al. (2011) and Güttler et al. (2013b). Though small, the winter (DJF) differences between the RegCM simulations over eastern Europe are statistically significant.

When judging relative magnitude of the model *SWR* errors, one should bear in mind that the difference between ERA-Interim and GEWEX/SRB is relatively large – over eastern Europe it amounts to approximately 30 W $m^{-2}$ from April to July. Also, the non-negligible differences between the two GEWEX/SRB algorithms indicate uncertainties in the observational data: for example, over the Sahara desert the maximum difference of 35 W $m^{-2}$ is seen in May (Fig. 3.5d) and over Russia this difference is between 10 and 20 W $m^{-2}$ in the warm half of the year (Fig. 3.5a). In some months uncertainties in *SWR* estimates appear to be as large as the modelling biases, implying that the differences between various observational data question our knowledge of the actual values. For example, regardless of the algorithm used, the model overestimates *SWR* over the Sahara from March to August and over eastern Europe from May to July. Because *SWR* strongly affects other processes related to land surface, excessive *SWR* may, for example, force excessive surface evaporation and dry out soil moisture (Betts et al. 1996).

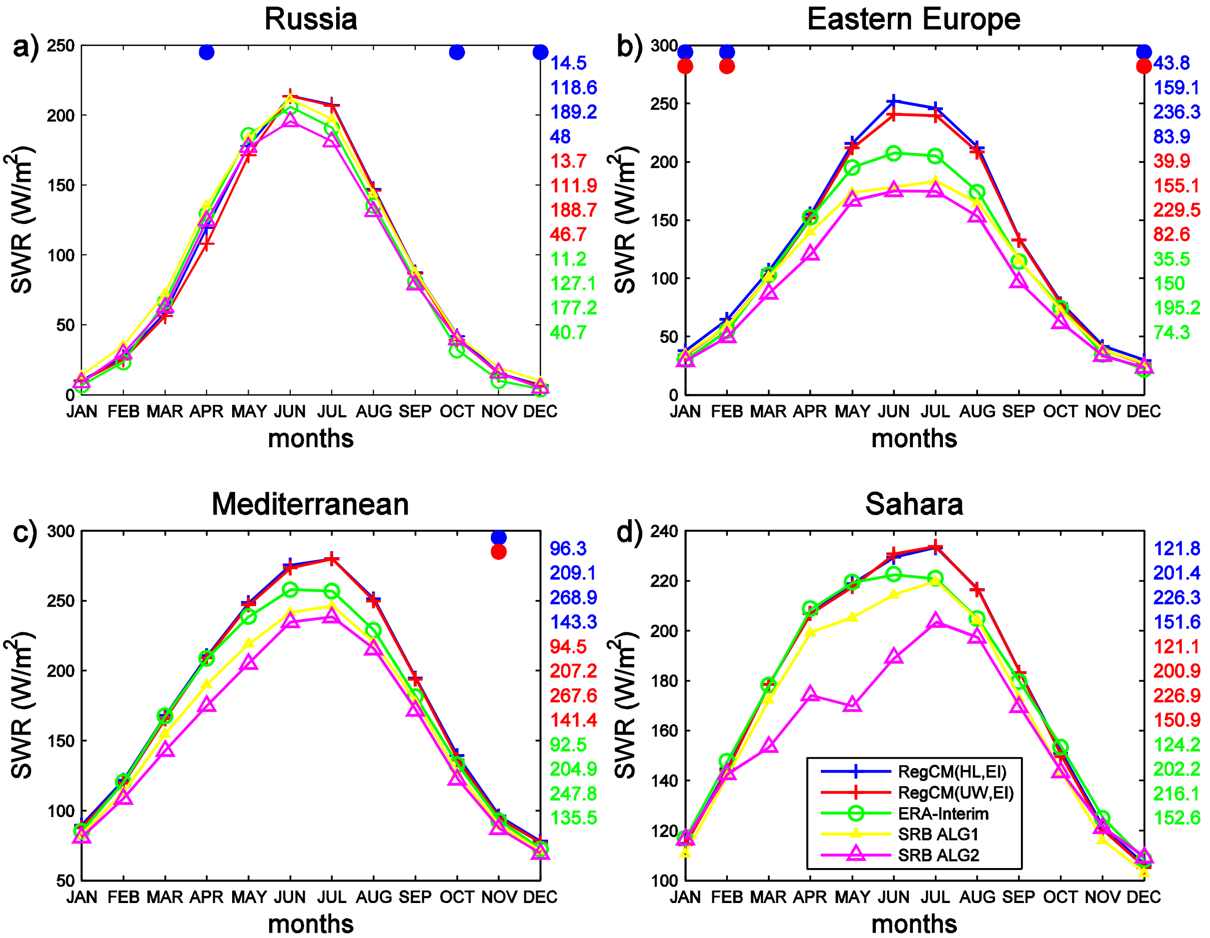


Fig. 3.5 Annual cycle of the net surface shortwave radiation *SWR* for RegCM(HL,EI) (blue plus marker), RegCM(UW,EI) (red plus marker), ERA-Interim (green circles), SRB ALG1 (yellow triangles) and SRB ALG2 (magenta triangles) datasets over selected regions. The period analysed is January 1989 - December 1998. Units are W m$^{-2}$. Blue (red) solid circles at the top of each panel mark the months when the difference between the medians of RegCM(HL,EI) and RegCM(UW,EI) monthly area averages are statistically significant at the 90% (95%) confidence level. The coloured numbers outside the y-axes are the mean seasonal values (DJF, MAM, JJA and SON) corresponding to identically coloured annual cycles (e.g. blue numbers correspond to seasonal means of RegCM(HL,EI)).

Errors in *SWR* over eastern Europe could be, at least partly, related to the representation of clouds. The underestimated *CLD* in two RegCM realisations and ERA-Interim (Fig. 3.6b) corresponds to the increased *SWR*, particularly in the summer (Fig. 3.5b). However, when compared against all observational datasets, the total cloud cover *CLD* in RegCM(UW,EI) during summer shows a major improvement in RegCM(HL,EI): it is increased from 0.4 in the

RegCM(HL,EI) up to 0.5 when the UW scheme is used. Although over the Sahara the observed *CLD* is generally low (Fig. 3.6d), it is nevertheless underestimated by the model and ERA-Interim; such an underestimation of *CLD* strongly corresponds to positive *SWR* errors (Fig. 3.5d). On the other hand, *SWR* over Russia during the cold half of the year (Fig. 3.5a) seems to be insensitive to a large variation (errors) of a relatively high cloud cover (Fig. 3.6a), possibly because of very low *SWR* values (only about 10 W m$^{-2}$). In addition, the amplitude of *LWR* outweighs that of *SWR* (cf. Fig. 3.8a below), i.e. the net surface radiation flux is weak negative.

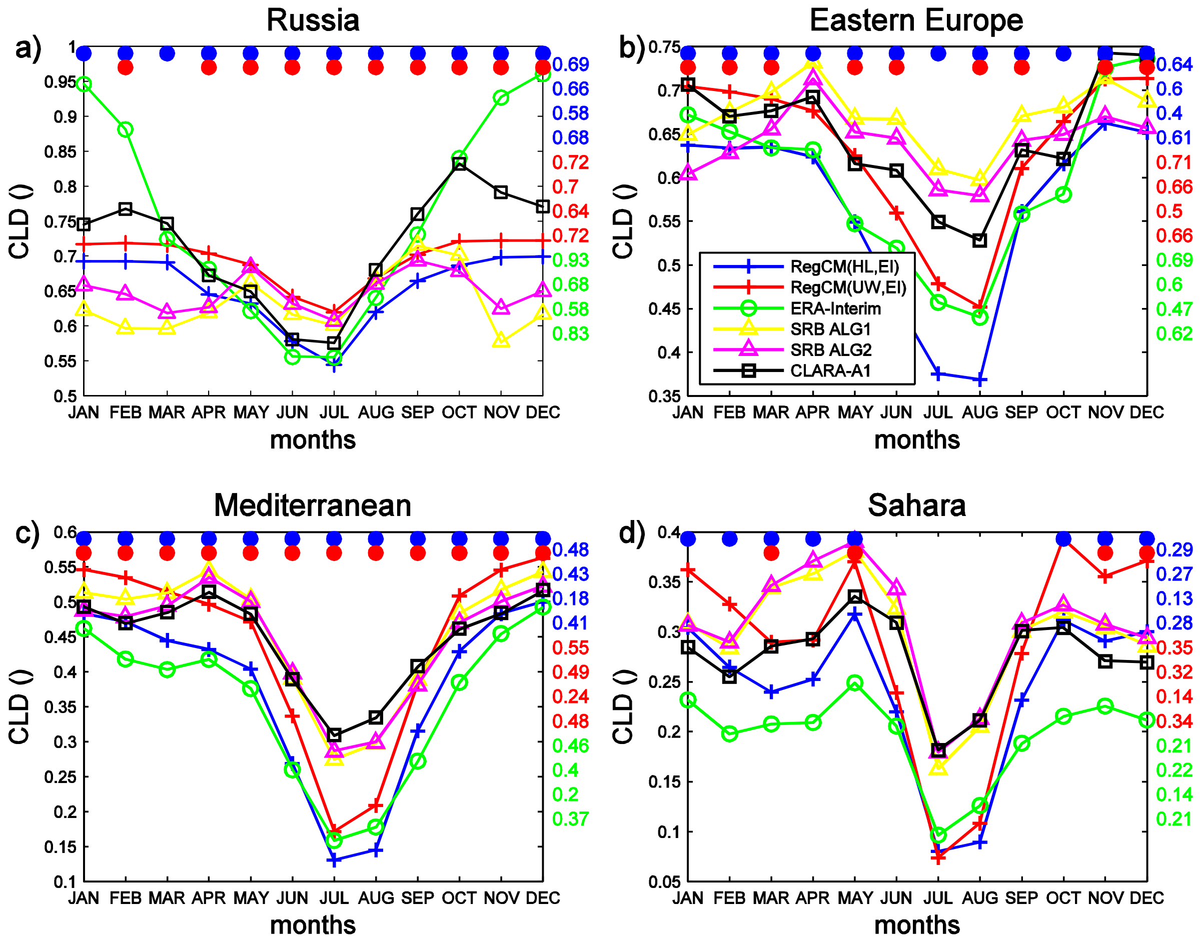


Fig. 3.6 Same as Fig. 3.5 but for total cloud cover *CLD* (from 0 to 1). Additionally, the annual cycles from the CM SAF CLARA-A1 dataset are shown (black squares).

The impact of surface albedo *ALB* over Russia and eastern Europe (Fig. 3.7a,b) on the *SWR* during the warm period seems to be less important than that of clouds, consistent with the results from Kothe et al. (2011). Over eastern Europe, the nearly constant and low model *ALB* values from April to October (~0.1) cannot account for the modelled variation in *SWR* in the same period (Fig. 3.5b). However, a close relationship between *ALB* and *SWR*, i.e. the lower albedo causing the higher SWR still holds among different data sources. On the other hand, the snow-related increase in albedo (and associated errors) in the cold period, particularly over Russia, does not point towards substantial differences in *SWR*, most probably due to the very low *SWR* values. Over the Sahara and the Mediterranean differences in the shape of the annual cycle of *ALB* between various datasets are present (Fig. 3.7c,d). Also, differences between the two satellite-based albedo estimates over the Sahara and the Mediterranean limit our ability to interpret possible link between the *ALB* and *SWR* errors. However, both RegCM simulations underestimate the satellite-based estimates of *ALB* and that by ERA-Interim and have the tendency to follow the ERA-Interim annual cycle.

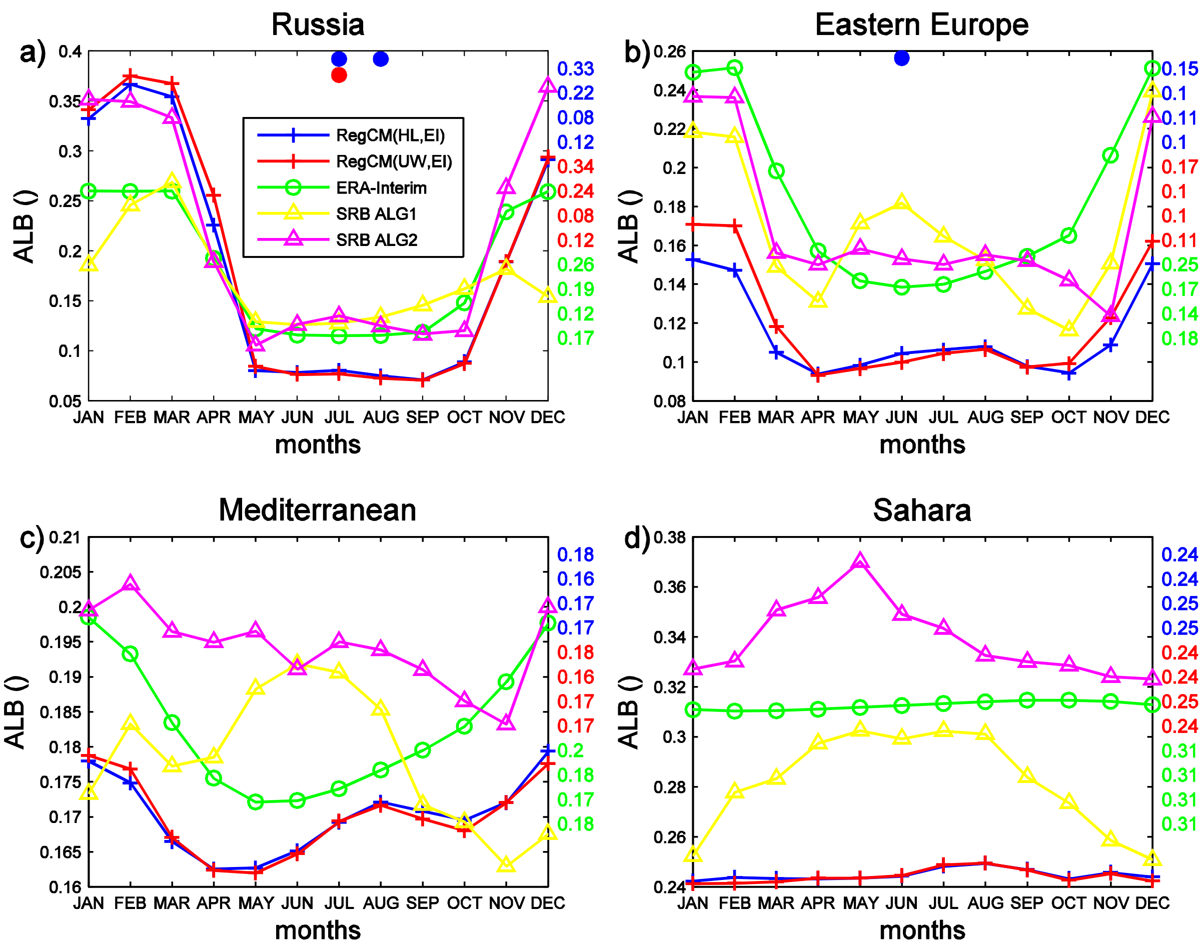


Fig. 3.7 Same as Fig. 3.8 but for surface albedo *ALB* (from 0 to 1) except CM SAF CLARA-A1 data are not included.

*3.4 Net surface longwave radiation LWR*

The largest RegCM errors in *LWR*, ranging between 20 and 30 W m$^{-2}$, are seen in the warm half of the year over eastern Europe (Fig. 3.8b). Here, ERA-Interim is very close to GEWEX/SRB and CLARA-A1 estimates and the modelling errors indicate an overestimation of *LWR* (in absolute terms). In the cold period, RegCM deviates less from GEWEX/SRB, CLARA-A1 and ERA-Interim, except over Russia where the errors are of similar magnitude (around 10 W m$^{-2}$) as the differences between the two GEWEX/SRB algorithms. Over the Sahara, an even larger discrepancy (20-30 W m$^{-2}$) is seen between the two GEWEX/SRB algorithms throughout the year (Fig. 3.8d) which suggests a cautious evaluation of this surface energy budget component.

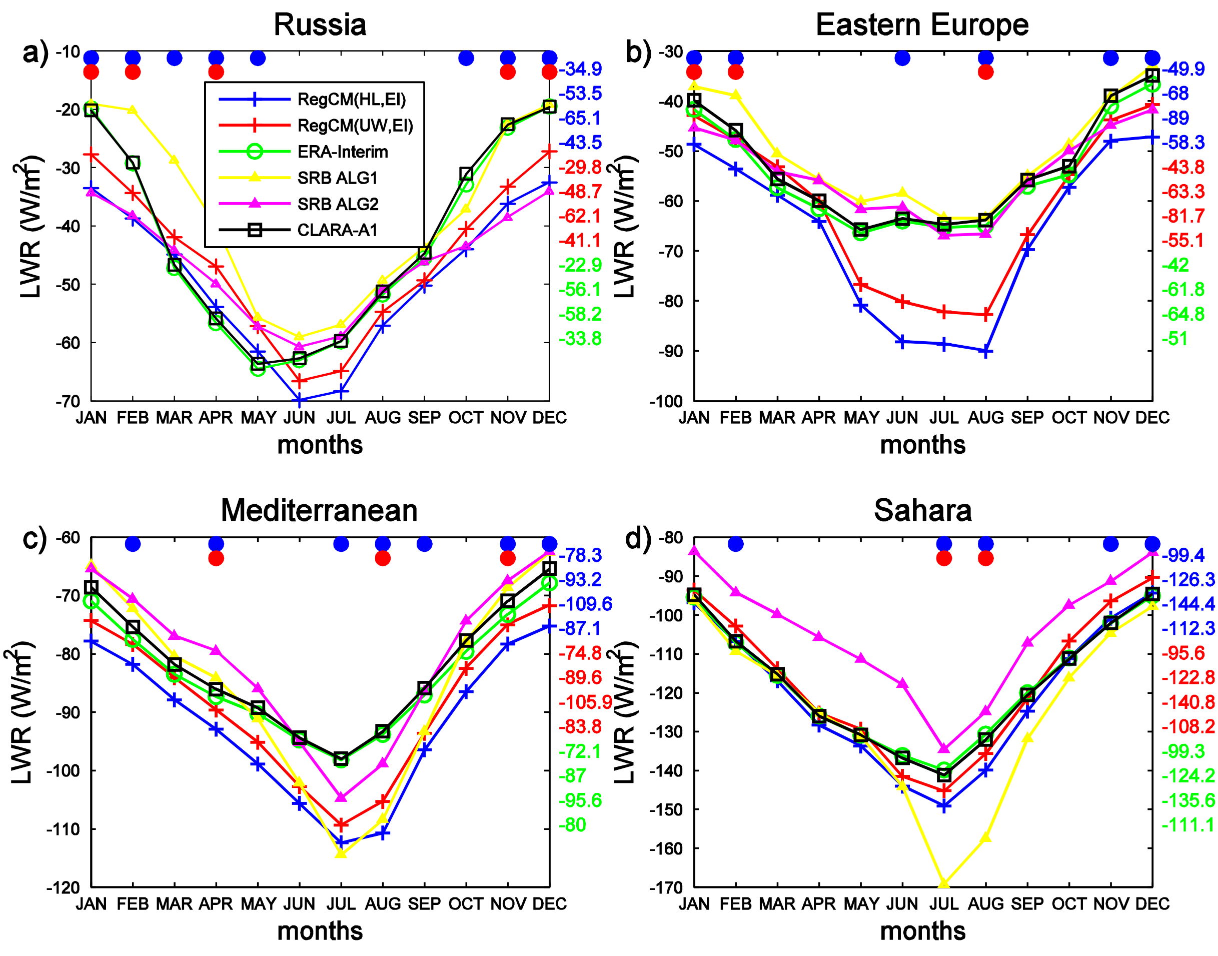


Fig. 3.8 Same as Fig. 3.5 but for the net surface longwave radiation *LWR*. Units are W m$^{-2}$. Additionally, the annual cycles from the CM SAF CLARA-A1 dataset are shown (black squares).

Errors in *LWR* are generally smaller than in *SWR*, but their interpretation and association with individual processes or relevant variables is by no means less demanding. In RegCM simulations, the errors in both total cloud cover and in near-surface temperature (cf. surface temperature in Güttler et al. 2013b) during the warm period could play a role in generating errors in *LWR* with respect to observations and ERA-Interim. Over eastern Europe, for example, both the reduction in *CLD* (Fig. 3.6b) and the increase in *T2m* (Fig. 3.2b) act in the direction that eventually yields an overestimation of *LWR* in RegCM (in the absolute terms; Fig. 3.8b). However, all three variables (*LWR, CLD* and *T2m*) from the RegCM(UW,EI) experiment indicate typically lower systematic errors over eastern Europe when compared to the referent RegCM(HL,EI) experiment. A sharp decrease of nearly 20% in *CLD* from June to July over the Sahara in both RegCM simulations (Fig. 3.6d) does not have the corresponding *LWR* counterpart (Fig. 3.8d); that is, the *LWR* annual cycle follows more closely the annual cycle of the near-surface air temperature *T2m* than that of *CLD* (cf. Güttler et al. 2013b). In the cold period, the variation of *LWR* among different sources is less pronounced than during the warm half of the year.

*3.5 Surface turbulent heat fluxes – SHF and LHF*

The magnitude of sensible heat flux *SHF* depends largely on the temperature difference between the surface and the atmosphere above (cf. (2.15)). The downward direction (positive values) of *SHF* over Russia and eastern Europe during the cold half of the year indicates that the atmosphere is warmer than the underlying surface (Fig. 3.9a,b). During the rest of the year and over other two regions, *SHF* conveys energy upwards, from the surface into the atmosphere. No consistent RegCM response is seen for *SHF*: for example, over eastern Europe and the Mediterranean, *SHF* is larger in RegCM than in ERA-Interim between 20 and 40 W $m^{-2}$ (in absolute values) in the summer, but it is smaller over Russia; over the Sahara, the RegCM simulations coincide with ERA-Interim during many months. Though relatively close, the differences between the two RegCM simulations are statistically significant for several months over the Sahara and over Russia during the winter. Over eastern Europe, on the other hand, the RegCM(UW,EI) summer *SHF* is closer to ERA-Interim than the reference RegCM(HL,EI);

however, it appears that these differences between the two RegCM simulations are not statistically significant.

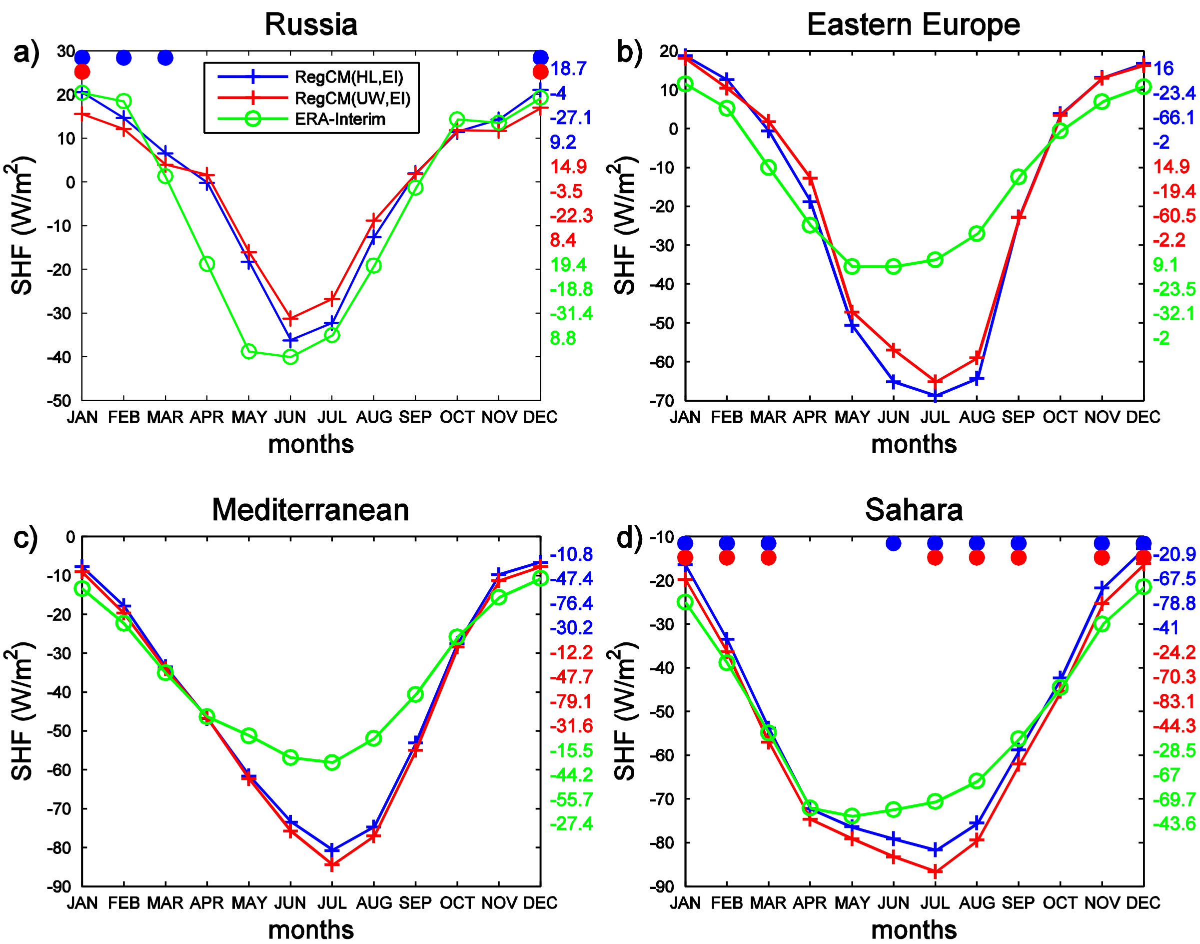


Fig. 3.9 Annual cycle of sensible heat flux *SHF* for RegCM(HL,EI) (blue plus markers), RegCM(UW,EI) (red plus markers) and ERA-Interim (green circles) datasets over selected regions. The period analysed is January 1989 - December 1998. Units are W m$^{-2}$. Blue (red) solid circles at the top of each panel mark the months when the difference between the medians of RegCM(HL,EI) and RegCM(UW,EI) monthly area averages are statistically significant at the 90% (95%) confidence level. The coloured numbers outside the y-axes are the mean seasonal values (DJF, MAM, JJA and SON) corresponding to identically coloured annual cycles (e.g. blue values correspond to the seasonal means of the RegCM(HL,EI)).

The latent heat flux *LHF* annual cycle for ERA-Interim is very pronounced over Russia and eastern Europe, somewhat weaker over the Mediterranean and almost non-existent over Sahara (Fig. 3.10). In terms of amplitude and shape, the RegCM simulations closely follow ERA-Interim over Russia and eastern Europe. The narrow range of *LHF* values over the Sahara, from -

6 W m$^{-2}$ to -2 W m$^{-2}$, indicates an almost identical impact of predominantly dry soil that generates weak upward *LHF* in all three sources considered. In both RegCM simulations the shape of the *LHF* annual cycle over the Mediterranean region strongly differs from that from ERA-Interim, particularly during the warm part of the year (Fig. 3.10c). While in Figures 3.9c and 3.10c RegCM and ERA-Interim *SHF* and *LHF* differ in terms of amplitude (and in terms of shape for *LHF*) of corresponding annual cycles, they are very close when the two turbulent fluxes over land and summed up (not shown). This may imply that the difference in the Bowen ratio (i.e. *SHF*/*LHF*) and soil moisture between RegCM and ERA-Interim may be more crucial over the Mediterranean region then the other regions.

The two RegCM simulations differ in terms of the *LHF* amplitude, but differences are rarely significant. RegCM(UW,EI) has tendency of stronger *LHF* and this is consistent with more precipitation (Figs. 3.3 and 3.4) and soil moisture (not shown) when compared to RegCM(HL,EI).

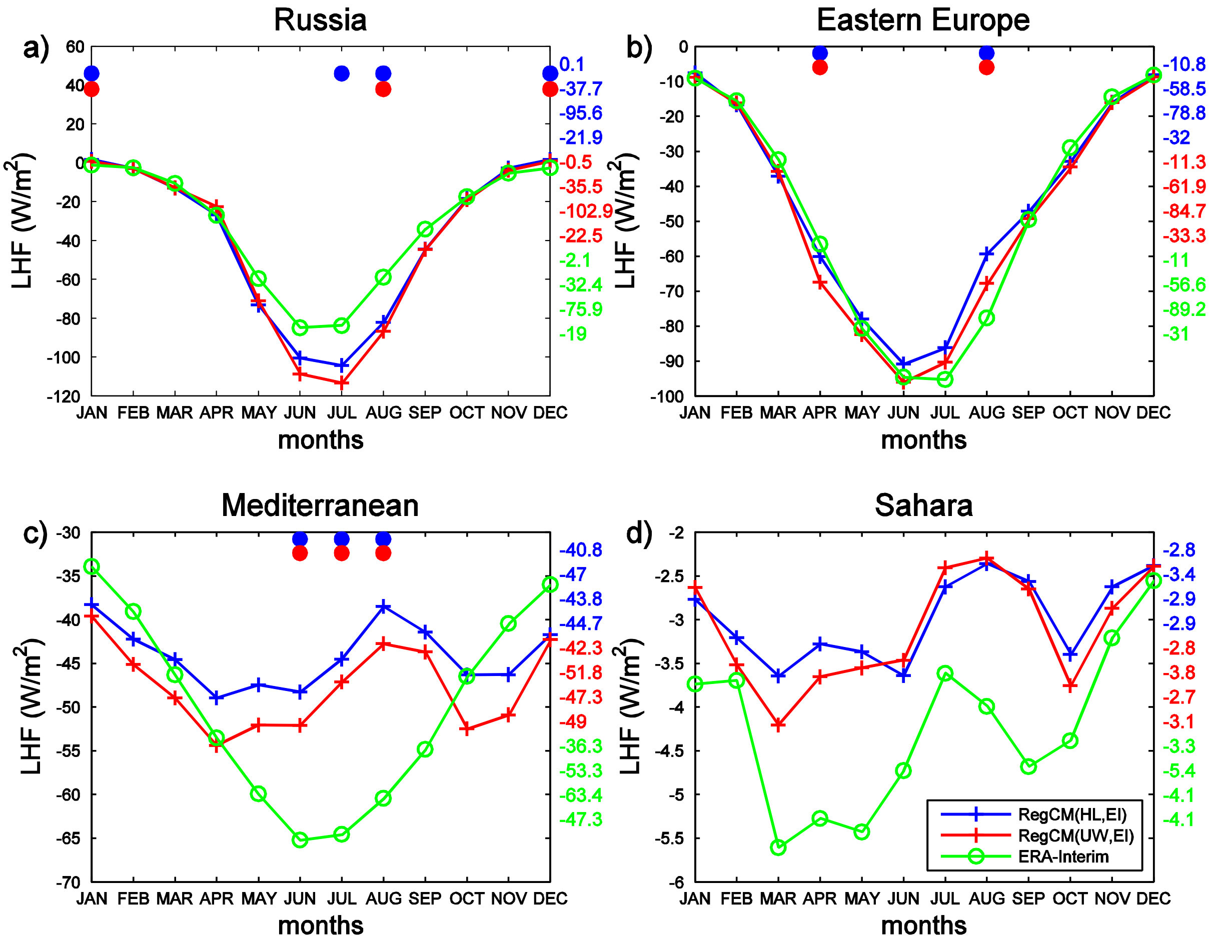


Fig. 3.10 Same as Fig. 3.9 but for latent heat flux *LHF*. Units are W m$^{-2}$.

*3.6 The PDF analysis of surface turbulent heat fluxes*

In this section, the PDF analysis of sensible and latent heat fluxes (*SHF* and *LHF*) for RegCM experiments with both PBL schemes, observations and ERA-Interim is presented. For all data sources, PDFs were based on the 3-hourly time series, thus enabling comparison of a wide range of *SHF* and *LHF* values. The RegCM heat fluxes are first evaluated against observations from the C-SRNWP Programme that were available at various station locations in Europe for the period 2008-2010 (see section 2.4.3 for details). For this purpose, it was necessary to make two additional RegCM experiments with the Holtslag and UW schemes for the same 3-year period, because the years 2008-2010 were not covered by the main set of experiments. This comparison is extended also to heat fluxes from ERA-Interim. For both RegCM and ERA-Interim, the heat fluxes at the grid points nearest to the C-SRNWP stations were estimated and compared with the observations. The Perkins Skill Score (PSS; Perkins et al. 2007) is used to measure how similar are the PDFs from different data sources (cf. subsection 2.4.3 and for more details see Güttler et al. 2013a; their Supplement 2).

The comparison of the RegCM and ERA-Interim heat fluxes against the C-SRNWP data for the 2008-2010 period (a “grid-cell” comparison) can be summarized as follows (Güttler et al. 2013a). For *SHF* in winter, a good agreement among PDFs from all data sources is found at three out of four C-SRNWP locations. However, model simulations and ERA-Interim overestimate the variability of the observed PDF, i.e. their PDF distributions are wider than the observed. In the summer, the observed variability is overestimated as well and the simulated PDFs tend to be shifted towards the higher negative values (i.e. the larger downward heat fluxes associated with stably stratified conditions). When compared against observations (or against ERA-Interim), RegCM(UW,EI) yields overall better results than RegCM(HL,EI) for sensible heat flux *SHF* but not for latent heat flux *LHF*. This may be indicative of a deficient representation of the near-surface humidity in the UW scheme.

From Güttler et al. (2013a) it also follows that qualitatively similar results to those for selected stations are obtained when heat fluxes from the RegCM model are compared with those from ERA-Interim over the four regions considered in this study (Russia, eastern Europe, the Sahara and the Mediterranean; as an example of the actual PDFs, see Fig. A1 for the winter *SHF* PDFs over selected four regions). In other words, in spite of some perceived deficiencies ERA-

Interim may be considered representative and can be used to evaluate RegCM simulations in the period 1989-1998. For *SHF*, the PDFs from the RegCM(UW,EI) agree better than RegCM(HL,EI) with PDFs from ERA-Interim in 12 out of 16 combinations (with one neutral), i.e. the second bar in Fig. 3.11, is taller than the first bar in 12 cases; this is confirmed by the positive values at the top of each panel. The largest improvement by the UW scheme in terms of PSS is seen over the Sahara and the Mediterranean in DJF and MAM, followed by eastern Europe in DJF and JJA. Only over Russia the UW scheme brings no improvement in terms of PSS.

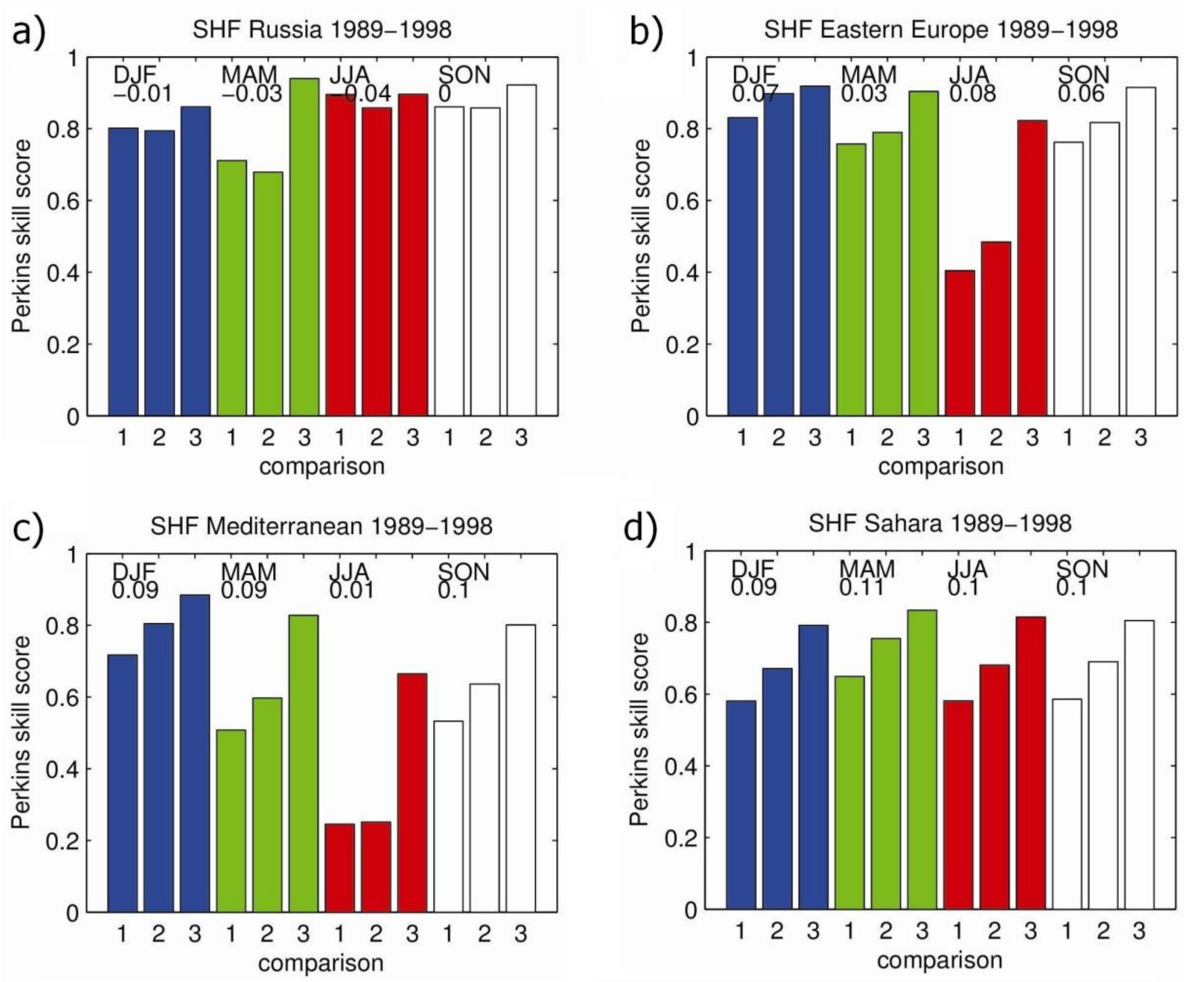


Fig. 3.11 Perkins skill scores (PSSs) for PDFs of sensible heat flux *SHF* over selected regions Period: 1989-1998. The three coloured bars in each season indicate the comparisons for: 1) RegCM(HL,EI) vs. ERA-Interim, 2) RegCM(UW,EI) vs. ERA-Interim and 3) RegCM(UW,EI) vs. RegCM(HL,EI). The numbers bellow DJF, MAM, JJA and SON are the differences between comparisons 1 and 2. In each panel, PDFs of the flux during summer JJA are

additionally shown: RegCM(HL,EI) green lines, RegCM(UW,EI) red lines, ERA-Interim black lines. The areas are: a) Russia, b) Eastern Europe, c) the Mediterranean and d) the Sahara (see Güttler et al. 2013a for more details).

In terms of PSS, for *LHF* (Fig. 3.12), RegCM(UW,EI) is more successful than RegCM(HL,EI) (10 vs. 5 cases, 1 neutral); however, this advantage is less pronounced when compared with the results for *SHF*. The improvements with RegCM(UW,EI) are seen over eastern Europe and the Mediterranean in all seasons except DJF. For the other two regions, the comparison of the model PDFs with ERA-Interim indicates that in the case of *LHF* neither scheme is superior.

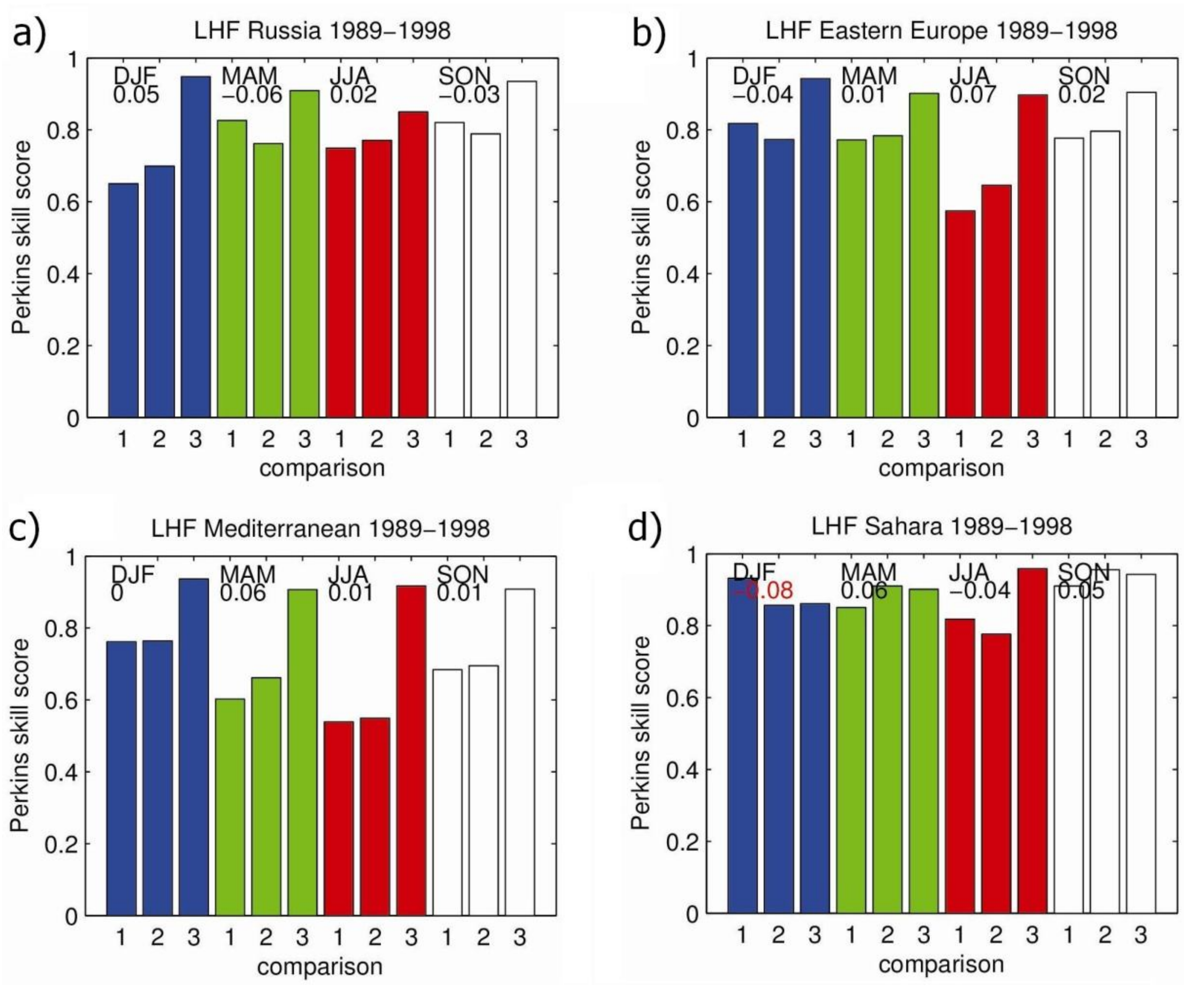


Fig. 3.12 Same as Fig. 3.11 but for latent heat flux *LHF*.

The results of this analysis could be viewed in the following perspective. The improvement in the RegCM(UW,EI) heat fluxes over eastern Europe during summer (Fig. 3.9b and Fig. 3.11b) is consistent with the reduction of the *T2m* warm bias over the same region (Fig. 3.1d and Fig. 3.2b). On the other hand, over Russia, the reduction of the winter *T2m* warm bias (Fig. 3.1b and Fig. 3.2a) is not reflected as an improvement in the RegCM(UW,EI) sensible heat flux (Fig. 3.9a and Fig. 3.11a). Conversely, the improvement in the RegCM(UW,EI) *SHF* over the Sahara in summer (Fig. 3.11d) coincides with the worsening of the *T2m* errors (Fig. 3.1d and Fig. 3.2d) and with the increased *SHF* errors in the RegCM(UW,EI) annual cycle (Fig. 3.9d). These latter results suggest that the PBL parameters other than heat fluxes, but not considered here, may contribute to the reduction of *T2m* in the UW scheme and that the impact of the PBL scheme can have contrasting effects on different quantities (e.g. improvement in *T2m* vs. deterioration in *SHF*). Although this analysis indicates that RegCM(UW,EI) is by no means superior to RegCM(HL,EI) in all regions, the basic "statistics" of the Perkins skill scores indicates that the use of UW scheme in the RegCM model can be beneficial and brings an improvement in the representation of that part of PBL physics which is related to the surface turbulent heat fluxes.

### *3.7 Surface energy budget residual*

According to (2.17), the residual of surface energy budget corresponds to the sum of ground heat flux *GHF* and snowmelt heat flux *SMF*. Since *GHF* and *SMF* were not available from the data sources considered, the residual discussed here reflects the effect of both components taken together. Over Russia, the residual is strongest in April and May (Fig. 3.13a) and is related to local snowmelt (Güttler et al. 2013b). It decreases gradually towards summer and early autumn; in RegCM, the residual is close to 0 W $m^{-2}$ in July and about two months later in ERA-Interim. Thus, the main contributor to the residual is the spring *SMF*, but its role diminishes later in the year and *GHF* becomes more important (e.g. Tsuang 2005).

At the end of the year, when snow starts to accumulate at the surface, the decrease of residual can be explained by decreasing *GHF* due to the freezing ground in addition to snow that is not melting (Güttler et al. 2013b). Similar arguments may be applied to eastern Europe, the difference mainly being an earlier start of snowmelt (March) and the lower amounts of the residual and snow than over Russia (Fig. 3.13a,b). Over the Sahara region, snow melt from the

Atlas Mountains and subsequently available soil moisture are negligible and most of the budget residual could be attributed to *GHF* (Fig. 3.13d).

Although various components of the surface energy budget in RegCM can substantially diverge from the ERA-Interim estimates (and observation-based products), relatively small differences in the residual annual cycles over selected regions imply it is the partitioning into the surface energy components at the surface that needs further evaluation in RegCM.

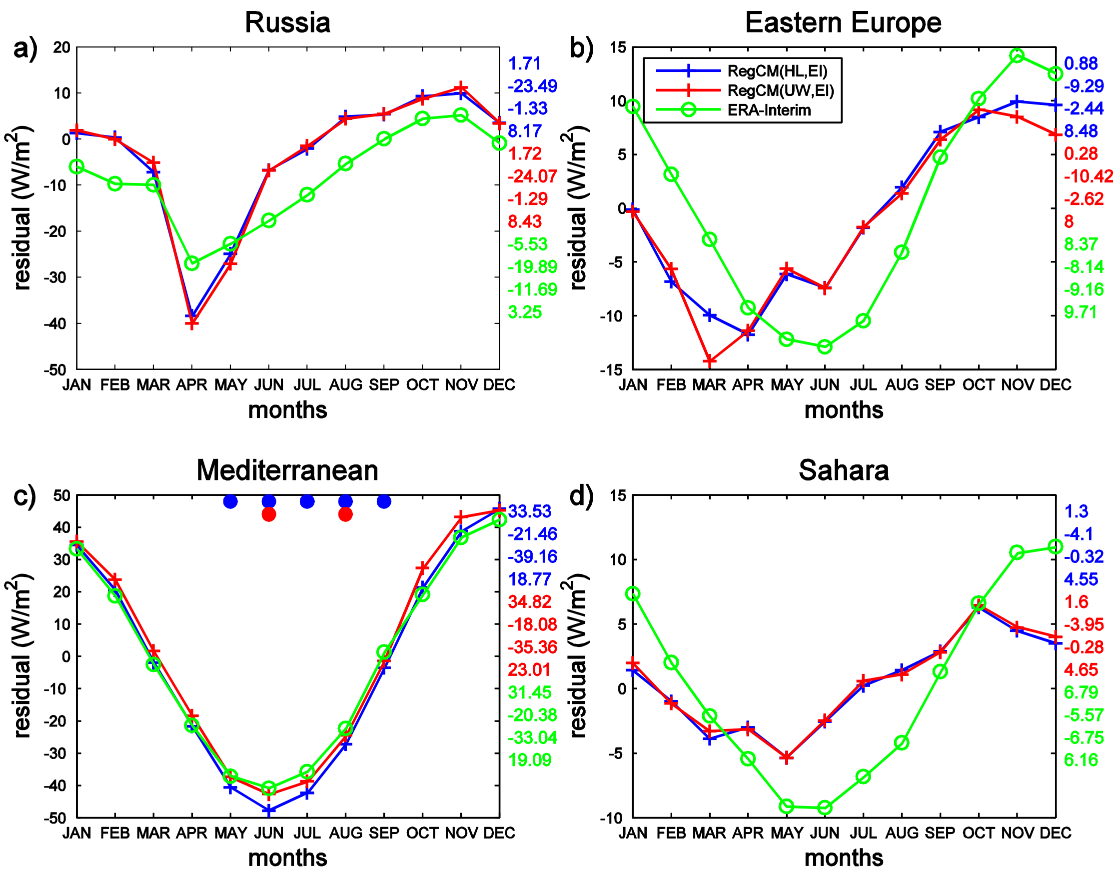


Fig. 3.13 Same as Fig. 3.9 but for the surface energy budget residual. Units are W m$^{-2}$.

# 4. THE IMPACT OF PBL PARAMETERISATIONS ON SYSTEMATIC ERRORS

In the previous chapter, model systematic errors in *T2m* and precipitation, derived from a 10-year period, in experiments with the two PBL schemes were compared. It was shown that the *T2m* climatology of the RegCM(UW,EI) experiment differ from that derived for the RegCM(HL,EI) experiment. In the following, vertical profiles of air temperature and water vapour mixing ratio (both being prognostic variables in RegCM and closely related to the near-surface temperature and precipitation) over four selected regions are compared. Next, the eddy heat diffusivity and tendencies in temperature and water vapour mixing ratio due to different PBL schemes are analyzed and possible mechanisms that could be responsible for detected differences are suggested. Finally, the sensitivity of *T2m*, near-surface specific humidity *q2m*, and eddy heat diffusivity $K_H$ to perturbations of three different parameters (Table 1) in the UW scheme is explored in an ensemble of the 3-year long RegCM simulations. Work presented in this chapter is based on Güttler et al. (2013a).

## *4.1 Vertical profiles*

The following analysis can be viewed as a comparison between non-local and local PBL schemes in the full model framework. In a sense, it follows the approach by Bretherton and Park (2009) who compared non-local and local PBL schemes but in a controlled 1-D framework. In their study three types of PBLs are simulated and compared against large eddy simulations and observations: (1) dry convective boundary layer; (2) stably stratified boundary layer, and (3) nocturnal stratocumulus-topped boundary layer. In (1) both non-local and local schemes performed equally well in general; in (2) the local scheme was modified by reducing the free-troposphere mixing length and thus made comparable to the non-local scheme; in (3) the non-local scheme (similar to the UW scheme used here) performed much better because of the inclusion of entrainment effects at the top of the cloud-topped PBL.

*4.1.1 Air temperature and water vapour mixing ratio*

The mean winter and summer vertical profiles of the air temperature *T* in RegCM with the Holtslag scheme (RegCM(HL,EI)) over selected regions are presented in Fig. 4.1a,b, and the impact of the UW scheme is shown in terms of the differences between RegCM(UW,EI) and RegCM(HL,EI) (Fig. 4.1c,d). Fig. 4.1a,b clearly indicates the impact of the regional geophysical properties on temperature profiles: Russia is the coldest and the Sahara the warmest region in both seasons throughout the atmospheric column considered. The differences between the two PBL schemes (Fig. 4.1c,d) are in general larger during JJA, when RegCM(UW,EI) exhibits cooling between 1 °C and 2 °C, than during DJF. In the winter, a dominant cooling between 0 °C and 1 °C (over Russia up to 2 °C) is mostly confined to the model low levels (cf. Park and Bretherton 2009). Weak differences of the opposite sign are found at the lower tropospheric levels, but at the stratospheric levels they reach up to 2 °C over eastern Europe (cf. Güttler et al. 2013a). Fig. 4.1c,d indicates a substantial sensitivity of the model air temperature and temperature profiles to the choice of PBL scheme at atmospheric layers where turbulent mixing is important. For example, during summer, when turbulent mixing induced by solar heating of the surface is strongly active in the lowest model layers, a prominent cooling with the UW scheme takes place in all regions except Russia (Fig. 4.1d). This is indicative of reduced turbulent mixing in RegCM integration with the UW scheme (see section 4.1.2 below). In contrast, during DJF, the strongest cooling is found over the Russian region at the lowest levels, again indicating that reduced eddy diffusivity, as the main characteristics of the UW scheme, contributes to further cooling of the PBL during winter. As seen in the previous chapter, the cooling with the UW scheme is consistent with the improvements in the *T2m* climatology when compared against CRU and E-OBS data over this region.

For water vapour mixing ratio *qv*, Fig. 4.2 shows that in winter, Russia is much drier than the Sahara (however, cloud water mixing ratio is higher over Russia; not shown), but in summer (Fig. 4.2b) there is a little difference among the regions except the Sahara. The mean summer differences between RegCM(UW,EI) and RegCM(HL,EI) indicate an increase of *qv* at the model lowest levels and a decrease around $\sigma$=0.7 (Fig. 4.2d). During DJF, the *qv* profiles show an increase when the UW scheme is used over the three regions except Russia. Fig. 4 demonstrates that model sensitivity to the PBL scheme is again most expressed during JJA with the largest increase of *qv* at the lowest model levels of up to 0.6 g kg$^{-1}$ over the Mediterranean and a decrease of up to 0.4 g kg$^{-1}$ in the mid-tropospheric layers over eastern Europe and the Sahara. The moistening of the lower atmosphere over Russia, eastern Europe and the Mediterranean (Fig. 4.2c,d) is consistent with the increased precipitation amounts when the UW scheme is employed in RegCM (Fig. 3.3b,d and Fig. 3.4a,b,c).

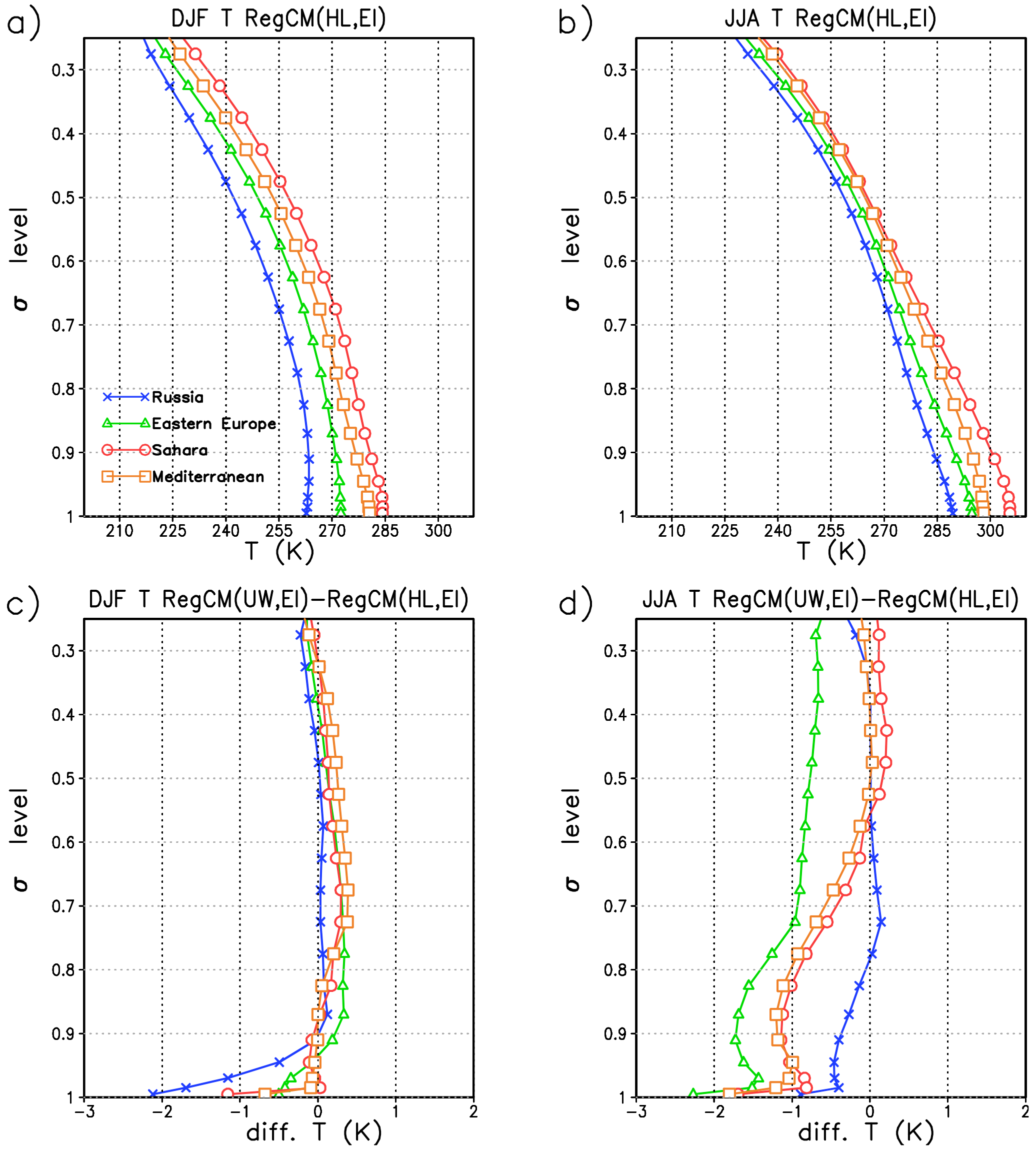


Fig. 4.1 Vertical profiles of the regional- and seasonal-mean air temperature *T* in RegCM(HL,EI) (RegCM with the Holtslag PBL scheme; top) and the difference between RegCM(UW,EI) (RegCM with the UW scheme) and RegCM(HL,EI) (bottom). Winter profiles are on the left, summer profiles are on the right. The period analysed is 1989–1998 and selected regions are shown in Fig. 2.1. Profiles over Russia are marked by crosses, over eastern Europe by triangles, over the Sahara by circles and over the Mediterranean by squares. Units are K. See Güttler et al. (2013a) for details.

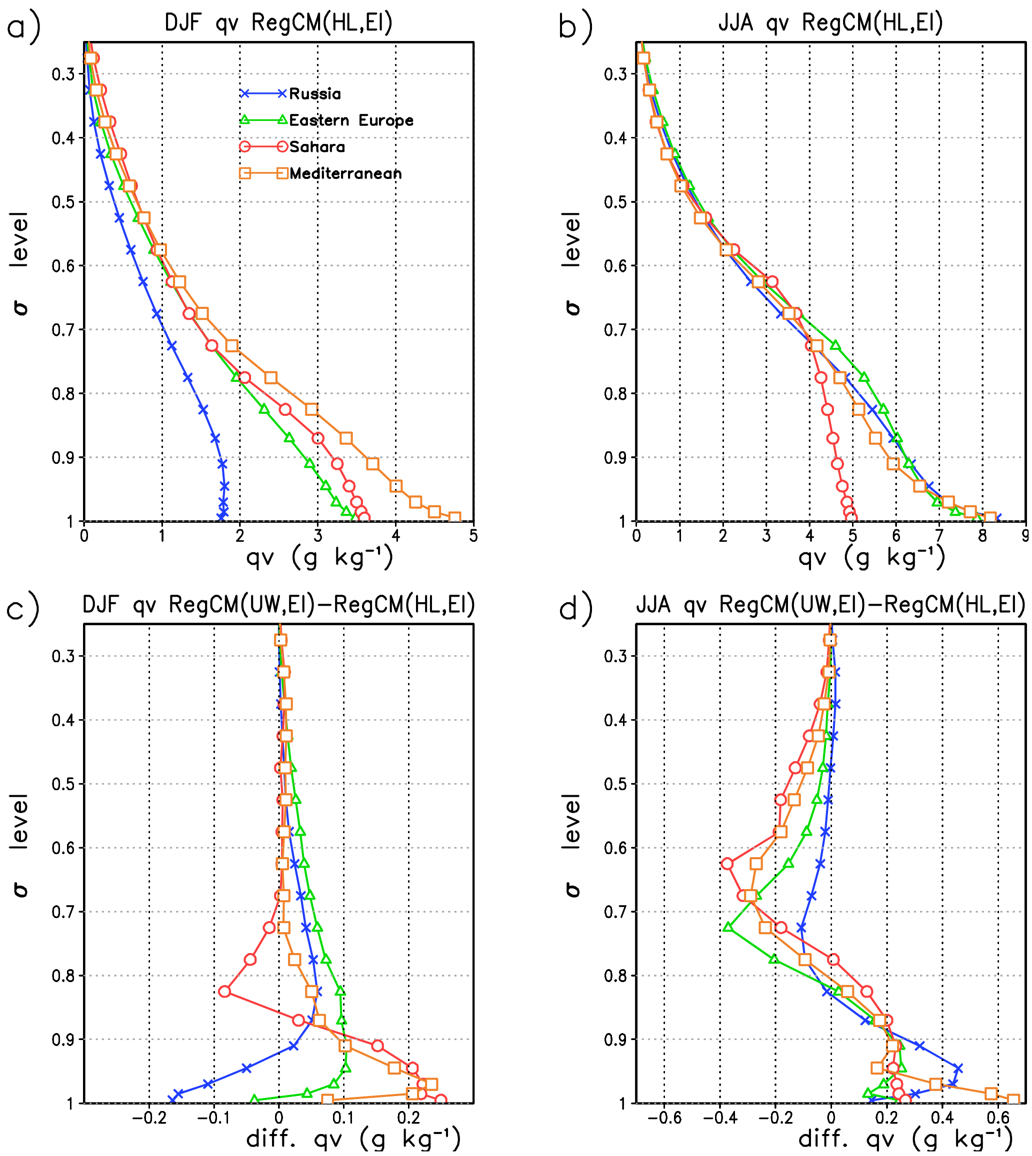


Fig. 4.2 Same as Fig. 4.1 but for water vapour mixing ratio *qv*. Units are g kg$^{-1}$. See Güttler et al. (2013a) for details.

The differences between the two schemes are also seen in the cloud-related variables: cloud water mixing ratio and cloud cover fraction. While the differences in the cloud water mixing ratio are highly variable in space (i.e. over different regions) and seasons (not shown), the cloud cover fraction in RegCM(UW,EI) is consistently increased relative to RegCM(HL,EI) in almost all vertical layers in all four regions and in both seasons (Fig. 4.3c,d) (cf. Park and Bretherton 2009). The resulting lower temperatures in the UW experiment thus indicates that, in the experiment with the Holtslag scheme, the total cloud cover *CLD* is underestimated and the net surface shortwave radiation *SWR* is overestimated yielding too high temperatures in RegCM(HL,EI), as seen in Chapter 3 (cf. Güttler et al. 2013b).

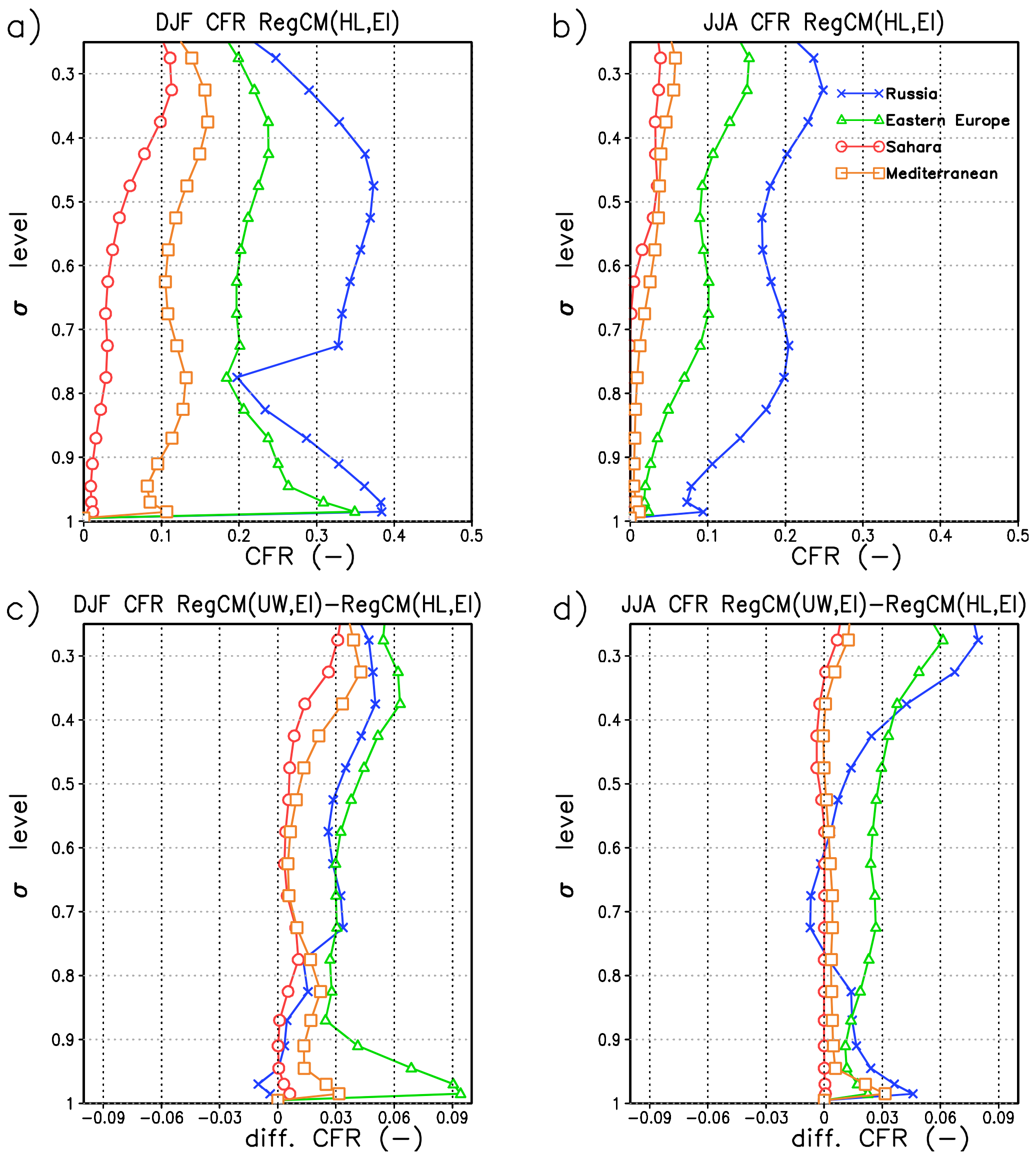


Fig. 4.3 Same as Fig. 4.1 but for the cloud cover fraction *CFR* (from 0 to 1).

We note in passing that the current implementation of the Holtslag scheme in RegCM does not include the contribution of the counter-gradient term to the calculation of tendencies in prognostic equation for water vapour mixing ratio (as it does for temperature; Giorgi et al. 1993). This is a variation from the original Holtslag et al. (1990) formulation and was implemented in RegCM by Giorgi et al. (2012) in order to reduce too dry conditions in the lower atmosphere.

This modification in the Holtslag scheme simplifies its comparison with the UW scheme since, by design, in the UW scheme no counter-gradient term is included.

### *4.1.2 Eddy heat diffusivity*

Vertical profiles of eddy heat diffusivity $K_H$ (see (2.3), (2.4) and (2.5)) in the default experiment RegCM(HL,EI) show the maximum in the lower atmosphere (between the surface and $\sigma$=0.9) with the mean JJA magnitude of up to 160 $m^2\ s^{-1}$ over the Sahara region, and between 40 $m^2\ s^{-1}$ and 90 $m^2\ s^{-1}$ in other regions (Fig. 4.4b). Giorgi et al. (1993) documented even higher values of $K_H$, but these included monthly means for specific hourly profiles (e.g. monthly means of all vertical profiles at 12 UTC; see also Grenier and Bretherton 2001; Bretherton and Park 2009). The winter $K_H$ maxima in Fig. 4.4a do not exceed 30 $m^2\ s^{-1}$ and are decreasing from the south to the north. The DJF eddy heat diffusivity profiles over the Mediterranean region are similar to the profiles over the Sahara (Fig. 4.4a,c) and in JJA to the profiles over the eastern Europe (Fig. 4.4b,d). For the winter, this may partially reflect the impact of sea surface temperature (SST) on turbulent mixing over the nearby coastal land areas because in the Mediterranean region land points are intermingled with sea points: comparatively high SST during DJF is associated with more instability, thus possibly influencing the surrounding land. In the summer, the sea is cooler than surrounding land and the eddy heat diffusivity is much lower than over hot Sahara region.

Similar to air temperature and water vapour mixing ratio, shown in Figs. 4.1 and 4.2 respectively, the differences in $K_H$ between the experiments with the two PBL schemes are mainly in the lower atmosphere with the JJA differences being larger than those during DJF (Fig. 4.4c,d). The UW scheme is less diffusive (i.e. the differences are predominantly negative) indicating a reduced vertical turbulent mixing than in the Holtslag scheme, with the differences of up to 60 $m^2\ s^{-1}$ over the Sahara in JJA and between 20 $m^2\ s^{-1}$ and 40 $m^2\ s^{-1}$ over other regions. This is consistent with the result of Cuxart et al. (2006) who found, for a moderately stably stratified PBL, a general reduction of turbulent mixing in prognostic schemes when compared to diagnostic schemes. Additionally, a secondary layer with a slightly increased eddy turbulent diffusivity in RegCM(UW,EI) is seen near $\sigma$=0.3 (~330 hPa), pronounced in the winter. These increased values of $K_H$ at high altitudes (Fig. 4.4c) can be associated with the shear-induced mixing in the UW scheme near the jet stream regions. A double-peak structure in the summer $K_H$ differences, seen between $\sigma$=1.0 and $\sigma$=0.9 in Fig. 4.4d over eastern Europe and the Sahara (and less obvious over Russia and the Mediterranean) is the consequence of a slight lowering of the $K_H$ maximum in the UW scheme and a sharper increase of the $K_H$ from the surface upwards.

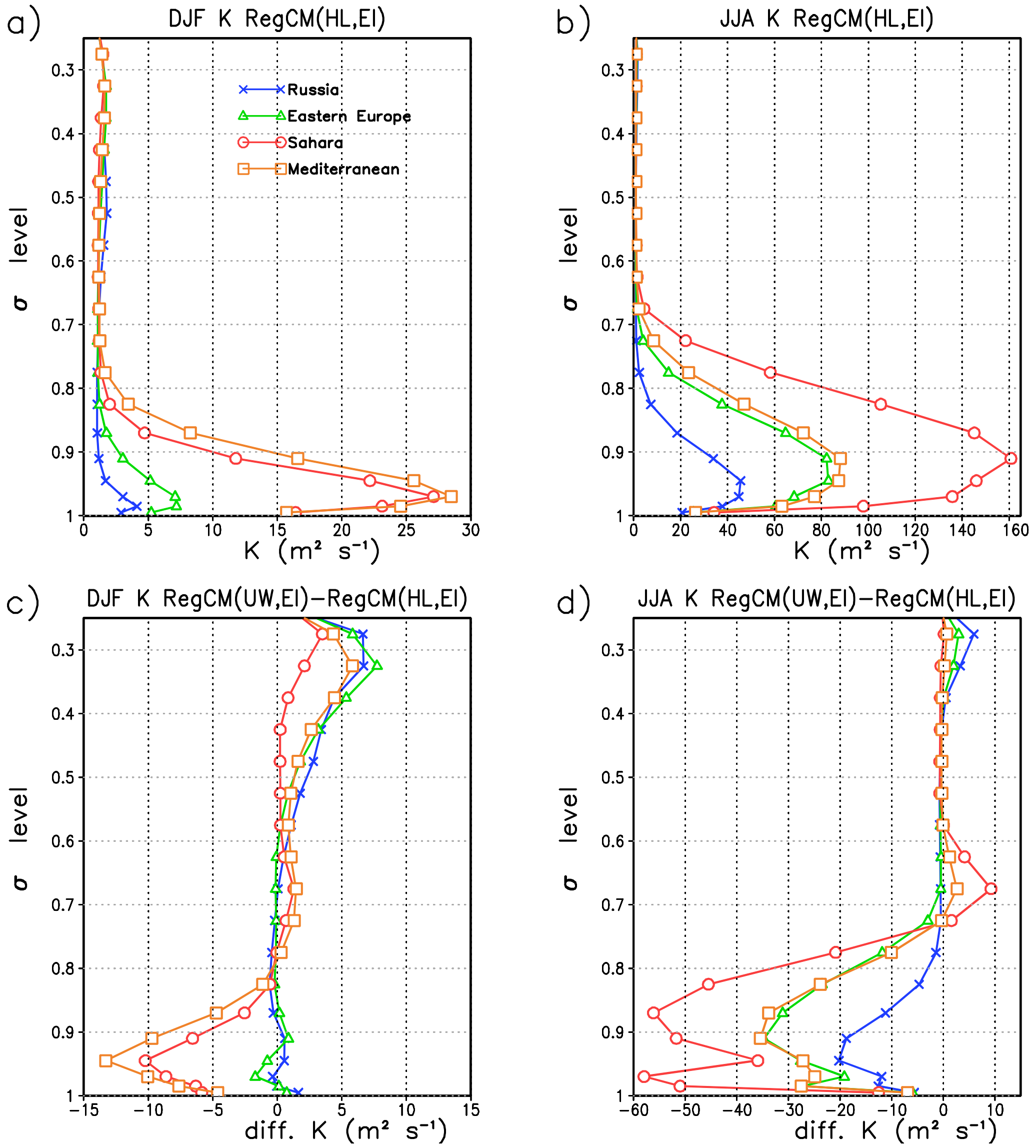


Fig. 4.4 Same as Fig. 4.1 but for the eddy heat diffusivity $K_H$. Units are m$^2$ s$^{-1}$ (cf. Güttler et al., 2013a).

By ignoring the counter-gradient term and rewriting it in a simplified form, i.e. only in terms of air temperature $T$, (2.1) can be converted into

$$\frac{\partial T}{\partial t} = \frac{\partial}{\partial z}\left(K_H \frac{\partial T}{\partial z}\right) = K_H \frac{\partial^2 T}{\partial z^2} + \frac{\partial K_H}{\partial z}\frac{\partial T}{\partial z}. \tag{4.1}$$

From (4.1) it is clear that both the magnitude of $K_H$ (always positive or near zero; Fig. 4.4a,b) and the slope $\partial K_H/\partial z$ (positive below the maximum and negative above at model levels below $\sigma$=0.9), in interaction with the curvature ($\partial^2 T/\partial z^2$) and the slope ($\partial T/\partial z$) of the air temperature vertical profiles respectively, govern the sign and the magnitude of the temperature tendencies from the PBL scheme. The magnitude and slope of the $K_H$ profile in the UW scheme is generally reduced relative to that of the Holtslag scheme: (cf. Fig. 4.4c,d). A simplification similar to (4.1) and the corresponding discussion of vertical profiles also holds for the water vapour mixing ratio. The ultimate impact to the vertical profile of any prognostic variable depends on additional interactions between the PBL scheme and all other model components, so different signs of temperature tendency and different signs of the $T$ and $qv$ differences between RegCM(HL,EI) and RegCM(UW,EI) are also possible.

### *4.1.3 Temperature and water vapour tendencies*

General structure of the RegCM vertical profiles of the total temperature tendency from the Holtslag PBL scheme, shown in Fig. 4.5a,b (where temperature tendencies are split into total and counter-gradient terms), is comparable to that in Giorgi et al. (1993; their Fig. 6a), though the different temporal and spatial scales are analyzed here. It is governed by the eddy heat diffusivity profile: temperature tendency is the highest at lower levels where $K_H$ slope is substantial (cf. Fig. 4.4a,b in conjunction with the last term $\partial K_H/\partial z\ \partial T/\partial z$ in (4.1)). At levels with the maximum $K_H$, where the contribution of the $K_H$ slope is negligible ($\partial K_H/\partial z \approx 0$), temperature tendency is still positive, implying that the air temperature curvature contribution (i.e. $K_H \partial^2 T/\partial z^2$; (4.1)) is positive and dominant. Vertical mixing within PBL transfers heat from the surface upwards (cf. Fig. 3.9) thus contributing to the warming of the lower atmosphere, corresponding to a universally positive temperature tendency in Fig. 4.5a,b. The magnitude of the (positive) temperature tendency in Fig. 4.5a,b decreases with height and becomes negligible around $\sigma$=0.7 (~700 hPa). The total PBL temperature tendencies over Russia, eastern Europe and the Mediterranean during the winter are weaker than in summer due to a weaker insolation. However, over the Sahara, where solar heating generates and supports turbulent mixing essentially throughout the year, the winter and summer PBL temperature tendencies are of comparable magnitude.

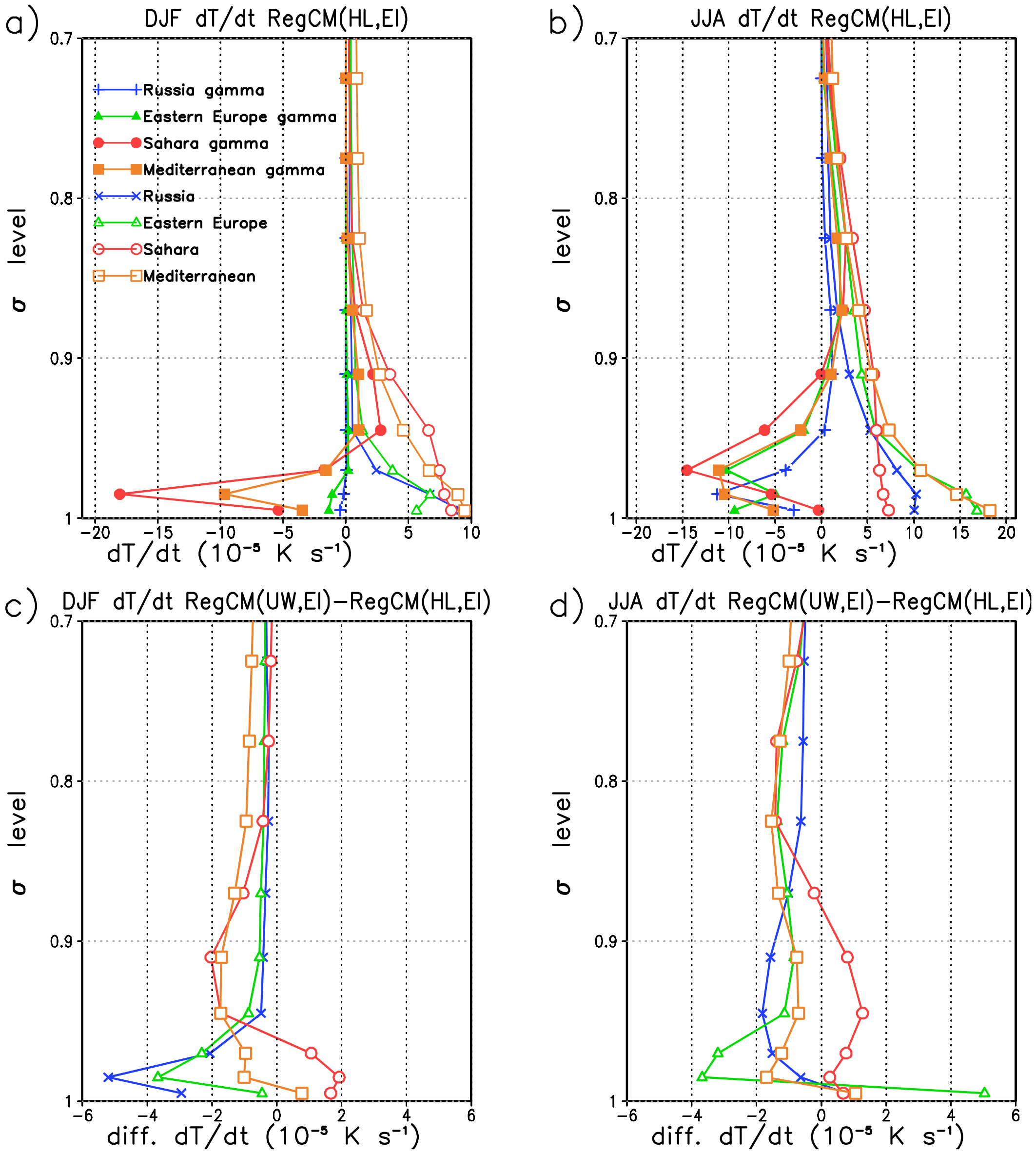


Fig. 4.5 Same as Fig. 4.1 but for the air temperature tendency due to the PBL scheme and in the lower troposphere, $\sigma$ = [1.0, 0.7]. Units are $10^{-5}$ K $s^{-1}$. Additionally, the air temperature tendency in the Holtslag scheme due to counter-gradient contribution (Eq. 1) is shown in the top row (the × marker for Russia and solid markers for other regions). See Güttler et al. (2013a) for details.

The contribution of the counter-gradient term (shown in Fig. 4.5a,b by solid markers and the + marker) to the total PBL tendency is important in all regions during JJA, but also during DJF over the Mediterranean and Sahara. The counter-gradient flux tends to reduce temperature tendency in the lower PBL and slightly warms the atmosphere around $\sigma$=0.8 (~800 hPa). It is associated with the parameterised deep eddies which originate in the lower parts of the convective PBL and transfer heat to the upper (sometimes slightly stably stratified) layers (Holtslag et al. 1990; Holtslag and Moeng 1991). According to Fig. 4.5, this process is simulated over all four regions in JJA and also over the arid northern Africa and Mediterranean region during DJF.

In both seasons and in most regions, the temperature tendency in the RegCM model with the UW scheme is reduced at many model levels in the lower atmosphere (Fig. 4.5c,d). This reduction is e.g. up to $6\times10^{-5}$ K $s^{-1}$ over Russia during DJF on the second model level relative to the same tendency in RegCM with the Holtslag scheme(this equals to almost 80% reduction for this specific case). The differences between the UW and Holtslag PBL temperature tendencies reflect the changes in the eddy heat diffusivity profiles. For example, the reduced values of eddy heat diffusivity $K_H$ in RegCM(UW,EI) are associated with the reduction of the slope in the $K_H$ vertical profile when compared to the default RegCM(HL,EI) experiment (cf. (2.1) and (4.1)).

The (negative) sign of the PBL-generated temperature tendency differences is generally consistent with the cooling of PBL in the UW scheme seen in Fig. 4.1. However, the opposite to this cooling response is found at the first model level during JJA in all regions as well as at the next few levels over the Sahara during both JJA and DJF. Here, the UW scheme produces a higher temperature tendency than the Holtslag making the differences in Fig. 4.5c,d positive. This is very likely a consequence of the inclusion of the counter-gradient flux in the Holtslag scheme which reduces the total temperature tendency, over the Mediterranean and Sahara regions (Fig. 4.5a,b, solid markers and the + marker).

The PBL-generated water vapour mixing-ratio tendencies in RegCM with the Holtslag scheme are positive in the bottom half of the atmospheric column in all four regions and in both seasons (Fig. A2; see Güttler et al. 2013a for more details). Vertical structure and the order of magnitude of the water vapour mixing-ratio tendencies are comparable to those from Giorgi et al. (1993). Differences between RegCM(UW,EI) and RegCM(HL,EI) include a major increase in the *qv* tendencies in almost entire vertical column in RegCM(UW,EI), with largest differences during DJF and over Russia and eastern Europe. This increase is often up to the two orders of magnitude larger than that in the original RegCM(HL,EI) profiles (cf. Güttler et al. 2013a; their Fig. 8a,b). The increase in the lower-atmospheric layers is consistent with the positive *qv* differences in the lower PBL, but other indirect processes may have also contributed to the final *qv* profile; for example, the *qv* vertical profile includes drying of PBL around $\sigma$=0.7 (Fig. 4.2c,d). Further research is needed to investigate possible contributions of other parameterisations and/or resolved processes to temperature and water vapour mixing ratio tendencies (e.g. van de Berg et al. 2007). Nevertheless, using the UW scheme, RegCM simulations are more in line with the ERA-Interim reanalysis in terms of water vapour mixing ratio, relative humidity and temperature vertical profiles (Fig. A3; see Güttler et al. 2013a for more details).

*4.2 Perturbed physics ensemble of the UW simulations*

In this section, the RegCM(UW,EI) response in several near-surface variables is considered and compared with the default experiment RegCM(HL,EI) when three parameters (master turbulent length scale *l*, efficiency of evaporative enhancement of cloud-top entrainment $a_2$ and scaling parameter in stable boundary layer turbulent length scale $R_{STBL}$) in the UW scheme are varied according to the definitions in Table 1. For the purpose of this section the experiment RegCM(HL,EI) is denoted as EXP001 and the RegCM(UW,EI) experiments with perturbed parameters are denoted as EXP002 through EXP019, EXP002 being the default RegCM(UW,EI). For all experiments, the comparison is now based on the 3-year (1989-1991) averages.

In comparison with EXP001, the *T2m* response in RegCM with the UW PBL scheme to the perturbations of the chosen parameters is almost unique: temperature is decreased in almost all experiments EXP002 through EXP019 over all regions and in both DJF and JJA. Here, in Fig. 4.6a the results are presented for Russia (i.e. only region where grouping as a function of $R_{STBL}$ was detected; see Güttler et al. (2013a; their Fig. 9) for other regions). The amplitude of cooling reaches 3 °C over Russia during DJF (Fig. 4.6a), but also over eastern Europe during JJA. This cooling is consistent with the sign of the air temperature vertical profiles depicted in Fig. 4.1c,d. A negligible warming over Russia in Fig. 4.6a is detected during JJA in only one perturbed experiment. The negative differences in Fig. 4.6a indicate an improvement in RegCM with the UW scheme because the *T2m* bias seen in RegCM(HL,EI) is reduced (see Fig. 3.2a for biases in the default experiments over Russia). This improvement is larger in DJF than in JJA suggesting an improved simulation of stably stratified PBLs over Russia in the winter period when the UW scheme is used in RegCM.

The only systematic grouping of experiments in Fig. 4.6a, associated with different perturbed parameters is seen during winter when the experiments with $R_{STBL}$=1.00 (blue crosses in EXP003, 6, 9, 12, 15, 18) tend to be cooler than the other experiments, sometimes twice as much for the same efficiency $a_2$. These are the experiments where $R_{STBL}$ is reduced relative to other perturbed experiments (cf. Table 1) and associated with the reduction of the master turbulent mixing length (cf. (2.8)). Thus, in stably stratified conditions the reduced $R_{STBL}$ can induce less vertical mixing of the cool surface air and the warmer air above (cf. Fig. 4.1a) resulting as additional cooling in experiments with $R_{STBL}$=1.00. Furthermore, an inspection of vertical profiles reveals a dominant tropospheric cooling with the amplitude of up to 3 °C in all members of the UW ensemble (not shown). This is comparable to the results of the 10-year UW experiment in Fig. 4.1.

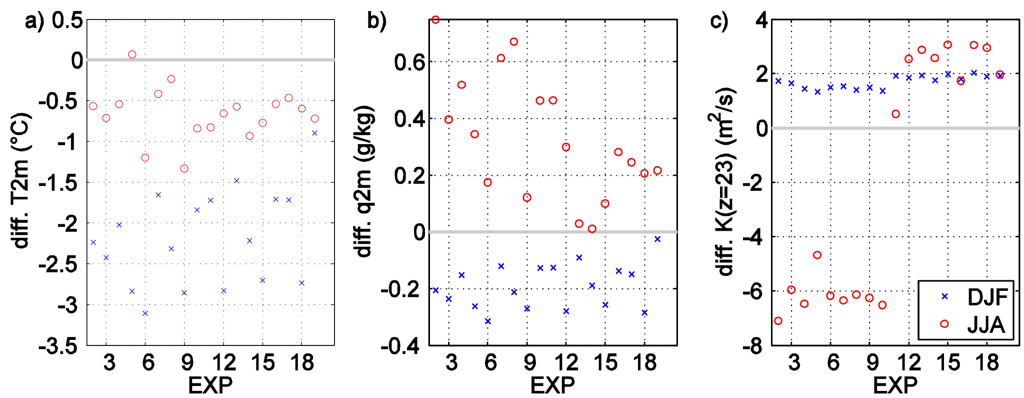


Fig. 4.6 Differences in an ensemble of UW PBL simulations relative to RegCM(HL,EI) over Russia for a) near-surface temperature *T2m* (units °C), b) near-surface specific humidity *q2m* (units g/kg) and c) eddy heat diffusivity at the lowest model level (units $m^2$/s) during DJF (blue crosses) and JJA (red circles). The period analysed is 1989-1991.

For the near-surface specific humidity *q2m*, the model response is more complex than for *T2m*. Here again the values over Russia are only presented (Fig. 4.6b), but see Güttler et al. (2013a; their Fig. 10) for other regions. In JJA, a large majority of the differences in the UW experiments indicate an increase of *q2m* in all regions, consistent with the increased precipitation in RegCM with the UW scheme (Fig. 3.3d). This is also in agreement with an increase in water vapour mixing ratio *qv* over all regions during JJA and over the dry Sahara and Mediterranean regions during DJF (Fig. 4.2c,d). In the winter, on the other hand, a general reduction of *q2m* in the UW experiments is seen over Russia with the magnitude of up to 0.3 g $kg^{-1}$ (Fig. 4.6b), but such a reduction is also present over eastern Europe (cf. Güttler et al. 2013a). From Fig. 4.6b, it can be deduced that in winter over Russia the experiments with $R_{STBL}$=1.00 tend to be drier than the other experiments. This again can be associated with the decrease in vertical mixing which is expected for the reduced values of $R_{STBL}$ (cf. (2.8)).

When considering eddy heat diffusivity $K_H$, a strong sensitivity to the formulation of the master turbulent length scale $l$ is found, particularly in the summer (Fig. 4.6c). Here, eddy heat diffusivity at the first model level above the ground is shown, but the same response is detected also at several higher levels (not shown, but see the $K_H$ vertical profiles and differences between RegCM(HL,EI) and RegCM(UW,EI) in Fig.4.4). The grouping of the differences in $K_H$ is largely according to the choice of $l$: in general, the use of $l_1$ yields the larger eddy heat diffusivity differences near the surface when compared to $l_2$. This may be expected from (2.6) and (2.7). However, no clear grouping of the RegCM simulations according to the other two parameters ($a_2$ and $R_{STBL}$) is detected.

To summarize, the amplitude of the *T2m* and *q2m* differences in the perturbed RegCM experiments with the UW scheme (experiments EXP003 to EXP019) does not differ dramatically from that in EXP002, which is the default experiment for the UW scheme and the spread among the UW experiments may be considered as relatively small to moderate. The small spread in the UW ensemble and similarity of the responses over different geographic regions implies that the default parameter settings in RegCM(UW,EI) will likely yield similar results in simulations over other regions and time intervals. Although for certain combinations of parameters these differences may be occasionally larger than in RegCM(UW,EI), generally this is neither systematic nor significant. This may support the choice of the default $a_2$ and $R_{STBL}$ (at least over the European domain). However, sensitivity of some aspects of model climatology (i.e. the $K_H$ profiles) can motivate further research and implementation of e.g. more refined master turbulent mixing length scale formulations (Grisogono 2010).

# 5. THE IMPACT OF PBL PARAMETERISATIONS ON THE PROJECTED CLIMATE CHANGE

In this chapter the time-dependent changes in the near-surface and surface variables simulated by the RegCM model using the UW and Holtslag PBL schemes under the RCP4.5 and RCP8.5 IPCC GHG scenarios and forced by the HadGEM2-ES Earth System Model (cf. subsection 2.1.1) are analysed. The RegCM simulations with the UW and Holtslag schemes are referred to as RegCM(UW,HA) and RegCM(HL,HA), respectively. The impact of the two PBL schemes on projected climate is presented and discussed as the differences between future periods (P1: 2011-2040, P2: 2041-2070 and P3: 2071-2098) and the historical period (P0: 1971-2000). The focus of the analysis is the Mediterranean region, where substantial temperature increase and precipitation decrease are expected in the 21$^{st}$ century (Giorgi 2006; Christensen et al. 2007). First, the near-surface air temperature *T2m* and total precipitation *R* annual cycles and projections are discussed, followed by a comparison of various components of the surface energy budget. For mean seasonal *T2m* and *R* systematic errors, differences between RegCM simulations and simulated climate change signal under the RCP8.5 scenario see Figs. A4 and A5. It is emphasised that in this chapter the RegCM model version, integration domain and historic period do not coincide with those discussed in Chapters 3 and 4, however, the Mediterranean region considered here is the same as before. Experiments analysed in this chapter will provide an estimation of the impact of the different climatology in RegCM simulations using two different PBL schemes on the simulated climate change signal.

### *5.1 Near-surface temperature T2m*

In the historical period P0, the mean monthly near-surface temperature *T2m* ranges between 6 °C and 25 °C in both RegCM(UW,HA) and RegCM(HL,HA) (Fig. 5.1a). *T2m* is lower in RegCM(UW,HA) than in RegCM(HL,HA) and the differences between two simulations are statistically significant in most of the year, except in the winter (Fig. 5.1b, open circles). The difference between RegCM(UW,HA) and RegCM(HL,HA) is thus comparable to the ERA-Interim forced experiments (Fig. 3.2c), i.e. RegCM(UW,HA) is consistently colder than RegCM(HL,HA). This similarity in the *T2m* results for the historic period in RegCM4.2 and

RegCM4.3 indicates that the differences in the model configuration (see section 2.1.1) do not substantially affect the impacts that the two PBL schemes exert on the temperature pattern. The cooling pattern in the RegCM(UW,HA) relative to RegCM(HL,HA) is also projected for the last period (P3) of the 21$^{st}$ century under both RCP scenarios (Fig. 5.1b, square markers). The largest difference (cooling) between the two schemes, up to 1.2 °C, is in the summer (Fig. 5.1b), and is overall slightly larger in the P3 period than in P0, particularly for the RCP8.5 scenario.

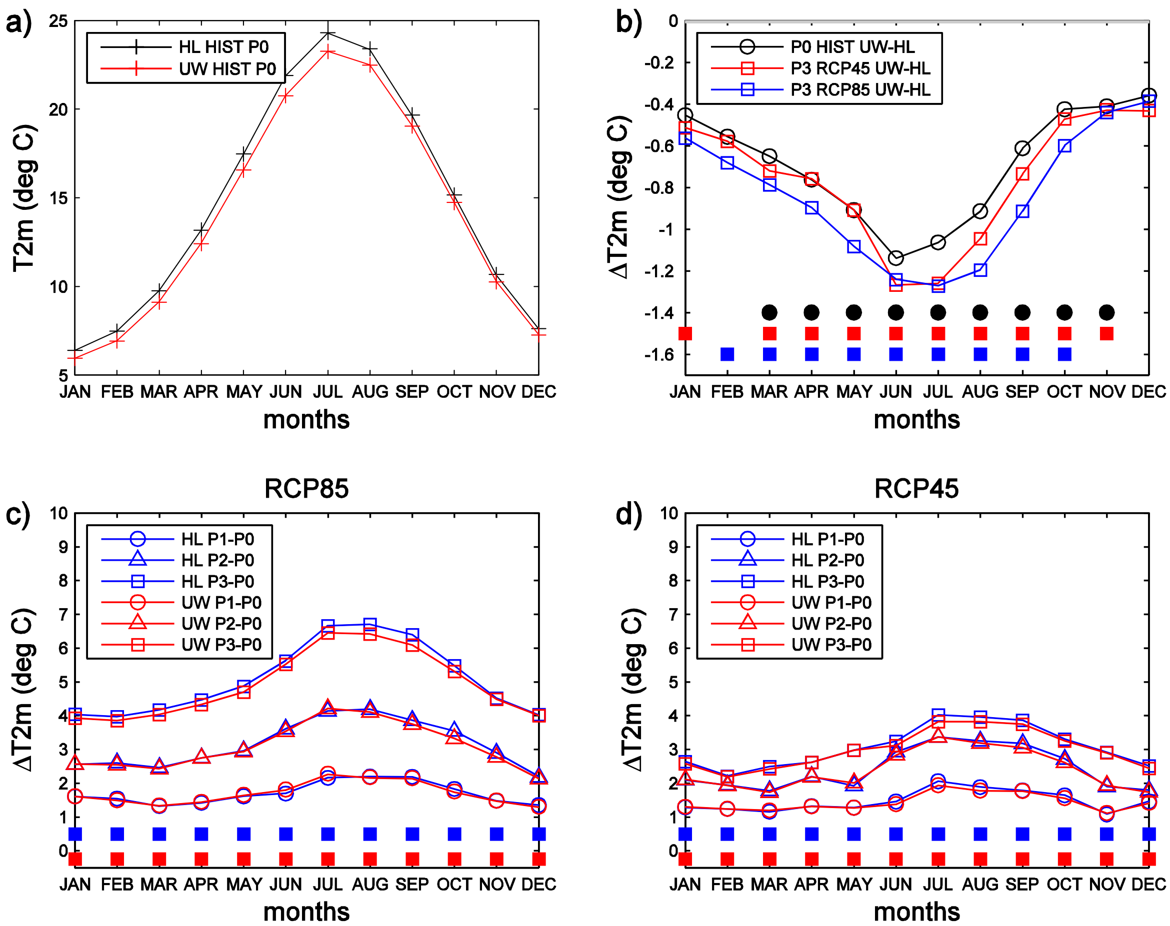


Fig 5.1 Annual cycle of the near-surface air temperature *T2m* over the Mediterranean region a) in RegCM(HL,HA) (black) and RegCM(UW,HA) (red) with HadGEM2-ES boundary conditions during the P0 period; b) differences between RegCM(UW,HA) and RegCM(HL,HA) in P0 (black) and for RCP4.5 (red) and RCP8.5 (blue) scenarios in the P3 period. Differences between future P1 (open circle), P2 (triangle) and P3 (square) periods and historical period P0 in RegCM(HL,HA) (blue) and RegCM(UW,HA) (red) under c) RCP8.5 and d) RCP4.5 scenarios. Months when medians of RegCM(HL,HA) and RegCM(UW,HA) monthly area averages in b) are different at the 95% confidence level are denoted by corresponding solid markers; statistically significant differences between P3 and P0 in c) and d) are denoted by corresponding solid square marker. P0: 1971-2000, P1: 2011-2040, P2: 2041-2070, P3: 2071-2098. Units are °C.

Since the averages shown in Fig. 5.1 are related to land points only, a possible interpretation of the larger *T2m* differences in P3 than in P0 between RegCM(UW,HA) and RegCM(HL,HA) should be linked with land surface processes in RegCM. The generally warmer RegCM with the Holtslag scheme than RegCM with the UW scheme in the historical and future periods (Fig. 5.1) implies that the overall drying of the land surface (the reduction of soil moisture) is stronger in RegCM with the Holtslag scheme than in RegCM with the UW scheme (Fig. 5.2).

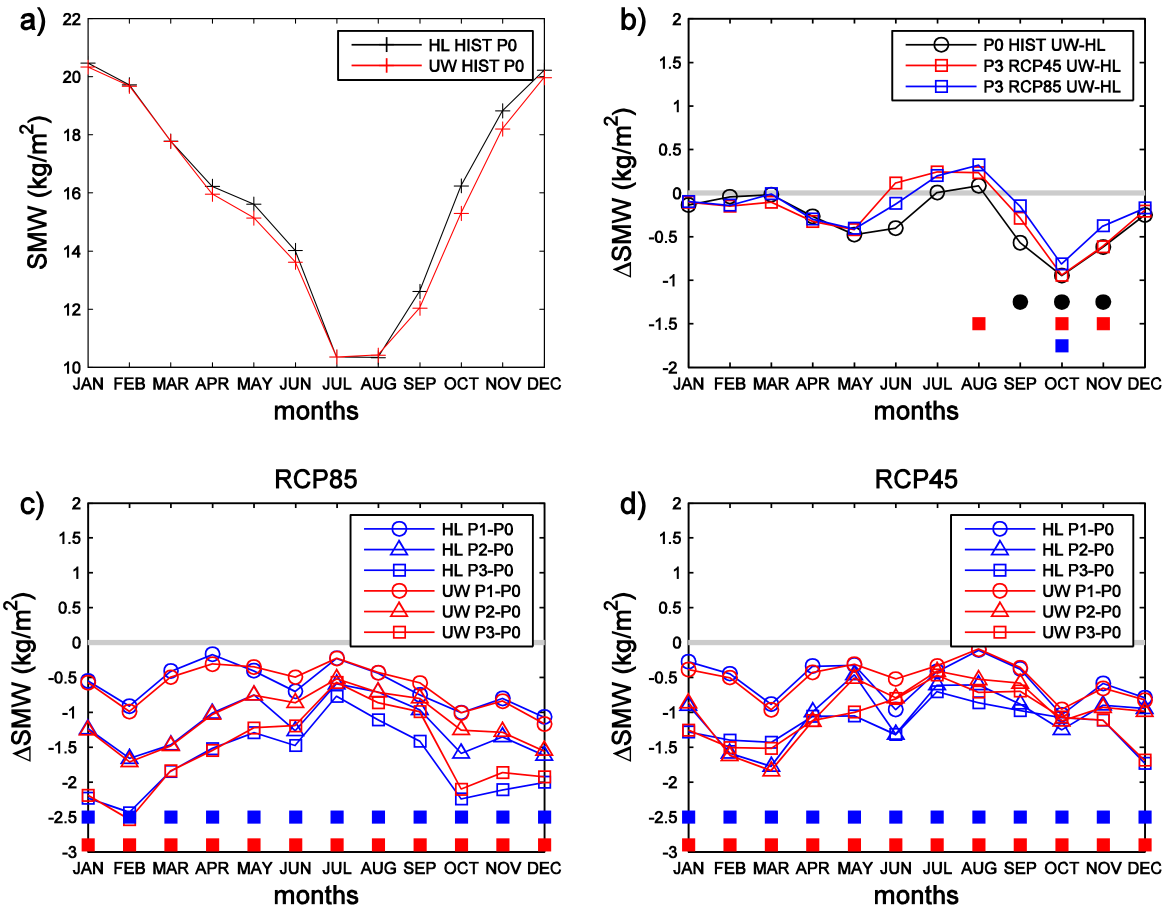


Fig 5.2 Same as Fig. 5.1 but for the soil moisture *SMW* in the first layer. Units are kg m$^{-2}$.

When comparing the RCP projections, RegCM(UW,HA) and RegCM(HL,HA) are similar in terms of the amplitude of climate change and its significance. Irrespective of the PBL scheme used, the projections are characterized by the largest warming in P3 in July and August (between 6 and 7 °C) for the RCP8.5 scenario (Fig. 5.1c). By the end of the 21$^{st}$ century the amplitude of warming forced by RCP4.5 is almost the same as the amplitude in the RCP8.5 scenario in the middle of the 21st century (Fig. 5.1c,d). Additionally, the warming from P0 to P3 is statistically significant for every month in both scenarios and with both PBL schemes applied. We can conclude that, although the use of particular PBL scheme may induce different mean climatology (cf. Fig. 3.1), it yields no substantially different response in terms of the *T2m* climate change over the Mediterranean region. This is in agreement with Jerez et al. (2013) who investigated the impact of the choice of various parameterisations on the climate change signal over the Iberian Peninsula. However, Fig. 5.1c also shows that in most of the year the warming with RegCM(UW,HA) in P3 is consistently slightly smaller than with RegCM(HL,HA).

*5.2 Total precipitation R*

In both RegCM(HL,HA) and RegCM(UW,HA) the minimum in the total precipitation *R* is found in July (~0.5 mm day$^{-1}$) while the maximum is in late autumn and early winter (~2.5 mm day$^{-1}$; Fig. 5.3a). More precipitation in the winter months in RegCM(UW,HA) than in RegCM(HL,HA) is consistent with the results when RegCM is forced by the ERA-Interim boundary conditions (see Chapter 3). However, in May and June, when statistically significant differences between RegCM(UW,HA) and RegCM(HL,HA) in the P0 period are found, the opposite is seen, i.e. RegCM(HL,HA) is wetter than RegCM(UW,HA) (Fig. 5.3b). Thus the wetter RegCM(HL,HA) is in contrast to the results when RegCM is forced by ERA-Interim: Fig. 3.4c indicates more drying during the above two months in RegCM(HL,EI) than in RegCM(UW,EI). This result implies that possibly other differences in the model setup considered here and those in Chapters 3 and 4 (e.g. boundary conditions, domain size, the choice of other parameterisations (see Section 2.1.1)) could influence the model behaviour and overcome the impact due to changes from the PBL schemes alone. However, the overall similarity of the precipitation annual cycle in the rest of the year in RegCM4.2 and RegCM4.3 again confirms, as in case of *T2m*, that in our experiments the different model setup has a rather limited impact when compared with the impact of the two PBL schemes.

When compared to *T2m*, there are fewer months with significant climate change in precipitation *R* (cf. Fig. 5.3 c-d and 5.1 c-d). Also, the comparison of future periods and the historical period P0 reveals differences which are more variable in sign for precipitation than for

*T2m*. Although, irrespective of the PBL scheme used, in a larger part of the year future precipitation amounts are reduced, the differences between the future periods and P0 are larger and statistically significant more frequently in the RegCM(HL,HA) than in RegCM(UW,HA) (Fig. 5.3c,d). This might be, at least partly, attributed to stronger positive feedbacks in RegCM(HL,HA) than in RegCM(UW,HA), where the higher near-surface temperature corresponds to the larger drying (e.g. Seneviratne et al. 2010).

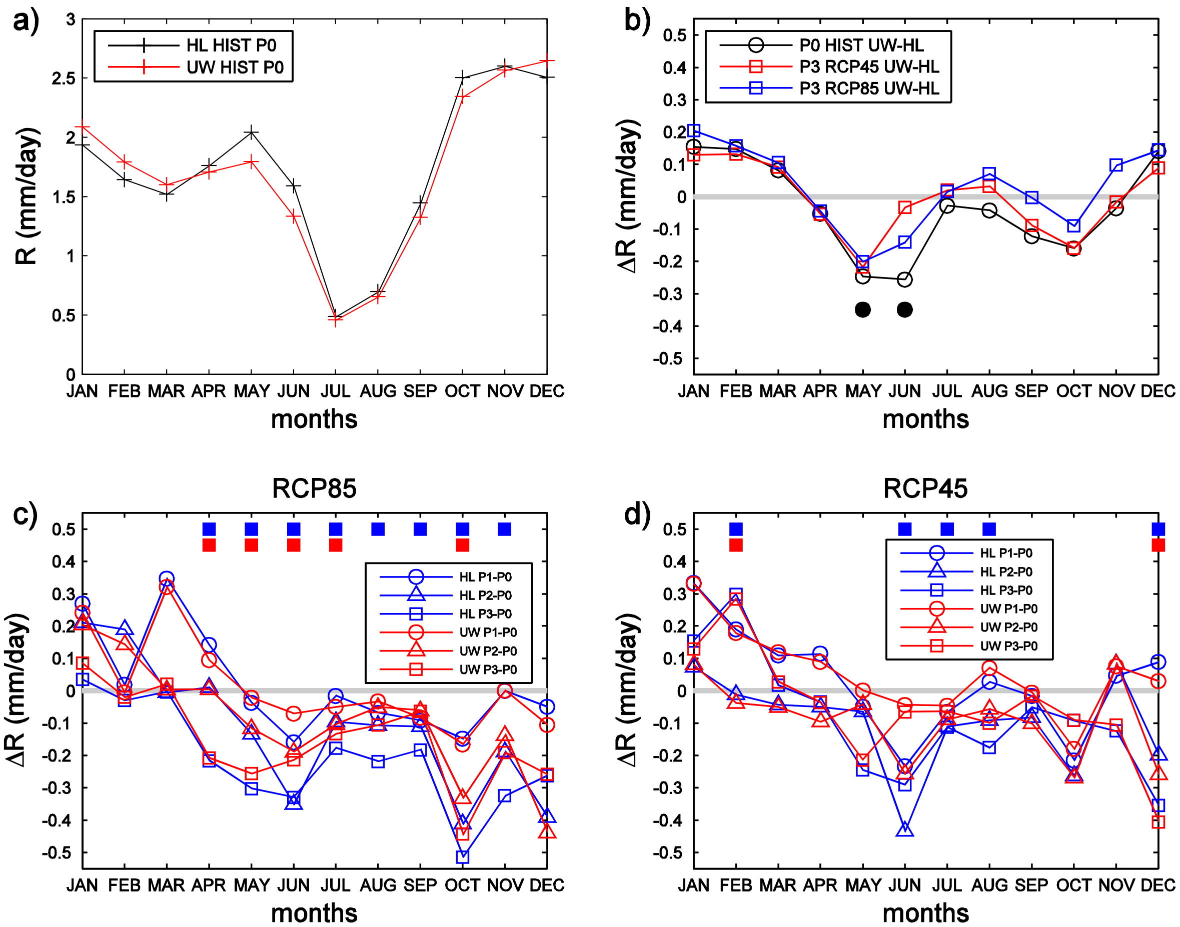


Fig 5.3 Same as Fig. 5.1 but for the total precipitation amount *R*. Units are mm day$^{-1}$.

Decrease in precipitation over the Mediterranean region is also a function of the applied RCP scenario forcing (see also Jacob et al. 2013). The largest decrease is found in RegCM(HL,HA) by the end of the 21$^{st}$ century in the autumn under the RCP8.5 scenario and amounts to about -0.5 mm day$^{-1}$ relative to P0 (Fig. 5.3c). A possible explanation of the reduction in precipitation during most of the year could include the impact of the reduced latent heat flux (e.g. Andrews 2009) and the warming contrast between land and sea (e.g. Rowell and Jones, 2006).

*5.3 Radiative fluxes, total cloud cover and surface albedo*

The net surface shortwave radiation *SWR* in the P0 period is significantly different between the two RegCM simulations throughout the annual cycle over the Mediterranean region (Fig. 5.4a,b). The amplitude of *SWR* is larger in RegCM(HL,HA) than in RegCM(UW,HA) and the difference between the two RegCM experiments peaks in May.

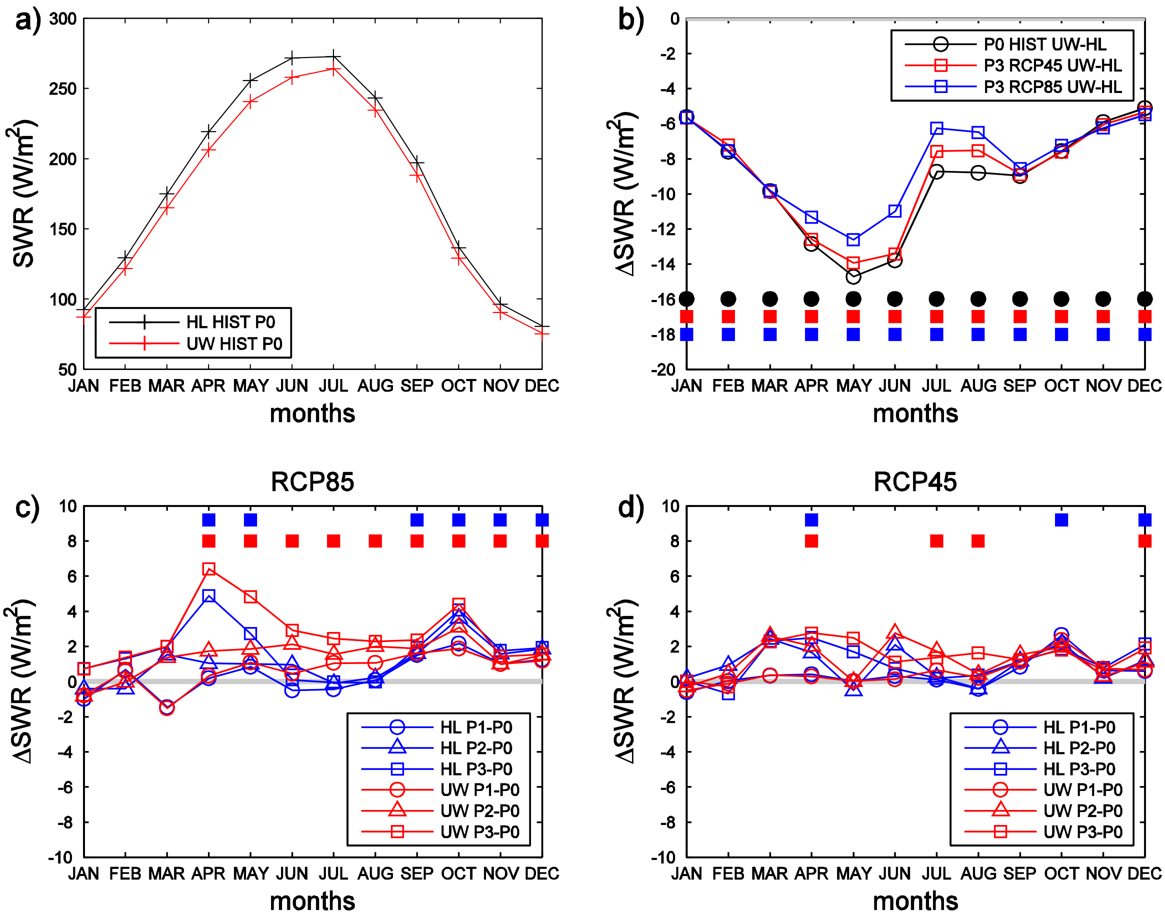


Fig 5.4 Same as Fig. 5.1 but for the net surface shortwave radiation *SWR*. Units are W m$^{-2}$.

In the previous chapters, where the RegCM experiments forced by ERA-Interim were analysed, a strong dependence of *SWR* on the total cloud cover *CLD* and less strong dependence of *SWR* on surface albedo *ALB* was identified. Therefore, similar dependency in the experiments when RegCM is forced by the HadGEM2-ES Earth System Model may be expected. Indeed, the larger *SWR* in RegCM(HL,HA) than in RegCM(UW,HA) (Fig. 5.4a) can be associated with the lower *CLD* in RegCM(HL,HA) (Fig. 5.5a) implying that more shortwave radiation reaches the surface and in turn forces higher *T2m* and/or increase in the turbulent heat fluxes (Andrews et al. 2009, Tang et al. 2012). This relationship between the two PBL schemes is also seen in the last 30-year period of the 21$^{st}$ century (P3) and does not depend substantially on the RCP scenario applied (Fig. 5.4b). Moreover, the differences in *SWR* between RegCM(UW,HA) and RegCM(HL,HA) when going from P0 to P3 are reduced in spring and summer (Fig. 5.4b) and they are consistent with the reduction of differences between the two experiments in total cloud cover *CLD* (Fig. 5.5b).

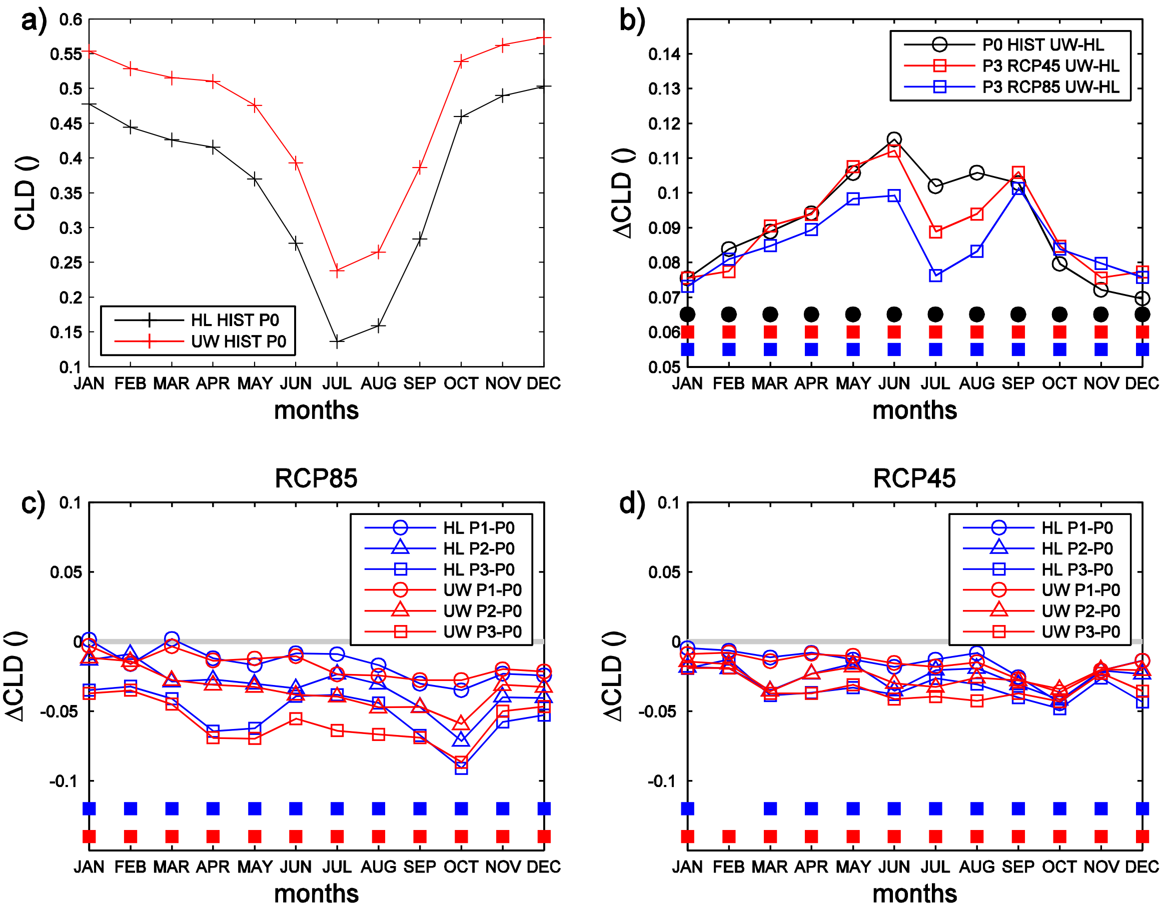


Fig 5.5 Same as Fig. 5.1 but for the total cloud cover *CLD*.

Although the *SWR* differences between future periods and P0 vary from -2 W m$^{-2}$ to +6 W m$^{-2}$, they are largely dominated by the increased *SWR* in future climate (Fig. 5.4c,d). Similar increase of *SWR* in the future projections is also found by Lenderink et al. (2007) in the ensemble of RCM simulations under the IPCC A2 scenario over Spain during the summer, thus indicating that the *SWR* increase over the Mediterranean region may be a robust feature in various experimental designs. The *SWR* differences between P0 and P3 under the RCP8.5 scenario, are statistically significant in most months in RegCM(UW,HA).

The *SWR* increase in future periods (Fig. 5.4c,d) is consistent with the reduction of *CLD* (Fig. 5.5c,d) irrespective of the RCP scenario applied. At the same time, surface albedo *ALB* is slightly increased, except in the winter months (Fig. 5.6c,d).

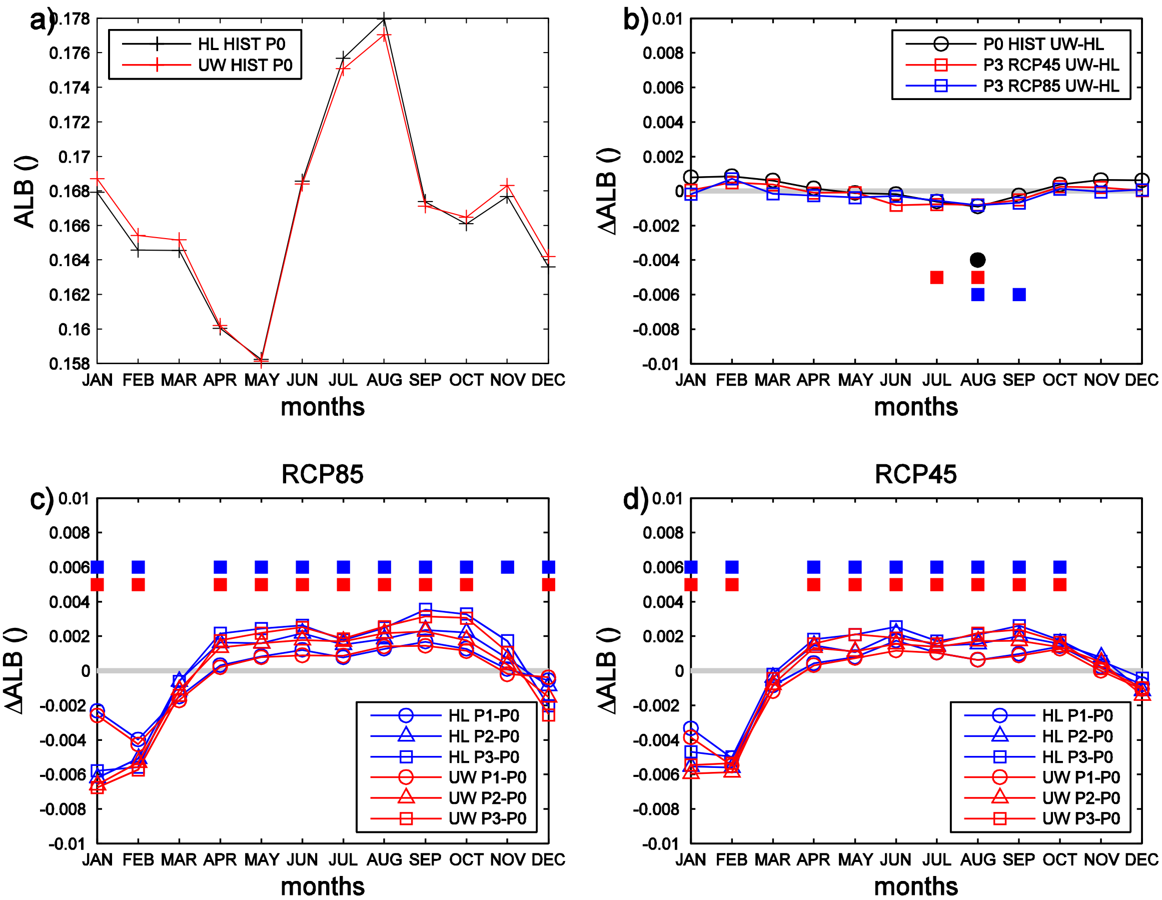


Fig 5.6 Same as Fig. 5.1 but for the surface albedo *ALB*.

The featured future changes in *CLD* and *ALB* have the opposite effects on *SWR*: decrease in *CLD* acts in the sense as to increase *SWR*, and increase in *ALB* acts as to decrease *SWR*. Since Fig. 5.4c,d indicates an overall increase of the future *SWR*, it may be inferred that the decrease in *CLD* overcomes the tendency of surface albedo to reduce *SWR*. The *ALB* increase is linked with the reduction of precipitation and soil moisture (Fig. 5.3c,d and Fig. 5.2c,d) because the drier soil is generally brighter and reflects more shortwave radiation; this effect is included in the RegCM land-surface scheme BATS (e.g. Dickinson et al. 1993; Seneviratne et al. 2010). The origin of the *ALB* decrease in the winter months may be due to the reduction of snow cover in future climate over mountainous parts of the Mediterranean region, but also due to increased winter precipitation (Fig. 5.3 c,d).

For the net surface longwave radiation *LWR* in the historic period P0, differences between the two RegCM simulations are less than 10 W m$^{-2}$ and statistically significant during the whole year (Fig. 5.7a,b). The larger *LWR* (in absolute terms) is found in RegCM(HL,HA); this is consistent both with higher *T2m* (Fig. 5.1a) and lower *CLD* (Fig. 5.5a) in RegCM(HL,HA) than in RegCM(UW,HA) and the same relationship also holds in the last period of the 21$^{st}$ century (Fig. 5.7b).

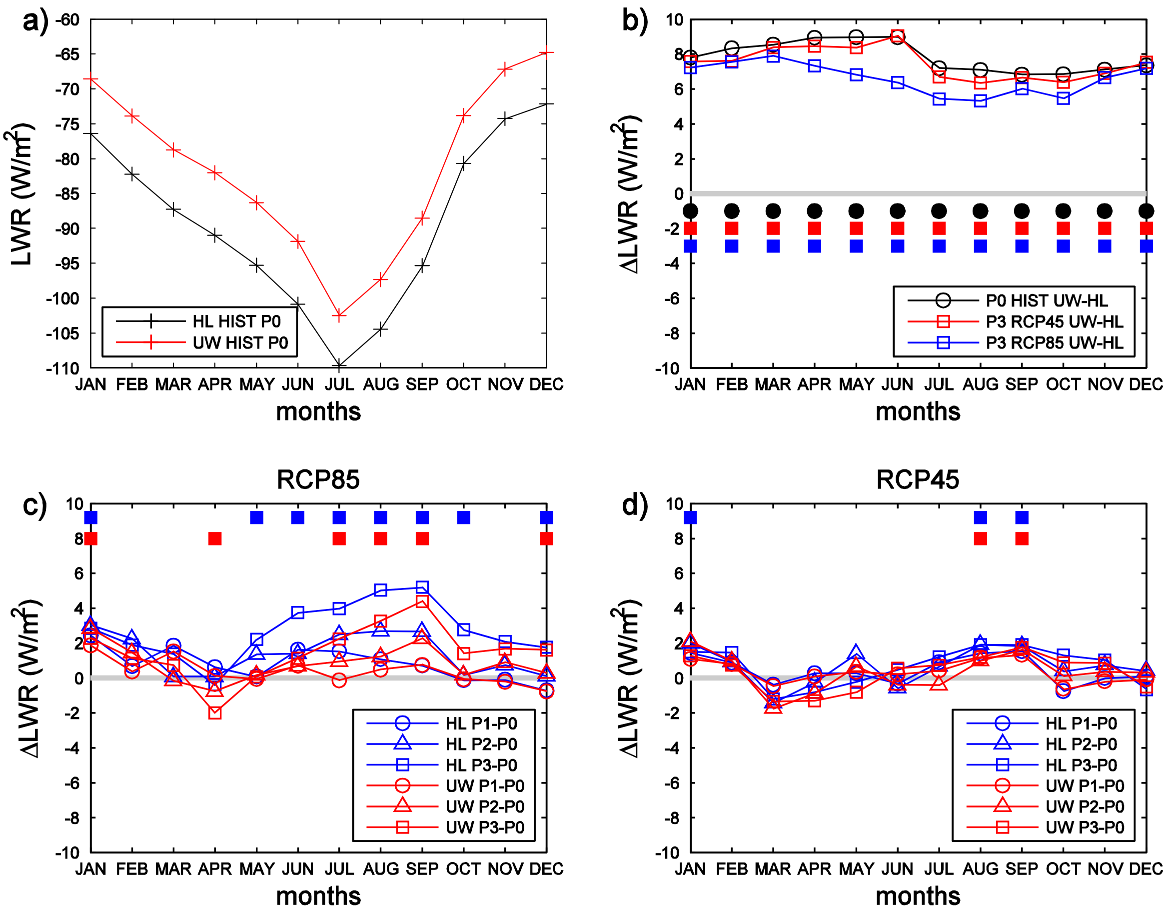


Fig 5.7 Same as Fig. 5.1 but for the net surface longwave radiation *LWR*. Units are W m$^{-2}$.

The *LWR* changes between the future and historical periods are, similar to *SWR*, confined to between -2 and +6 W $m^{-2}$ (Fig. 5.7c,d) and under the RCP8.5 scenario are mostly positive indicating a reduction of *LWR* in absolute terms in the future climate. In contrast to *SWR*, significant changes of *LWR* occur in RegCM(HL,HA) more frequently than in RegCM(UW,HA). The prevailing positive *LWR* change, when comparing future and historical periods (Fig. 5.7c,d), is not dependent on the *T2m* increase and *CLD* decrease alone. For example, although according to (2.14) increase in surface temperature (but also in *T2m* considered here) would imply increase (in absolute terms) in *LWR*, this simple diagnostic model of the *LWR* dependency on temperature and cloudiness does not fully explain positive *LWR* change because it does not include the dependency of *LWR* on the water vapour amount in the atmospheric column (Kothe et al. 2011). Nevertheless, this positive *LWR* change in the future (indicating a decrease of *LWR* in absolute terms) is consistent with the results of e.g. Andrews et al. (2009), where, on global scale, various GCMs simulated the *LWR* decrease (in absolute terms) in a future warmer and moisture atmosphere. They asserted that this decrease of *LWR* was the effect of an increase in the downward surface longwave radiation *LWD* which thus outweighed the thermal response of the surface (and associated surface outgoing longwave radiation). In RegCM experiments analysed here, positive *LWR* change is somewhat larger in RegCM(HL,HA) under the RCP8.5 scenario and in the P3 period relative to P0 (Fig. 5.7c); this larger *LWR* increase in RegCM(HL,HA) than in RegCM(UW,HA) is linked and consistent with the larger *LWD* in RegCM(HL,HA) simulation (Fig. 5.8c).

The downward surface longwave radiation *LWD* (Fig. 5.8c,d) exhibits much stronger climate change signal than the net longwave radiation *LWR* (Fig. 5.7c,d) and it is projected to be higher in the future periods than in historical period (cf. Lenderink et al. 2007). In the P3 period and for RCP8.5, changes in the *LWD* reach almost 50 W $m^{-2}$, or nearly 15% increase relative to P0, and both the differences between the two PBL schemes (Fig. 5.8b) and differences between future and historical periods are statistically significant throughout the year (Fig. 5.8c,d). Only during the P3 period, the two RegCM simulations are very close in terms of summer *LWD* (Fig. 5.8b). Reduced differences in the *LWD* between two PBL schemes in P3 (Fig. 5.8b) are consistent with reduced differences in the *CLD* (Fig. 5.5b) in the same period.

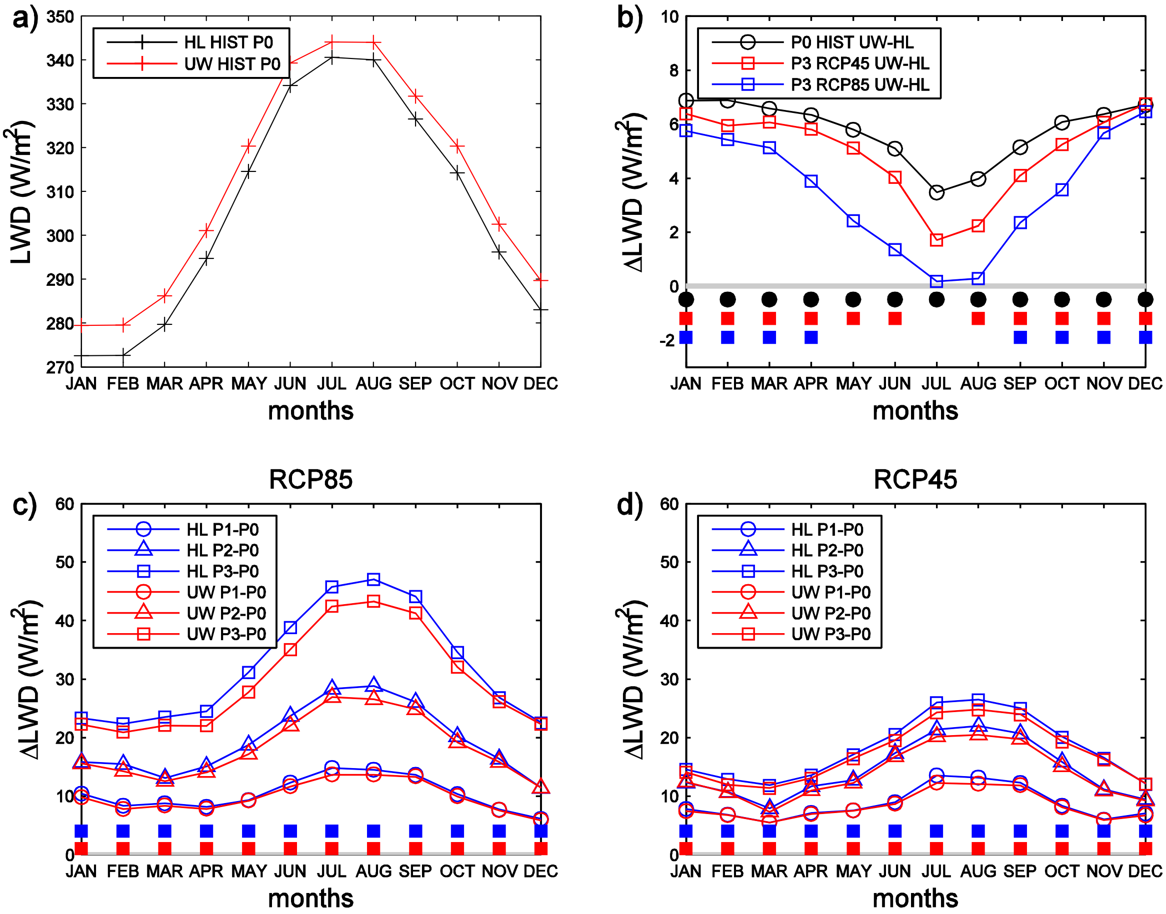


Fig 5.8 Same as Fig. 5.1 but for the downward surface longwave radiation *LWD*. Units are W m$^{-2}$.

### *5.4. Turbulent heat fluxes*

In the Mediterranean region sensible heat flux *SHF* in the RegCM model is directed from the land surface into the atmosphere throughout the year, i.e. it is manifested as the heat loss from the surface, with the largest loss occurring in the summer (Fig. 5.9a). In P0 and P3 periods, heat loss is stronger in RegCM(UW,HA) than in RegCM(HL,HA) and the differences of up to 5 W m$^{-2}$ are statistically significant in almost every month (Fig. 5.9b). In the future, the heat loss due to *SHF* is projected to increase up to 6 W m$^{-2}$ under the RCP4.5 scenario and almost up to 10 W m$^{-2}$ in RCP8.5 in P3, and both RegCM experiments with different PBL schemes exhibit similar response (Fig. 5.9c,d).

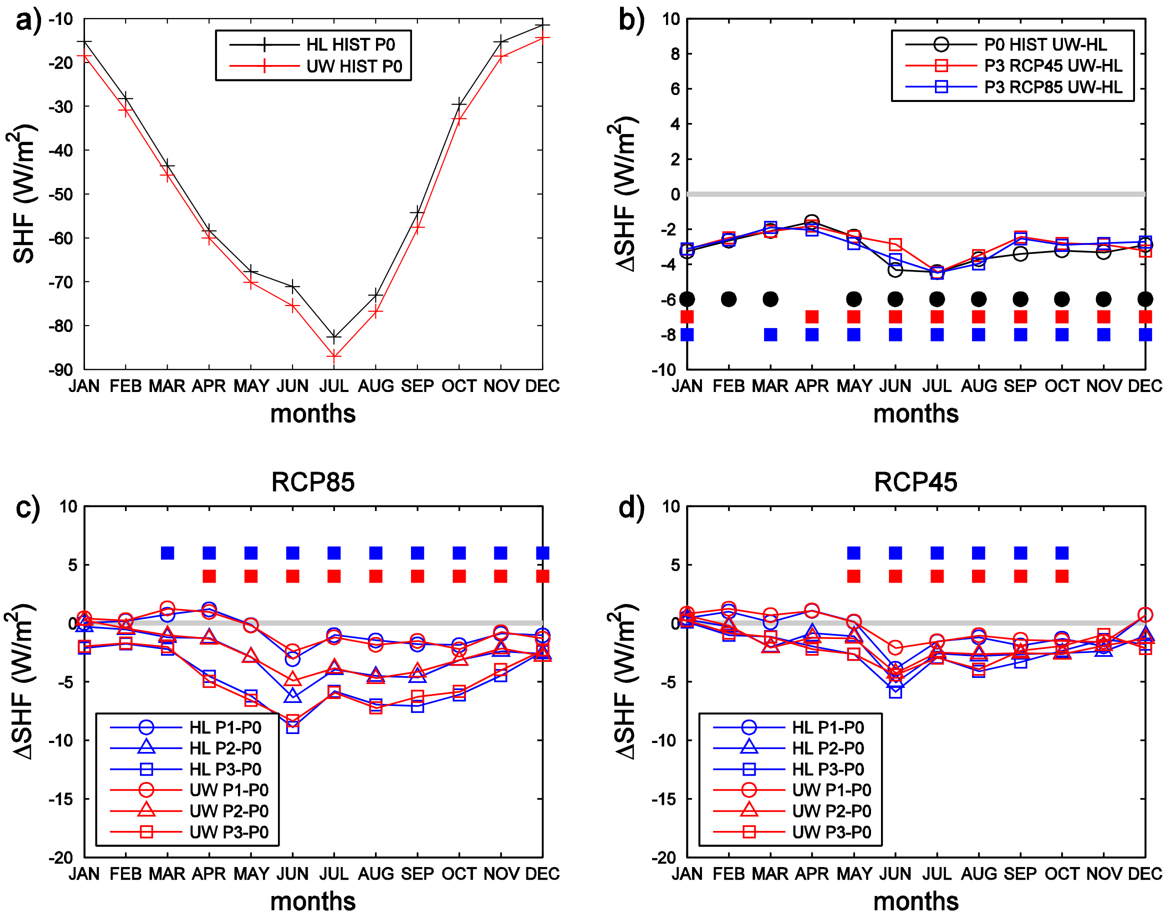


Fig 5.9 Same as Fig. 5.1 but for the sensible heat flux *SHF*. Units are W m$^{-2}$.

The maximum heat loss from the surface due to latent heat flux *LHF* is in May and June when the strongest evapotranspiration occurs; the *LHF* minimum is in the winter coinciding with the minimum in solar insolation and in July and August when soil in the Mediterranean region is the driest in the year (Fig. 5.10a). *LHF* is stronger in RegCM(HL,HA) than in RegCM(UW,HA) in late spring and early summer, but the opposite is seen during the cold period. Under both RCP scenarios, the *LHF* heat loss is generally projected to increase (Fig. 5.10c,d), with the smallest change occurring in June, the month when the maximum *LHF* (in absolute terms) is attained (Fig. 5.10a). From Fig. 5.10c,d it may be inferred that a relative small projected (absolute) increase of *LHF* in the summer would reduce somewhat the future role of *LHF* over the land points in the Mediterranean region; this could be explained partly because of the reduction in the total precipitation (Fig. 5.3) and partly because of the reduction in soil moisture (Fig. 5.2). Consequently, *SHF* takes more prominent role over *LHF* in maintaining the energy balance of land surface (Fig. 5.9c,d) in summer. Reduced evapotranspiration during the summer (associated with less *LHF*) is also found in other RCMs and GCMs over parts of southern Europe suggesting that a strong control of *LHF* by available soil moisture is taking place over this region (e.g. Lenderink et al. 2007; Boé and Terray 2008; Seneviratne et al. 2010).

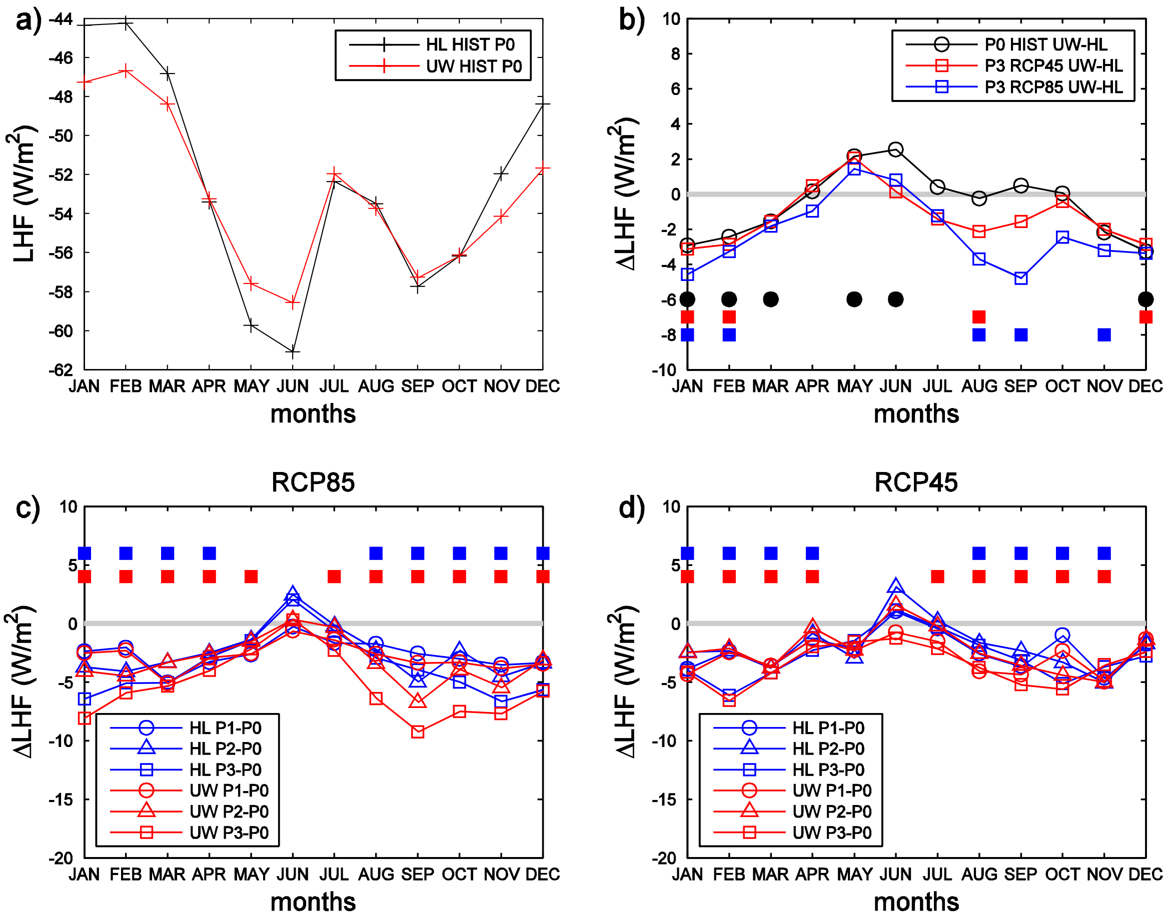


Fig 5.10 Same as Fig. 5.1 but for the latent heat flux *LHF*. Units are W m$^{-2}$.

*LHF* (or evapotranspiration) increase alone cannot explain the precipitation reduction in RegCM(UW,HA) and RegCM(HL,HA) (see e.g. Andrews et al. (2009) for the discussion of the link between reduction in precipitation and reduction in *LHF* on global scale). However, the reduction of total precipitation *R* and total cloud cover *CLD* over Mediterranean region (cf. Figs. 5.3c,d and 5.5c,d) in the RegCM set of experiments could be linked using the hypothesis of the land-sea warming contrast (e.g. Manabe et al. 1992; Rowell and Jones 2006; Boé and Terray 2014). In order to confirm this hypothesis and to fully disentangle different contributions to *R* and *CLD* changes (e.g. various land-atmosphere interactions, changes in the large-scale flow patterns, interplay between local and large-scale processes) additional analysis is needed and is beyond the scope of this thesis.

In terms of the impact of different PBL schemes on the projected *LHF* change, one can notice that the future *LHF* tends to be larger in RegCM(UW,HA) than in RegCM(HL,HA) (Fig. 5.10c,d), i.e. more water is available for evapotranspiration from the surface in RegCM(UW,HA). This is consistent with a smaller reduction of soil moisture in the future in RegCM(UW,HA) than in RegCM(HL,HA) (Fig. 5.2c,d) thus confirming that the UW PBL scheme would yield a somewhat wetter future climate (Fig. 5.3c,d).

In summary, the two PBL schemes used in the historical RegCM simulations over the Mediterranean region may affect climatology of various quantities that differ in statistical sense; however, most of the differences in the 21$^{st}$ century induced by climate change forcing are not sensitive to the choice of the PBL scheme.

# 6. CONCLUSIONS

Sensitivity of the regional climate model RegCM4.2 simulations to the choice of the PBL parameterisation was studied in the context of the model systematic errors in near-surface temperature *T2m* and precipitation. The two PBL schemes implemented in RegCM4.2 were the default Holtslag scheme (Holtslag et al. 1990) and the recently implemented UW scheme (Grenier and Bretherton 2001). From the 10-year (1989-1998) model climatology with the default scheme, relatively large erroneous warming is revealed over the north-eastern Europe in the winter and over central Europe in the summer. The model also exhibits a wet winter bias in the north-eastern part of the integration domain as well as a non-negligible dry summer bias in central Europe; these biases are reduced when the UW scheme is used in RegCM. The main goal of this study was to identify physical processes and parameters in the default Holtslag PBL scheme which contribute to the above systematic errors and to assess their behaviour in the UW PBL scheme. In addition, some changes inside the UW scheme are investigated in order to establish whether further improvements with this scheme could be attained. Both Holtslag and UW schemes are then used in additional RegCM model simulations of future climate (until the year 2098) and the differences between them are analysed and discussed when the forcing by the two IPCC scenarios, RCP4.5 and RCP8.5, was applied.

First, the model version RegCM4.2 was forced by ERA-Interim reanalysis over the European/north African domain for the 10-year period 1989-1998. The analysis focused on the surface energy budget (SEB) components: net surface shortwave and longwave radiative fluxes (*SWR* and *LWR*), and sensible and latent heat fluxes (*SHF* and *LHF*). The modelled net surface radiative fluxes were compared against the same fields derived from satellite datasets and the approach from Kothe et al. (2011) was applied to interpret the differences between various data sources. In a simple diagnostic analysis, radiative fluxes are related to surface temperature, total cloud fraction (*CLD*) and albedo (*ALB*). The RegCM sensible and latent heat fluxes at the grid-cell level were validated by the ground measurements, while on regional scales they were compared with the turbulent heat fluxes from ERA-Interim. An important validation feature was revealed, that is, the non-negligible differences between various algorithms of the satellite-based products. These differences were often as large as model biases, indicating uncertainties in our knowledge of true values (Güttler et al. 2013b). In addition, although ERA-Interim is normally considered as a reference dataset, in some cases it diverged considerably from the corresponding satellite-based observations.

The main difference in RegCM simulations, when compared with ERA-Interim and/or satellite estimates, is strong overestimation of *SWR* over eastern Europe during summer which, in turn, affects other components of SEB. The above overestimation of *SWR* is associated with deficient representation of realistic cloud cover in the model: for example, *CLD* is severely underestimated over central Europe and less severe, but still significantly, over parts of northern Africa. This is found to be the main source of errors in SEB which then affects near-surface temperature *T2m*. The use of the UW scheme in RegCM brings an improvement in representation of the total cloud cover *CLD*, most clearly over eastern Europe in the summer. The increase in the total cloud cover *CLD* in experiments with the UW scheme reduces net surface shortwave flux *SWR* and significantly reduces the near-surface temperature errors over central Europe during summer. However, a consistent reduction of *T2m* in the UW simulations further deteriorates the cold bias over northern Africa that existed in the default Holtslag simulations. The following potential sources of such near-surface temperature bias over northern Africa in RegCM could be identified: limitations and/or deficiencies in specification of albedo in the land-surface scheme (Sylla et al. 2010), overestimation of the total cloud cover over this region during DJF (Güttler et al. 2013b) and the need to include the aerosol-related processes in RegCM simulations (Solmon et al. 2012).

Strong overestimation of *SWR* over eastern Europe during summer is also manifested as an overestimation (in absolute terms) of *LWR* and *SHF* in the model, while for *LHF* a somewhat complex pattern of differences between RegCM and ERA-Interim is revealed. In terms of interaction between land surface and near-surface atmospheric fields, the evaluation of latent heat flux suggests that RegCM simulations with the UW scheme are not superior to those with the Holtslag scheme, but the evaluation of sensible heat flux clearly indicates benefits of using the UW scheme.

The differences between the two PBL schemes in terms of temperature and water vapour mixing ratio can be partially ascribed to different vertical profiles of eddy heat diffusivity and associated tendencies induced by turbulent mixing. Eddy heat diffusivity is substantially reduced in the UW simulations relative to the control simulation with the Holtslag PBL scheme, especially during JJA when it normally reaches the maximum in the annual cycle. However, this reduction is not homogeneous in the vertical; the vertical slope of eddy heat diffusivity is also changed, resulting in the reduced temperature tendencies. Other possible sources of differences in the temperature and water vapour tendencies between the two PBL schemes are found to be related to the changes in the characteristics (slope and curvature) of vertical profiles of prognostic variables. Vertical profiles of the water vapour mixing ratio ($qv$) tendencies reveal a major increase of the PBL-generated $qv$ tendency in the prognostic equation when the UW scheme is used.

Sensitivity of the UW scheme to different formulations is also investigated in a series of the 3-year experiments by testing the master turbulent mixing length scale in unstably stratified conditions and by perturbing two unconstrained parameters, associated with (a) the entrainment efficiency and (b) the formulation of the master turbulent length scale in stably stratified conditions. The results reveal that this sensitivity can be detected as the changing values of eddy heat diffusivity. However, the results indicate that the simulated near-surface temperature and specific humidity are relatively insensitive to the changes in the UW scheme formulation. Furthermore, it was also demonstrated that the UW scheme is not very sensitive to the perturbations of two unconstrained parameters (the efficiency of evaporative enhancement of the cloud-top entrainment $a_2$ and the scaling parameter in statically stable boundary layer turbulence length scale $R_{STBL}$). An exception is found, however, in the northern parts of the domain, where the reduction in the default $R_{STBL}$ is systematically followed by the reduction of $T2m$.

The second set of RegCM experiments, with the model version RegCM4.3, was performed with the aim to evaluate the impact of different PBL schemes on the signal of climate change when forced by the HadGEM2-ES Earth System Model in the historical period and for the 21$^{st}$ century under the IPCC RCP4.5 and RCP8.5 scenarios. The differences between the two experiments with the two different PBL scheme are similar to those when RegCM was forced by ERA-Interim, i.e. they include a reduced near-surface temperature and higher total cloud cover in the experiments with the UW PBL scheme. This similarity may indicate that the differences between the RegCM4.2 and RegCM4.3 configurations appear less important than the differences inferred by using the two different PBL schemes. Although the statistically significant differences between the Holtslag and the UW scheme experiments do exist in the historical period, and are generally maintained into the 21$^{st}$ century, there are no substantial differences in the signal of the climate change under variable PBL scheme. For example, the warming by the end of the 21st century under RCP8.5 over the Mediterranean region equals to 4 °C in the winter and between 6 °C and 7 °C in the summer (with differences in warming between two schemes 0.1 °C during the winter and 0.2 °C during the summer). The increased near-surface air temperature $T2m$ and the general reduction of the total precipitation $R$ over the Mediterranean region are consistent with other studies, but the lack of sensitivity in the climate change signal related to different PBL schemes can not be generalized to other parameterisations (e.g. Jerez et al. 2013).

The following areas of future research emerged while working on the thesis: since a PBL scheme impacts other model prognostic variables, a careful experimental design to study these impacts should include an analysis of model tendencies due to all simulated processes; because in both PBL schemes only the simplest formulations of the master mixing length scale were implemented, this question deserves further detailed investigation; and finally, an exercise similar to that for the future climate simulations should be repeated using other subgrid physics options in RegCM (e.g. Torma and Giorgi 2014) and an analysis of the changes in prognostic tendencies is strongly suggested.

# 7. APPENDIX

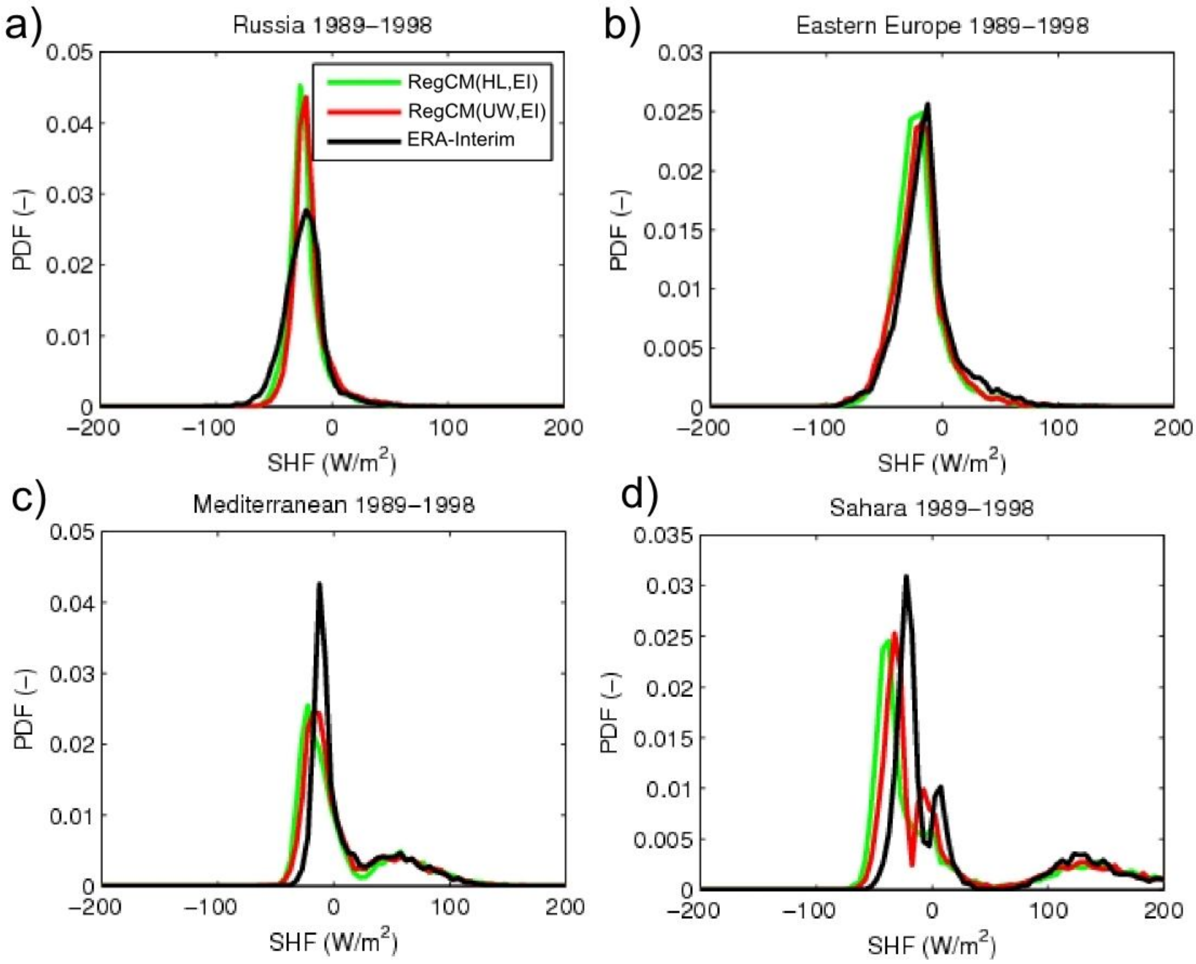


Fig. A1 PDFs of sensible heat flux *SHF* over analysed regions (cf. Fig. 2.1a) simulated by RegCM(HL,EI) (green), RegCM(UW,EI) (red) and ERA-Interim (black). Period: 1989-1998. Season: DJF.

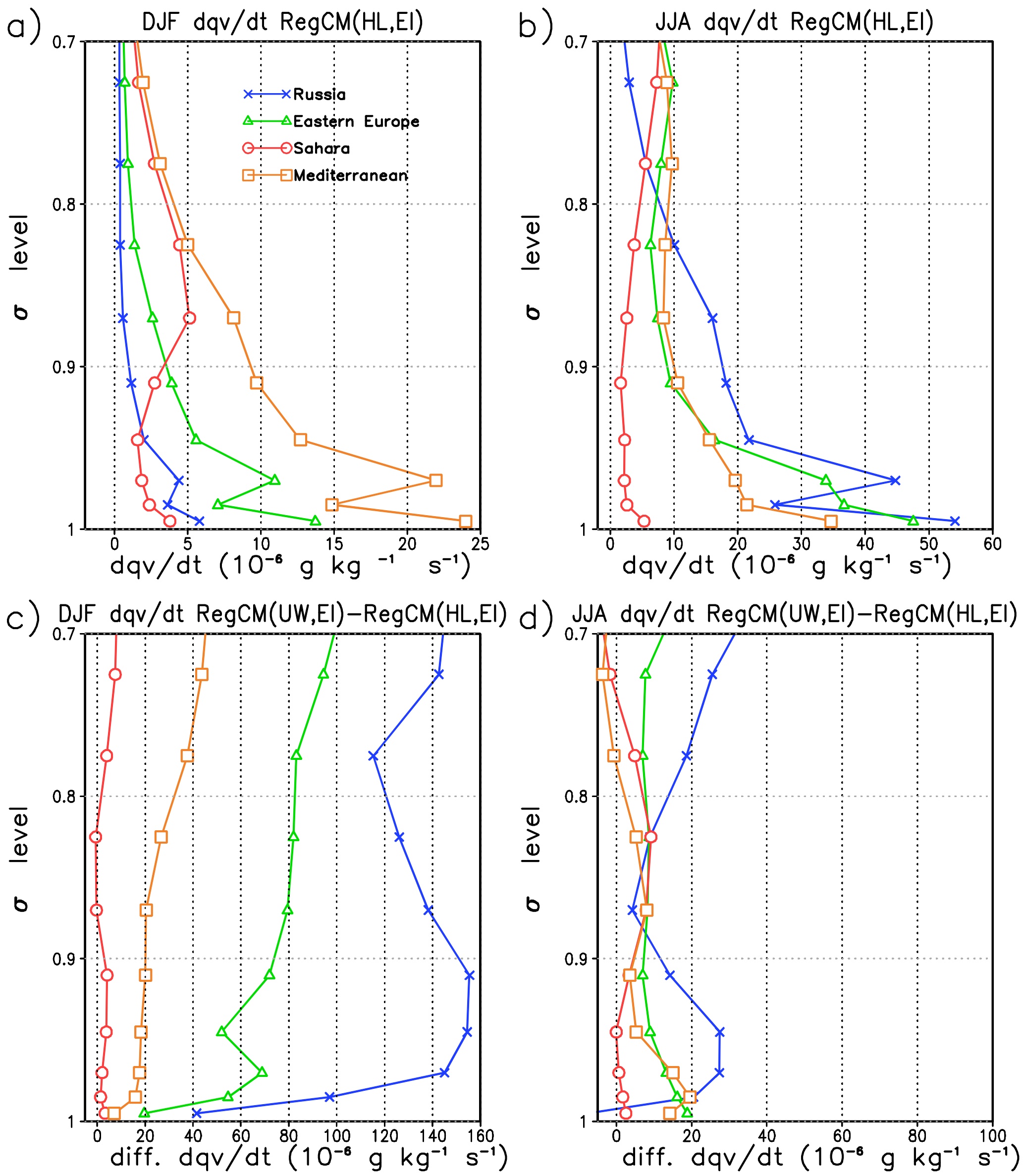


Fig. A2 Vertical profiles of the regional- and seasonal-mean water vapour mixing ratio tendency due to the PBL scheme in RegCM(HL,EI) (RegCM with the Holtslag PBL scheme; top) and the difference between RegCM(UW,EI) (RegCM with the UW scheme) and RegCM(HL,EI) (bottom). Winter profiles are on the left, summer profiles are on the right. The period analysed is 1989–1998 and selected regions are shown in Fig. 2.1. Profiles over Russia are marked by crosses, over eastern Europe by triangles, over the Sahara by circles and over the Mediterranean by squares. Units are $10^{-6}$ g kg$^{-1}$ s$^{-1}$. See Güttler et al. (2013a) for details.

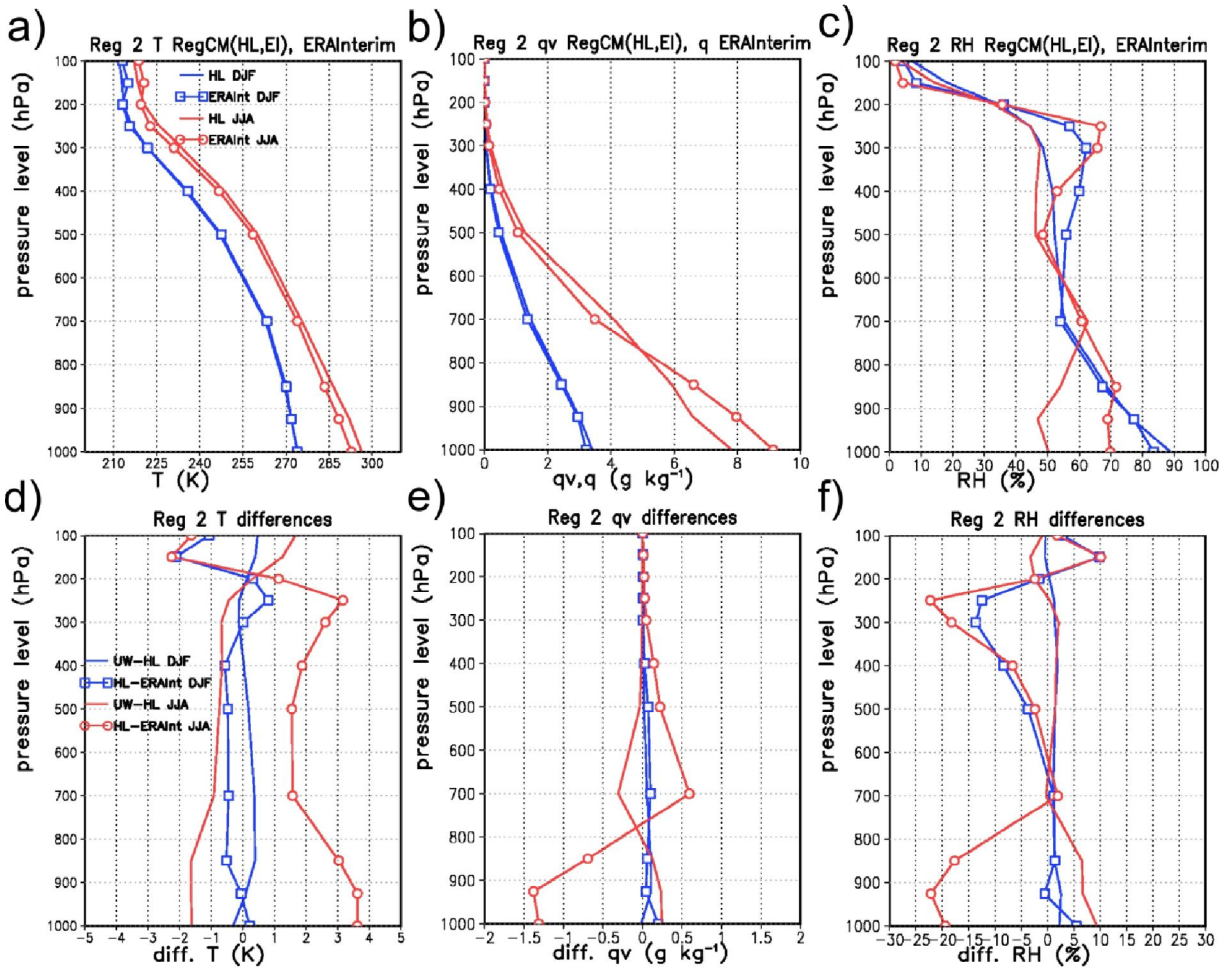


Fig. A3 Vertical profiles of air temperature, water vapour mixing ratio and relative humidity over eastern Europe during winter and summer. Top: the full RegCM(HL,EI) (blue graphs for DJF and red graphs for JJA) and ERA-Interim profiles (blue squares for DJF and red circles for JJA); bottom: differences between RegCM(UW,EI) and RegCM(HL,EI) (blue graphs for DJF and red graphs for JJA) and between RegCM(HL,EI) and ERA-Interim (blue squares for DJF and red circles for JJA). See Güttler et al. (2013a) for details.

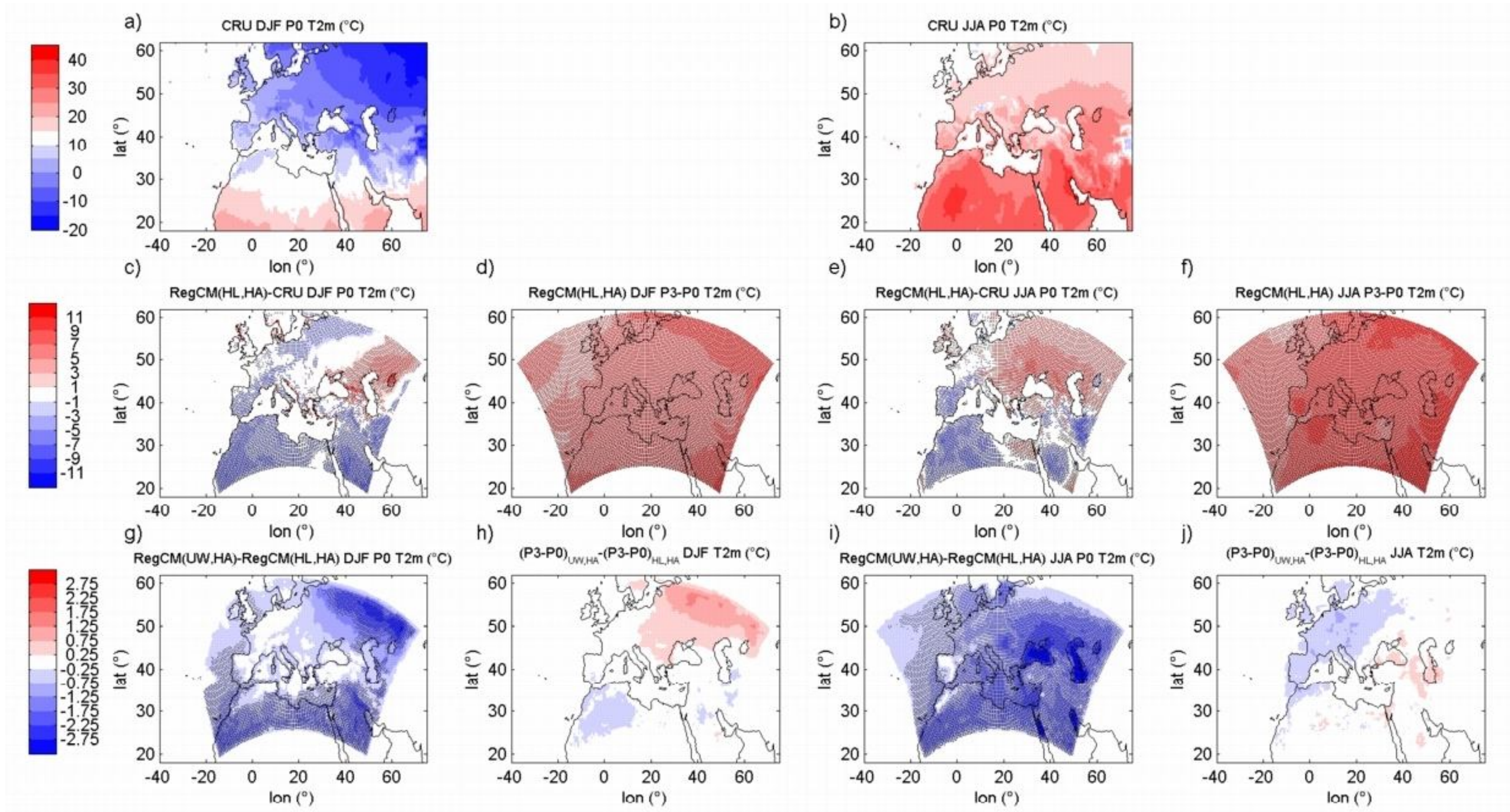

Fig. A4 Mean seasonal air temperature at 2 m *T2m* in CRU TS 3.0 in a) winter (DJF) and b) summer (JJA). RegCM(HL,HA) *T2m* systematic errors when compared to CRU in c) winter and e) summer. The *T2m* climate change signal P3-P0 simulated by RegCM(HL,HA) under the RCP8.5 scenario in d) winter and f) summer. The *T2m* differences between RegCM(UW,HA) and RegCM(HL,HA) in historical P0 period in g) winter and i) summer. Differences in *T2m* climate change signal P3-P0 in RegCM(UW,HL) versus RegCM(HL,HA) simulations. Grid cells where statistically significant differences/changes occur (according to the WMW test and 95% confidence level) in panels c), d), e), f), g) and i) are marked by dots. Periods of analysis: P0: 1971-2000 and P3: 2071-2098. Units are °C.

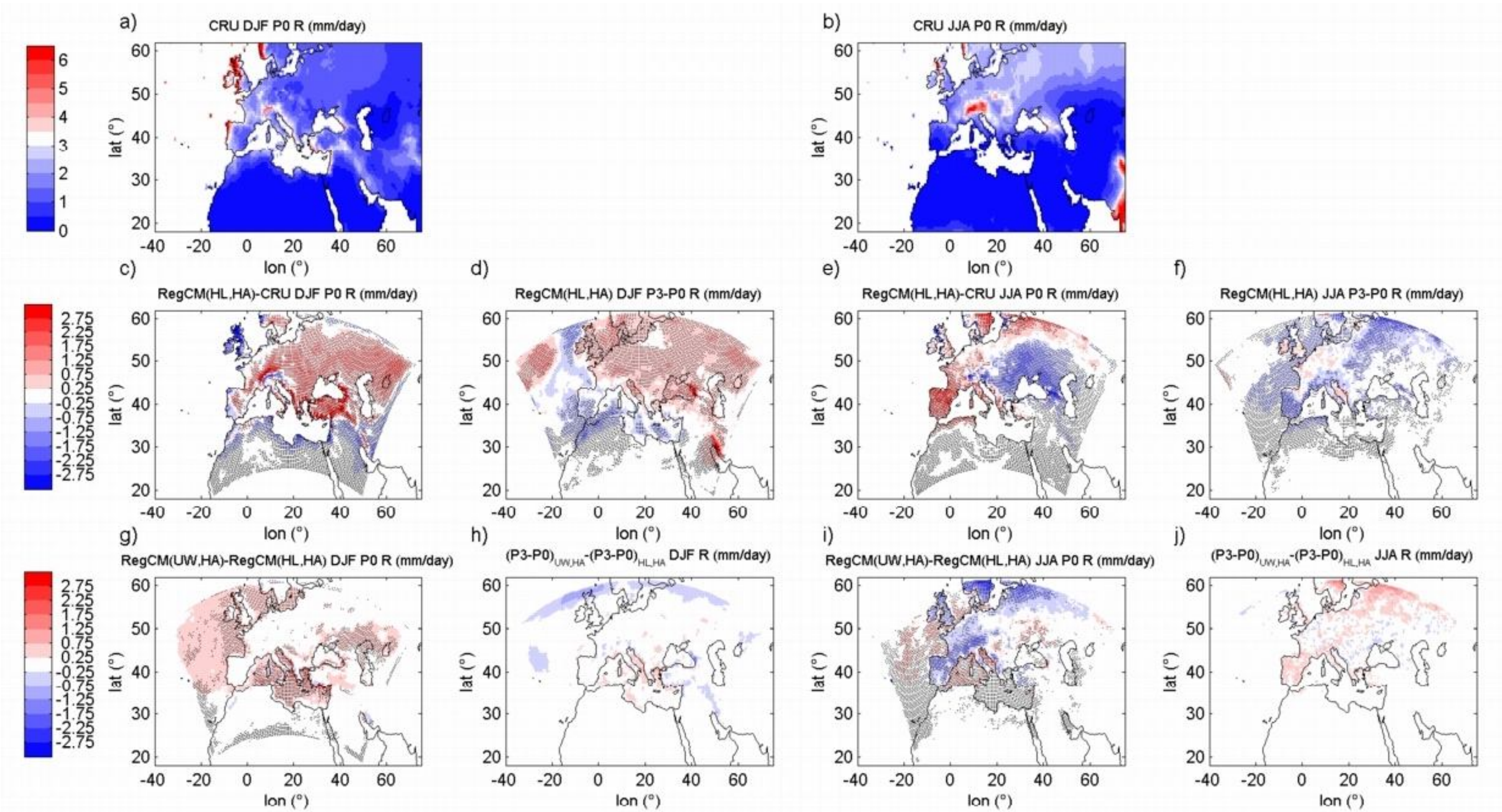


Fig. A5 Same as Fig. A4 but for total precipitation *R*. Units are mm day$^{-1}$.

# 8. REFERENCES


1. Andrews, T. (2009) Forcing and response in simulated $20^{th}$ and $21^{st}$ century surface energy and precipitation trends. *J. Geophys. Res.,*114(D17100), doi: 10.1029/2009JD011749
2. Andrews, T., Forster, P. M., Gregory, J. M. (2009) A surface energy perspective on climate change. *J. Climate,* 22:2557–2570
3. Baklanov, A., Grisogono, B., Bornstein, R., Mahrt, L., Zilitinkevich, S., Taylor, P., Larsen, S., Rotach, M., Fernando, H. J. S. (2011) On the nature, theory, and modeling of atmospheric planetary boundary layers. *Bull. Amer. Meteor. Soc.,* 92:123–128
4. Bellprat, O., Kotlarski, S., Lüthi, D., Schär, C. (2012) Exploring perturbed physics ensembles in a regional climate model. *J. Climate,* 25:4582–4599
5. Berbery, E. H., Mitchell, K. E., Benjamin, S., Smirnova, T., Ritchie, H., Hogue, R., Radeva, E. (1999) Assessment of land–surface energy budgets from regional and global models. *J. Geophys. Res.,*104 (D16):19,329–19,348
6. Berner, J., Jung, T., Palmer T. N. (2012) Systematic model error: the impact of increased horizontal resolution versus improved stochastic and deterministic parameterizations. *J. Climate*, 25: 4946–4962
7. Betts, A. K., Ball, J. H., Beljaars, A. C. M., Miller, M. J., Viterbo, P. A. (1996) The land surface-atmosphere interaction: A review based on observational and global modeling perspectives. *J. Geophys. Res.,*101(D3):7209–7225
8. Betts, A. K., Viterbo, P. (2000) Hydrological budgets and surface energy balance of seven subbasins of the Mackenzie river from the ECMWF model. *J. Hydrometeor.,* 1:47–60
9. Blackadar, A. K. (1962) The vertical distribution of wind and turbulent exchange in a neutral atmosphere. *J. Geophys. Res.,* 67:3095–3102
10. Boberg, F., Christensen, J. H. (2012) Overestimation of Mediterranean summer temperature projections due to model deficiencies. *Nature Climate Change,* 2:433–436
11. Boé, J., Terray, L. (2008) Uncertainties in summer evapotranspiration changes over Europe and implications for regional climate change. *Geophys. Res. Lett.,* 35(L05702), doi:10.1029/2007GL032417
12. Boé, J., Terray, L. (2014) Land-sea contrast, soil-atmosphere and cloud-temperature interactions: interplays and roles in future summer European climate change. *Clim. Dyn.,* 42:683–699
13. Branković, Č., Gregory, D. (2001) Impact of horizontal resolution on seasonal integrations. *Clim. Dyn.*, 18: 123–143
14. Branković, Č., Molteni, F., Viterbo, P. (2006) GCM sensitivity experiments with locally modified

land surface properties over tropical South America. *Clim. Dyn.,* 26:729–749

15. Branković, Č., Patarčić, M., Güttler, I., Srnec, L. (2012) Near-future climate change over Europe with focus on Croatia in an ensemble of regional climate model simulations. *Clim. Res.,* 52:227–251
16. Branković, Č., Güttler, I., Gajić-Čapka, M. (2013) Evaluating climate change at the Croatian Adriatic from observations and regional climate models' simulations. *Clim. Dyn.*, 41:2353–2373
17. Bretherton, C. S., Park, S. (2009) A new moist turbulence parameterization in the Community Atmosphere Model. *J. Climate,* 22:3422–3448
18. Christensen, J. H., Hewitson, B., Busuioc, A., Chen, A., Gao, X., Held, I., Jones, R., Kolli, R. K., Kwon, W.-T., Laprise, R., Magaña Rueda, V., Mearns, L., Menéndez, C. G., Räisänen, J., Rinke, A., Sarr, A., Whetton, P. (2007) Regional climate projections. In: Climate change 2007: The physical science basis. Contribution of Working Group I to the Fourth Assessment Report of the Intergovernmental Panel on Climate Change. Solomon, S. et al. (eds.). Cambridge, UK, and New York, NY: Cambridge University Press
19. Christensen, J. H., Christensen, O. B. (2007) A summary of the PRUDENCE model projections of changes in European climate by the end of this century. *Clim. Change,* 81:7–30
20. Christensen, J. H., Kjellström, E., Giorgi, F., Lenderink, G., Rummukainen, M. (2010) Weight assignment in regional climate models. *Clim. Res.*, 44:179–194
21. Coppola, E., Giorgi, F., Mariotti, L., Bi, X. (2012) RegT-Band: a tropical band version of RegCM4. *Clim. Res.,* 52:115–133
22. Curry, J. A., Webster, P. J. (2011) Climate science and the uncertainty monster. *Bull. Amer. Meteor. Soc.,* 92:1667–1682
23. Cuxart, J., Holtslag, A. A. M., Beare, R. J., Bazile, E., Beljaars, A., Cheng, A., Conangla, L., Ek, M., Freedman, F., Hamdi, R., Kerstein, A., Kitagawa, H., Lenderink, G., Lewellen, D., Mailhot, J., Mauritsen, T., Perov, V., Schayes, G., Steeneveld, G-J., Svensson, G., Taylor, P., Weng, W., Wunsch, S., Xu, K-M. (2006) Single-column model intercomparison for a stably stratified atmospheric boundary layer. *Bound-Layer. Meteor.,* 118:273–303
24. Davis, N., Bowden, J., Semazzi, F., Xie, L., Önol, B. (2009) Customization of RegCM3 regional climate model for eastern Africa and a tropical Indian ocean domain. *J. Climate,* 22:3595–3616
25. Dee, D. P., Uppala, S. M., Simmons, A. J., Berrisford, P., Poli, P., Kobayashi, S., Andrae, U., Balmaseda, M. A., Balsamo, G., Bauer, P., Bechtold, P., Beljaars, A. C. M., van de Berg, L., Bidlot, J., Bormann, N., Delsol, C., Dragani, R., Fuentes, M., Geer, A. J., Haimberger, L., Healy, S. B., Hersbach, H., Hólm, E. V., Isaksen, L., Kållberg, P., Köhler, M., Matricardi, M., McNally, A. P., Monge-Sanz, B. M., Morcrette, J.-J., Park, B.-K., Peubey, C., de Rosnay, P., Tavolato, C.,

Thépaut, J.-N., Vitart, F. (2011) The ERA–Interim reanalysis: configuration and performance of the data assimilation system. *Quart. J. R. Meteorol. Soc.,* 137:553–597

26. Denis, B., Laprise, R., Caya, D., Côté, J. (2002) Downscaling ability of one-way nested regional climate models: the Big-Brother Experiment. *Clim. Dyn.,* 18:627–646
27. Dethloff, K., Abegg, C., Rinke, A., Hebestadt, I., Romanov, V. F. (2001) Sensitivity of Arctic climate simulations to different boundary–layer parameterizations in a regional climate model. *Tellus,* 53A:1–26
28. Diak, G. R., Mecikalski, J. R., Anderson, M. C., Norman, J. M., Kustas, W. P., Torn, R. D., DeWolf, R. L. (2004) Estimating Land Surface Energy Budgets From Space: Review and Current Efforts at the University of Wisconsin-Madison and USDA-ARS. *Bull. Amer. Meteor. Soc.*, 85:65–78
29. Dickinson, R. E., Errico, R. M., Giorgi, F., Bates, G. T. (1989) A regional climate model for western United States. *Clim. Change,* 15:383–422
30. Dickinson, R. E., Henderson-Sellers, A., Kennedy, P. J. (1993) Biosphere-atmosphere transfer scheme (BATS) version 1e as coupled to the NCAR Community Climate Model. NCAR Tech. Note NCAR/TN–387+STR, NCAR, Boulder, Colorado, USA, 72 pp
31. Emanuel, K. A. (1991) A scheme for representing cumulus convection in large-scale models. *J. Atmos. Sci.,* 48:2313–2335
32. Esau, I., Zilitinkevich, S. (2010) On the role of the planetary boundary layer depth in the climate system. *Adv. Sci. Res.,* 4:63–69
33. Fu, Q., Liou, K. N., Grossman, A. (1997) Multiple scattering parameterization in thermal infrared radiative transfer. *J. Atmos. Sci.,* 54:2799–2812
34. Galperin, B., Kantha, L. H., Hassid, S., Rosati, A. (1988) A quasi-equilibrium turbulent energy model for geophysical flows. *J. Atmos. Sci.,* 45:55–62
35. García-Díez, M., Fernández, J., Fita, L., Yagüe, C. (2013) Seasonal dependence of WRF bias and sensitivity to PBL schemes over Europe. *Quart. J. R. Meteorol. Soc.,* 139:501–514
36. Gianotti, R. L., Zhang, D., Eltahir, E. A. B. (2012) Assessment of the Regional Climate Model Version 3 over the maritime continent using different cumulus parameterization and land surface schemes. *J. Climate,* 25:638–656
37. Giorgi, F., Mearns, L. O. (1991) Approaches to the simulation of regional climate change: A review. *Reviews of Geophysics,* 29(2):191–216
38. Giorgi, F., Marinucci, M. R., Bates, G. T. (1993) Development of a second–generation Regional Climate Model (RegCM2). Part I: Boundary-layer and radiative transfer processes. *Mon. Wea. Rev.,* 121:2794–2813

39. Giorgi, F., Mearns, L. O. (1999) Introduction to special section: Regional climate modelling revisited. *J. Geophys. Res.,* 104(D6):6335–6352
40. Giorgi, F. (2006) Climate change hot-spots. *Geophys. Res. Lett.*, 33(L08707), doi: 10.1029/2006GL025734
41. Giorgi, F., Coppola, E. (2010) Does the model regional bias affect the projected regional climate change? An analysis of global model projections. *Clim. Change,* 100:787–795
42. Giorgi, F., Elguindi, N., Cozzini, S., Giuliani, G. (2011) Regional Climatic Model RegCM User's Guide Version 4.2. Earth System Physics Section, The Abdus Salam International Centre for Theoretical Physics, Trieste, Italy
43. Giorgi, F., Coppola, E., Solmon, F., Mariotti, L., Sylla, M. B., Bi, X., Elguindi, N., Diro, G. T., Nair, V., Giuliani, G., Cozzini, S., Güttler, I., O'Brien, T. A., Tawfik, A. B., Shalaby, A., Zakey, A. S., Steiner, A. L., Stordal, F., Sloan, L. C., Brankovic, C. (2012) RegCM4: Model description and preliminary tests over multiple CORDEX domains. *Clim. Res.,* 52:7–29
44. Grell, G. A. (1993) Prognostic evaluation of assumptions used by cumulus parameterizations. *Mon. Wea. Rev.,* 121:764–787
45. Grenier, H., Bretherton, C. S. (2001) A moist PBL parameterization for large–scale models and its application to subtropical cloud–topped marine boundary layers. *Mon. Wea. Rev.,* 129:357–377
46. Grisogono, B. (2010) Generalizing 'z–less' mixing length for stable boundary layers. *Quart. J. R. Meteorol. Soc.,* 136:213–221
47. Gupta, S. K., Darnell, W. L., Wilber, A. C. (1992) A parameterization for longwave surface radiation from satellite data: Recent improvements. *J. Appl. Meteor.,* 31:1361–1367
48. Gupta, S. K., Kratz, D. P., Stackhouse Jr, P. W., Wilber, A. C. (2001) The Langley Parameterized Shortwave Algorithm for surface radiation budget studies (Vers. 1.0). NASA/TP–2001–211272, 31 pp
49. Gupta, S. K., Stackhouse Jr, P. W., Cox, S. J., Mikovitz, J. C., Zhang T (2006) Surface radiation budget project completes 22–year data set. *GEWEX WCRP News,* 16:12–13
50. Gutowski, W.J., Gutzler, D.S., Wang, W.-C. (1991) Surface energy balances of three general circulation models: Implications for simulating regional climate change. *J. Climate,* 4:121–134
51. Güttler, I. (2011) Reducing warm bias over the north-eastern Europe in a regional climate model. *Hrvatski Meteorološki Časopis/Croatian Meteorological Journal,* 44/45:19–29
52. Güttler, I., Branković, Č., O'Brien, T.A., Coppola, E., Grisogono, B., Giorgi, F. (2013a) Sensitivity of the regional climate model RegCM4.2 to planetary boundary layer parameterisation. *Clim. Dyn.*, doi:10.1007/s00382-013-2003-6
53. Güttler, I., Brankovič, Č., Srnec, L., Patarčić, M. (2013b) The impact of boundary forcing on

RegCM4.2 surface energy budget. *Clim. Change*, doi:10.1007/s10584-013-0995-x

54. Haylock, M. R., Hofstra, N., Klein Tank, A. M. G., Klok, E. J., Jones, P. D., New, M. (2008) A European daily high-resolution gridded dataset of surface temperature and precipitation. *J. Geophys. Res.* 113(D20), doi: 10.1029/2008JD010201
55. Holtslag, A. A. M., de Bruijn, E. I. F., Pan, H. L. (1990) A high resolution air mass transformation model for short-range weather forecasting. *Mon. Wea. Rev.,* 118:1561–1575
56. Holtslag, A. A. M., Moeng, C.-H. (1991) Eddy diffusivity and countergradient transport in the convective atmospheric boundary layer. *J. Atmos. Sci.,* 48:1690–1698
57. Holtslag, A. A. M., Boville, B. (1993) Local versus nonlocal boundary-layer diffusion in a global climate model. *J. Climate,* 6:1825–1842
58. Holtslag, A. A. M., Svensson, G., Baas, P., Basu, S., Beare, B., Beljaars, A. C. M., Bosveld, F. C., Cuxart, J., Lindvall, J., Steeneveld, G. J., Tjernström, M., Van De Wiel, B. J .H. (2013) Stable atmospheric boundary layers and diurnal cycles: Challenges for weather and climate models. *Bull. Amer. Meteor. Soc.*, 94:1691–1706
59. Hu, X.-M., Nielsen-Gammon, J. W., Zhang, F. (2010) Evaluation of three planetary boundary-layer schemes in the WRF model. *J. Appl. Meteor. Climatol.,* 49:1831–1844
60. Hunt, J. C. R., Olafsson, H., Bougeault, P. (2001) Coriolis effects on orographic and mesoscale flows. *Quart. J. R. Meteorol. Soc.*, 127: 601–633
61. Jacob, D., Bärring, L., Christensen, O. B., Christensen, J. H., de Castro, M., Déqué, M., Giorgi, F., Hagemann, S., Hirschi, M., Jones, R., Kjellström, E., Lenderink, G., Rockel, B., Sánchez, E., Schär, C., Seneviratne, S. I., Somot, S., van Ulden, A., van den Hurk, B. (2007) An inter-comparison of regional climate models for Europe: model performance in present-day climate. *Climatic Change,* 81:31–52
62. Jacob, D., Petersen, J., Eggert, B., Alias, A., Christensen, O. B., Bouwer, L. M., Braun, A., Colette, A., Déqué, M., Georgievski, G., Georgopoulou, E., Gobiet, A., Menut, L., Nikulin, G., Haensler, A., Hempelmann, N., Jones, C., Keuler, K., Kovats, S., Kröner, N., Kotlarski, S., Kriegsmann, A., Martin, E., van Meijgaard, E., Moseley, C., Pfeifer, S., Preuschmann, S., Radermacher, C., Radtke, K., Rechid, D., Rounsevell, M., Samuelsson, P., Somot, S., Soussana, J.-F., Teichmann, C., Valentini, R., Vautard, R., Weber, B., Yiou, P. (2013) EURO-CORDEX: new high-resolution climate change projections for European impact research. *Reg. Environ. Change.*, doi: 10.1007/s10113-013-0499-2
63. Jaeger, E.B., Anders, I., Lüthi, D., Rockel, B., Schär, C., Senevirante, S. (2008) Analysis of ERA-40 driven CLM simulations for Europe. *Meteorol. Z.,* 17(4):349–367

64. Jaeger, E. B., Stöckli, R., Seneviratne S. I. (2009) Analysis of planetary boundary layer fluxes and land-atmosphere coupling in the regional climate model CLM. *J. Geophys. Res.*, 114(D17106), doi: 10.1029/2008JD011658

65. Jerez, S., Montavez, J. P., Gomez-Navarro, J. J., Lorente-Plazas, R., Garcia-Valero, J. A., Jimenez-Guerrero, P. (2013) A multi-physics ensemble of regional climate change projections over the Iberian Peninsula. *Clim. Dyn.,* 41:1749–1768

66. Jones, C. D., Hughes, J. K., Bellouin, N., Hardiman, S. C., Jones, G. S., Knight, J., Liddicoat, S., O'Connor, F. M., Andres, R. J., Bell, C., Boo, K.-O., Bozzo, A., Butchart, N., Cadule, P., Corbin, K. D., Doutriaux-Boucher, M., Friedlingstein, P., Gornall, J., Gray, L., Halloran, P. R., Hurtt, G., Ingram, W. J., Lamarque, J.-F., Law, R. M., Meinshausen, M., Osprey, S., Palin, E. J., Parsons Chini, L., Raddatz, T., Sanderson, M. G., Sellar, A. A., Schurer, A., Valdes, P., Wood, N., Woodward, S., Yoshioka, M., Zerroukat, M. (2011) The HadGEM2-ES implementation of CMIP5 centennial simulations. *Geosci. Model. Dev.,* 4:543–570

67. Karlsson, K.-G., Riihelä, A., Müller, R., Meirink, J. F., Sedlar, J., Stengel, M., Lockhoff, M., Trentmann, J., Kaspar, F., Hollmann, R., Wolters, E. (2013) CLARA-A1: the CM SAF cloud, albedo and radiation dataset from 28 yr of global AVHRR data. *Atmos. Chem. Phys. Discuss.,* 13:935–982

68. Kiehl, J., Hack, J., Bonan, G., Boville, B., Breigleb, B., Williamson, D., Rasch, P. (1996) Description of the NCAR Community Climate Model (CCM3). NCAR Tech. Note NCAR/TN-420+STR. NCAR, Boulder, Colorado, USA, 152 pp

69. Kim, J., Waliser, D. E., Mattmann, C. A., Goodale, C. E., Hart, A. F., Zimdars, P. A., Crichton, D. J., Jones, C., Nikulin, G., Hewitson, B., Jack, C., Lennard, C., Favre, A. (2013) Evaluation of the CORDEX-Africa multi–RCM hindcast: systematic model errors. *Clim. Dyn.*, doi: 10.1007/s00382-013-1751-7

70. Knight, C. G., Knight, S. H. E., Massey, N., Aina, T., Christensen, C., Frame, D. J., Kettleborough, J. A., Martin, A., Pascoe, S., Sanderson, B., Stainforth, D. A., Allen, M. R. (2007) Association of parameter, software, and hardware variation with large–scale behaviour across 57,000 climate models. *Proc. Natl. Acad. Sci. USA,* 104:12259–12264

71. Kondratyev, K. Ya. (1969) Radiation in the Atmosphere. Academic Press, New York, 873 pp

72. Kothe, S., Ahrens, B. (2010) On the radiation budget in regional climate simulations for West Africa. *J. Geophys. Res.,* 115(D23120), doi: 10.1029/2010JD014331

73. Kothe, S., Dobler, A., Beck, A., Ahrens, B. (2011) The radiation budget in a regional climate model. *Clim. Dyn.,* 36:1023–1036

74. Laprise, R., de Elía, R., Caya, D., Biner, S., Lucas-Picher, P., Diaconescu, E., Leduc, M., Alexandru, A., Separovic, L., Canadian Network for Regional Climate Modelling and Diagnostics (2008) Challenging some tenets of Regional Climate Modelling. *Meteorology and Atmospheric Physics,* 100:3–22
75. Lenderink, G., van Ulden, A., van den Hurk, B., van Meijgaard, E. (2007) Summertime inter-annual temperature variability in an ensemble of regional climate model simulations: analysis of the surface energy budget. *Climatic Change,* 81:233–247
76. Lesins, G., Duck, T. J., Drummond, J. R. (2012) Surface energy balance framework for Arctic amplification of climate change. *J. Climate,* 25: 8277–8288
77. Mahrt, L., Vickers, D. (2003) Formulation of turbulent fluxes in the stable boundary layer. *J. Atmos. Sci.,* 60:2538–2548
78. Manabe, S., Spelman, M. J., Stouffer, R. J. (1992) Transient responses of a coupled ocean-atmosphere model to gradual changes of atmospheric $CO_2$. Part II: Seasonal Response. *J. Climate,* 5:105–126
79. Markovic, M., Jones, C. G., Winger, K., Paquin, D. (2009) The surface radiation budget over North America: gridded data assessment and evaluation of regional climate models. *Int. J. Climatol.,* 29: 2226–2240
80. Martin, G. M., Bellouin, N., Collins, W. J. and Coauthors. (2011) The HadGEM2 family of Met Office Unified Model climate configurations. *Geosci. Model Dev.*, 4: 723–757
81. Mauritsen, T., Svensson, G., Zilitinkevich, S. S., Esau, I., Enger, L., Grisogono, B. (2007) A total turbulent energy closure model for neutrally and stably stratified atmospheric boundary layers. *J. Atmos. Sci.,* 64: 4113–4126
82. McGregor, J.L. (1997) Regional Climate Modelling. *Meteorology and Atmospheric Physics*, 63:105–117
83. Mearns, L. O., Arritt, R., Biner, S., Bukovsky, M. S., McGinnis, S., Sain, S., Caya, D., Correia Jr., J., Flory, D., Gutowski, W., Takle, E. S., Jones, R., Leung, R., Muofouma-Okia, W., McDaniel, L., Nunes, A. M. B., Qian, Y., Roads, J., Sloan, L., Snyder, M. (2012) The North American Regional Climate Change Assessment Program: overview of Phase I results. *Bull. Amer. Meteor. Soc.,* 93: 1337–1362
84. Medeiros, B., Hall, A., Stevens, B. (2005) What controls the mean depth of the PBL? *J. Climate,* 18:3157–3172
85. Mellor, G., Yamada, T. (1982) Development of a turbulence closure model for geophysical fluid problems. *Rev. Astrophys. Space. Phys.,* 20:851–875
86. Mitchell, T. D., Jones, P. D. (2005) An improved method of constructing a database of monthly

climate observations and associated high–resolution grids. *Int. J. Climatol.,* 25:693–712

87. Moss, R. H., Edmonds, J. A., Hibbard, K. A., Manning, M. R., Rose, S. K., van Vuuren, D. P., Carter, T. R., Emori, S., Kainuma, M., Kram, T., Meehl, G. A., Mitchell, J. F. B., Nakicenovic, N., Riahi, K., Smith, S. J., Stouffer, R. J., Thomson, A. M., Weyant, J. P., Wilbanks, T. J. (2010) The next generation of scenarios for climate change research and assessment. *Nature,* 463:747–756
88. Murphy, J. M., Sexton, D. M. H., Barnett, D. N., Jones, G. S., Webb, M. J., Collins, M., Stainforth, D.A. (2004) Quantification of modelling uncertainties in a large ensemble of climate change simulations. *Nature,* 430:768–772
89. Nicholls, S., Turton, J. D. (1986) Observational study of the structure of stratiform cloud layers. Part II: Entrainment. *Quart. J. R. Meteorol. Soc.,* 112:461–480
90. Nieuwstadt, F. T. M. (1984) The turbulent structure of the stable, nocturnal boundary layer. *J. Atmos. Sci.,* 41: 2202–2216
91. Nogherotto, R., Coppola, E., Giorgi, F., Mariotti, L. (2013) Impact of Congo Basin deforestation on the African monsoon. *Atmos. Sci. Let.,* 14:45–51
92. Noguer, M., Jones, R., Murphy, J. (1998) Sources of systematic errors in the climatology of a regional climate model over Europe. *Clim. Dyn.,* 14:691−712
93. O'Brien, T. A., Chuang, P. Y., Sloan, L. C., Faloona, I. C., Rossiter, D. L. (2012) Coupling a new turbulence parametrization to RegCM adds realistic stratocumulus clouds. *Geosci. Model Dev. Discuss.,* 5:989–1008
94. Ozturk, T., Altinsoy, H., Türkeş, M., Kuranz, M. L. (2012) Simulation of temperature and precipitation climatology for the Central Asia CORDEX domain using RegCM 4.0. *Clim. Res.,* 52: 63–76
95. Pal, J. S., Small, E. E., Eltahir, E. A. B. (2000) Simulation of regional–scale water and energy budgets: representation of subgrid cloud and precipitation processes within RegCM. *J. Geophys. Res.,* 105(D24):29,579–29,594
96. Pal, J. S., Giorgi, F., Bi, X., Elguindi, N., Solmon, F., Gao, X., Rauscher, S. A., Francisco, R., Zakey, A., Winter, J., Ashfaq, M., Syed, F. S., Bell, J. L., Diffenbaugh, N. S., Karmacharya, J., Konaré, A., Martinez, D., Da Rocha, R. P., Sloan, L. C., Steiner, A. L. (2007) Regional climate modeling for the developing world: The ICTP RegCM3 and RegCNET. *Bull. Amer. Meteor. Soc.,* 88:1395–1409
97. Park, S., Bretherton, C. H. (2009) The University of Washington shallow convection and moist turbulence schemes and their impact on climate simulations with the Community Atmosphere Model. *J. Climate,* 22:3349–3469

98. Perkins, S. E., Pitman, A. J., Holbrook, N. J., McAneney, J. (2007) Evaluation of the AR4 climate models' simulated daily maximum temperature, minimum temperature, and precipitation over Australia using probability density functions. *J. Climate,* 20:4356–4376

99. Pielke, R.A., Sr. (2002) Mesoscale meteorological modeling. 2nd Edition, Academic Press, San Diego, CA, 676 pp

100. Pinker, R. T., Laszlo, I. (1992) Modeling surface solar irradiance for satellite applications on a global scale. *J. Appl. Meteor.,* 31:194–211

101. Pitman, A. J. (2003) The evolution of, and revolution in, land surface schemes designed for climate models: A review. *Int. J. Climatol.,* 23:479–510

102. Pope, V. D., Stratton, R. A. (2002) The processes governing horizontal resolution sensitivity in a climate model. *Clim. Dyn*., 19:211–236

103. Reboita, M. S., da Rocha, R. P., Ambrizzi, T., Caetano, E. (2010) An assessment of the latent and sensible heat flux on the simulated regional climate over Southwestern South Atlantic Ocean. *Clim. Dyn.,* 34:873–889

104. Rowell, D. P., Jones, R. G. (2006) Causes and uncertainty of future summer drying over Europe. *Clim. Dyn.,* 27:281–299

105. Rummukainen, M. (2010) State-of-the-art with regional climate models. *WIREs: Climatic Change*, 1(1):82–96

106. Sánchez, E., Yagüe, C., Gaertner, M. A. (2007) Planetary boundary layer energetics simulated from a regional climate model over Europe for present climate and climate change conditions. *Geophys. Res. Lett.,* 34(L01709), doi:10.1029/2006GL028340

107. Schär, C., Lüthi, D., Beyerle, U., Heise, E. (1999) The soil-precipitation feedback: a process study with a regional climate model. *J. Climate,* 12:722–741

108. Seneviratne, S. I., Lüthi, D., Litschi, M., Schär, C. (2006) Land-atmosphere coupling and climate change in Europe. *Nature,* 443:205–209

109. Seneviratne, S. I., Corti, T., Davin, E. L., Hirschi, M., Jaeger, E. B., Lehner, I., Orlowsky, B., Teuling, A. J. (2010) Investigating soil moisture–climate interactions in a changing climate: A review. *Earth-Science Reviews*, 99:125–161

110. Shin, S.-H., Ha, K.-J. (2007) Effects of spatial and temporal variations in PBL depth on a GCM. *J. Climate,* 20:4717–4732

111. Shi, X. L., Chan, J. C. L., Chow, K. C., Ding, Y. (2008) Effects of upstream surface heat fluxes on the evolution of the South China Sea summer monsoon. *Meteorology and Atmospheric Physics,* 100:303–325

112. Solmon, F., Elguindi, N., Mallet, M. (2012) Radiative and climatic effects of dust over West

Africa, as simulated by a regional climate model. *Clim. Res.,* 52:97–113

113. Stackhouse Jr., P. W., Gupta, S. K., Cox, S. J., Zhang, T., Mikovitz, J. C., Hinkelman, L. M. (2011) 24.5–Year Surface Radiation Budget Data Set Released. *GEWEX WCRP News,* 21:9–11
114. Stainforth, D. A., Aina, T., Christensen, C., Collins, M., Faull, N., Frame, D. J., Kettleborough, J. A., Knight, S., Martin, A., Murphy, J. M., Piani, C., Sexton, D., Smith, L. A., Spicer, R. A., Thorpe, A. J., Allen, M. R. (2005) Uncertainty in predictions of the climate response to rising levels of greenhouse gases. *Nature,* 433:403–406
115. Stainforth, D. A., Allen, M. R., Tredger, E. R., Smith, L. A. (2007) Confidence, uncertainty and decision–support relevance in climate predictions. *Philos. Trans. Roy. Soc. London,* A365: 2145–2161
116. Steiner, A. L., Pal, J. S., Giorgi, F., Dickinson, R. E., Chameides, W. L. (2005) The coupling of the Common Land Model (CLM0) to a regional climate model (RegCM). *Theor. Appl. Climatol.,* 82:225–243
117. Steiner, A. L., Pal, J. S., Rauscher, S. A., Bell, J. L., Diffenbaugh, N. S., Boone, A., Sloan, L. C., Giorgi, F. (2009) Land surface coupling in regional climate simulations of the West African monsoon. *Clim. Dyn.,* 33:869–892
118. Stensrud, D. J. (2007) Parameterization Schemes: Keys to Understanding Numerical Weather Prediction Models. Cambridge University Press, New York, 459 pp
119. Stephens, G. L., Li, J., Wild, M., Clayson, C. A., Loeb, N., Kato, S., L'Ecuyer, T., Stackhouse Jr., P. W., Lebsock, M., Andrews, T. (2012) An update on Earth's energy balance in light of the latest global observations. *Nature Geoscience*, 5:691–696
120. Stewart, R. W. (1979) The Atmospheric Boundary Layer, WMO No 523, World Meteorological Organization, Geneva, 44 pp
121. Stull, R. B. (1988) An introduction to boundary layer meteorology. Kluwer Academic Publishers, Dordrecht, 666 pp
122. Suklitsch, M., Gobiet, A., Truhetz, H., Awan, N. K., Göttel, H., Jacob, D. (2011) Error characteristics of high resolution regional climate models over the Alpine region. *Clim. Dyn.,* 37:377–390
123. Sylla, M. B., Coppola, E., Mariotti, L., Giorgi, F., Ruti, P. M., Dell'Aquila, A., Bi, X. (2010) Multiyear simulation of the African climate using a regional climate model (RegCM3) with the high–resolution ERA–Interim reanalysis. *Clim. Dyn.,* 35:231–247
124. Sylla, M. B., Giorgi, F., Stordal, F. (2012) Large–scale origins of rainfall and temperature bias in high resolution simulations over southern Africa. *Clim. Res.,* 52:193–211

125. Tang, Q., Leng, G., Groisman, P. Ya. (2012) European hot summers associated with a reduction of cloudiness. *J. Climate,* 25:3637–3644
126. Tebaldi, C., Knutti, R. (2007) The use of the multi–model ensemble in probabilistic climate projections. *Philos. Trans. Roy. Soc. London,* A365, 2053–2075
127. Torma, Cs., Giorgi, F. (2014) Assessing the contribution of different factors in regional climate model projections using the factor separation method. *Atmos. Sci. Let.* doi:10.1002/asl2.491
128. Trenberth, K. E., Fasullo, J. T., Kiehl, J. (2009) Earth's global energy budget. *Bull. Amer. Meteor. Soc.,* 90:311–323
129. Troen, I. B., Mahrt, L. (1986) A simple model of the atmospheric boundary layer: sensitivity to surface evaporation. *Bound-Layer. Meteor.,* 37:129–148
130. Tsuang, B.-J (2005) Ground heat flux determination according to land skin temperature observations from in situ stations and satellites. *J Hydrometeor.*, 6:371–390
131. Van de Berg, W. J., van den Broeke, M. R., van Meijgaard, F. (2007) Heat budget of the East Antarctic lower atmosphere derived from a regional atmospheric climate model. *J. Geophys. Res.,* 112, D23101, doi:10.1029/2007JD008613
132. Walter, K. M., Zimov, S. A., Chanton, J. P., Verbyla, D., Chapin III, F. S. (2006) Methane bubbling from Siberian thaw lakes as a positive feedback to climate warming. *Nature,* 443:71–75
133. Wang, Y., Leung, L. R., McGregor, J. L., Lee, D. K., Wang, W. C., Ding, Y. H., Kimura, F. (2004) Regional Climate Modeling: Progress, Challenges, and Prospects. *Journal of the Meteorological Society of Japan,* 82(6):1599–1628
134. Wilks, D. S. (2006) Statistical methods in the atmospheric sciences, 2nd edn. Elsevier Academic Press, San Diego, 627 pp
135. Winter, J. M., Pal, J. S., Eltahir, E. A. B. (2009) Coupling of Integrated Biosphere Simulator to Regional Climate Model Version 3. *J. Climate,* 22:2743–2757
136. Winter, J. M., Eltahir, E. A. B. (2010) The sensitivity of latent heat flux to changes in the radiative forcing: a framework for comparing models and observations. *J. Climate,* 23:2345–2356
137. Winton, M. (2006) Surface albedo feedback estimates for the AR4 climate models. *J. Climate,* 19:359–365
138. Wyngaard, J. C. (1985) Structure of the planetary boundary layer and implications for its modeling. *J. Clim. Appl. Meteorol.* 24:1131–1142
139. Xie, B., Fung, J. C. H., Chan, A., Lau, A. (2012) Evaluation of nonlocal and local planetary boundary layer schemes in the WRF model. *J. Geophys. Res.,* 117(D12103) doi:10.1029/2011JD017080
140. Yang, Z., Arritt, R. W. (2002) Test of a perturbed physics ensemble approach for regional

climate modeling. *J. Climate,* 15:2881–2986

141. Zhang, Y., Xie, S., Covey, C., Lucas, D. D., Gleckler, P., Klein, S. A., Tannahill, J., Doutriaux, C., Klein, R. (2012) Regional assessment of the parameter–dependent performance of CAM4 in simulating tropical clouds. *Geophys. Res. Lett.,* 39(L14708), doi:10.1029/2012GL052184
142. Zhu, P., Bretherton, C. S., Köhler, M., Cheng, A., Chlond, A., Geng, Q., Austin, P., Golaz, J.-C., Lenderink, G., Lock, A., Stevens, B. (2005) Intercomparison and interpretation of single-column model simulations of a nocturnal stratocumulus-topped marine boundary layer. *Mon. Wea. Rev.,* 133:2741–275

# 9. PROŠIRENI SAŽETAK

*9.1 Uvod*

Atmosferska i oceanska strujanja te izmjena količine gibanja, mase i energije između različitih sastavnica klimatskog sustava mogu se matematički formulirati u obliku numeričkog klimatskog modela. Klimatske modele možemo dijeliti na globalne i regionalne modele ovisno o domeni za koju se simulira klimatski sustav. Regionalni modeli koriste se za dinamičku prilagodbu prošlog, sadašnjeg i mogućeg budućeg stanja klime koja se izvorno može simulirati globalnim klimatskim modelima, atmosferskim reanalizama ili sezonskim prognozama (npr. Wang i sur. 2004). Pri tome je dinamička prilagodba metoda kojom se simulacije na gruboj prostornoj rezoluciji (s prostornim korakom od npr. 100 do 300 km) mogu regionalizirati na finiju prostornu rezoluciju (od npr. 10 do 50 km). U ovoj disertaciji, klima i njena promjenjivost na području Europe bit će istražena koristeći regionalni klimatski model RegCM (Pal i sur. 2007, Giorgi i sur. 2012). Za područje Europe je porast prostorne rezolucije na nekoliko desetaka kilometara ključan zbog značajne prostorne promjenjivosti i složenosti podloge, topografije i obale (npr. Branković i sur. 2013).

U smislu fizikalnih i matematičkih pretpostavki, regionalni klimatski modeli su slični numeričkim modelima za prognozu vremena. Prve regionalne klimatske simulacije opisane su u Dickinson i sur. (1989), a pregledi metodologije dani su u npr. Giorgi i Mearns (1991), McGregor (1997), Giorgi i Mearns (1999), Wang i sur. (2004), Laprise i sur. (2008) i Rummukainen (2010).

Usporedba rezultata klimatskih modela s mjerenjima može pružiti uvid u sustavne pogreške modela. Iako se amplituda i predznak sustavnih pogreška mogu razlikovati od modela do modela te ovise o području i sezoni koji se analiziraju, uobičajene srednje sezonske pogreške su na području Europe ±2.5°C za temperaturu zraka na 2 m te ±1.5 mm dan$^{-1}$ za ukupnu količinu oborine (Jacob i sur. 2007; Christensen i sur. 2010). Sustavne pogreške mogu biti izvorne pogreške samog regionalnog modela (zbog npr. nedostajućih ili nepotpuno uvaženih procesa) ili mogu biti unesene preko rubnih uvjeta iz globalnog modela ili reanalize (Noguer i sur. 1998). Važan izvor razlika između pojedinih modela jest u formulaciji fizikalnih procesa na prostornoj skali manjoj od one koja je razlučena na diskretnoj mreži modela. Tako na primjer model s prostornim korakom od 50 km ne može razlučiti pojedinačne oblake, turbulentne vrtloge, različite vrste atmosferskih valova, mikrofizikalne procese u oblacima, međudjelovanje zračenja i atmosferskih plinova, itd. Nerazlučeni procesi su stoga uključeni u model u obliku parametrizacija, tj. empiričkih ili poluempiričkih pristupa koji su temeljeni na izravnim mjerenjima u atmosferi, laboratorijskim mjerenjima i/ili na numeričkim simulacijama s finijom prostornom rezolucijom na kojoj su sami procesi razlučeni. Zbog brojnih mogućih pristupa ovom problemu, prisutna je velika različitost parametrizacija u klimatskim modelima. Primjeri ranijih istraživanja u kojima se za RegCM model istraživao utjecaj različitih parametrizacija ili utjecaj detalja određene parametrizacije na sustavne pogreške modela uključuju Pal i sur. (2000), Yang i Arritt (2002), Steiner i sur. (2005), Davis i sur. (2009), Gianotti i sur. (2012) i O'Brien i sur. (2012). Fokus ove disertacije su sustavne pogreške regionalnog klimatskog modela RegCM u nižoj atmosferi i pri tlu te uspješnost i prikladnost parametrizacija za turbulentno miješanje u atmosferskom (planetarnom) graničnom sloju (eng. *Planetary Boundary Layer*; PBL). Rezultati RegCM model bit će uspoređeni i diskutirani u odnosu na rezultate drugih klimatskih modela.

### *9.2 Metodologija*

U disertaciji se analiziraju dva osnovna skupa simulacija. U prvom skupu simulacija, RegCM je forsiran ERA-Interim reanalizom (Dee i sur. 2011) a domenu čini područje čitave Europe (Slika 2.1a) u razdoblju 1989.-1998. Ovim eksperimentima su pridružene oznake RegCM(HL,EI) i RegCM(UW,EI) gdje HL označava korištenje Holtslagove parametrizacije za procese u PBL-u, a UW označava korištenje parametrizacije razvijene na Sveučilištu Washington u SAD-u (*University of Washington*). RegCM(HL,EI) i RegCM(UW,EI) eksperimenti su analizirani u trećem i četvrtom poglavlju. U drugom skupu eksperimenata, RegCM je forsiran globalnim modelom HadGEM2-ES (Jones i sur. 2011) a domenu čini područje južne Europe i Sredozemlja (Slika 2.1b) za razdoblje 1971.-2098., pri čemu se od prosinca 2005. koriste scenariji koncentracije stakleničkih plinova RCP4.5 i RCP8.5 (Moss i sur. 2010). Ovim eksperimentima pridružene su oznake RegCM(HL,HA) i RegCM(UW,HA) te su analizirani u petom poglavlju.

Za procjenu sustavnih pogrešaka RegCM-a korišteni su CRU TS 3.0 (Mitchell i Jones 2005) i E-OBS 7.0 (Haylock i sur. 2008) podaci o ukupnoj količini oborine i temperaturi zraka na

2 m, satelitski podaci za ukupnu naoblaku i različite komponente zračenja iz GEWEX/SRB 3.0 (Gupta i sur. 2006) i CM SAF CLARA-A1 (Karlsson i sur. 2013) te stanična mjerenja turbulentnih tokova topline na lokacijama četiri postaje unutar mreže C-SRNWP (http://www.cosmo-model.org/srnwp/content/). Za veličine za koje nisu dostupna mjerenja na potrebnoj rezoluciji ili domeni (npr. turbulentni tokovi topline na cijelom području Europe), korištena je ERA-Interim reanaliza kao reprezentativan izvor podataka.

Godišnji hodovi odabranih veličina te vertikalni profili srednjih sezonskih polja analizirani su detaljnije za četiri područja karakterizirana različitim klimatskim svojstvima: dio Rusije u sjeveroistočnoj Europi, istočna Europa, sjeverna Afrika i dijelovi Sahare te kopneni dio u području Sredozemlja (Slika 2.1).

### *9.3 Sustavne pogreške u prizemnim varijablama*

U trećem poglavlju su srednje sezonske i mjesečne pogreške temperature zraka na 2 m *T2m* i količine oborine u RegCM simulacijama analizirane i povezane sa sustavnim pogreškama modela u komponentama energetske ravnoteže na površini. Dodatno, ukupna količina naoblake i albedo površine su povezani sa simuliranim i opaženim poljima zračenja. U trećem se poglavlju istražuje da li su sustavne pogreške RegCM modela koji koristi Holtslagovu parametrizaciju smanjene ukoliko se primjeni UW parametrizacija.

U referentnoj RegCM(HL,EI) simulaciji, *T2m* je podcijenjen u odnosu na CRU na području sjeverne Afrike tijekom zime s pogreškama u rasponu između -4 °C i -2 °C (Slika 3.1a). U središnjim dijelovima domene pogreške u *T2m* su između -1 °C i 1 °C. U sjevernim i sjeveroistočnim dijelovima domene RegCM(HL,EI) precjenjuje *T2m*, općenito u rasponu između 2 °C i 4 °C. U istom području je još i veće precjenjivanje *T2m* prisutno u ranijim verzijama RegCM-a te je povezano s nedostacima u simuliranju vrlo hladnih i statičkih stabilnih uvjeta povezanih s povećanom naoblakom (Güttler 2011). Pozitivne pogreške u temperaturi tijekom zime u RegCM simulacijama su detektirane i za ostala područja: npr. Sjeverna Amerika (Mearns i sur. 2012) i središnja Azija (Ozturk i sur. 2012). Tijekom ljeta, znatne se sustavne pogreške u *T2m* mogu pronaći u središnjim dijelovima Europe, i to u rasponu između 2 °C i 4 °C (Slika 3.1c).

Pogreške pozitivnog predznaka tijekom ljeta u središnjem dijelu domene te tijekom zime u sjeveroistočnom dijelu domene su smanjene u RegCM(UW,EI) simulaciji i iznose između 1 °C i 2 °C (Slika 3.1b,d). Međutim, pogreške negativnog predznaka tijekom zime u području sjeverne Afrike su povećane u RegCM(UW,EI) simulaciji. Općenito snižavanje *T2m* prilikom korištenja UW parametrizacije je dokumentirano u O'Brien i sur. (2012) za simulacije nad područjem Sjeverne Amerike. Unatoč povećanju pogrešaka u temperaturi na području sjeverne Afrike, primjenom UW parametrizacije ostvaruje se općenito poboljšanje simulirane temperature zraka na 2 m u RegCM modelu.

U RegCM(UW,EI) simulacijama nalazimo veću ukupnu količinu oborine od RegCM(HL,EI). Tako su npr. zimske pogreške u količini oborine u odnosu na CRU pozitivnog predznaka i iznosa između 0.5 mm dan$^{-1}$ i 1 mm dan$^{-1}$ u RegCM(HL,EI) dodatno povećane u RegCM(UW,EI) (Slika 3.3a,b). Ipak, općenito povećanje u količini oborine u RegCM(UW,EI) pridonosi smanjenju pogrešaka u središnjim dijelovima domene tijekom ljeta (Slika 3.3c,d).

Najveće razlike u ukupnom kratkovalnom zračenju na površini (*SWR*) nalaze se u toplom dijelu godine na području istočne Europe (Slika 3.5b). Obje RegCM simulacije bitno precjenjuju GEWEX/SRB podatke i također imaju veću amplitudu *SWR*-a u odnosu na ERA-Interim. Dok je srednji ljetni *SWR* na području istočne Europe 195.2 W m$^{-2}$, u RegCM(HL,EI) i RegCM(UW,EI) ovaj je iznos premašen za 21% odnosno 18%. U ostalim se područjima također nalaze sustavne pogreške u *SWR*-u pozitivnog predznaka ali manje amplitude nego na području istočne Europe (Slika 3.5 a,c,d). S obzirom da *SWR* bitno utječe na ostale procese na površini, previsok *SWR* može, na primjer, uzrokovati pojačano površinsko isparavanje i smanjenje vlage u tlu (Betts i sur. 1996). Pogreške *SWR*-a na području istočne Europe djelomično mogu biti povezane sa simuliranom naoblakom. Snižene vrijednosti ukupne naoblake u RegCM simulacijama (Slika 3.6) odgovaraju povećanom konačnom kratkovalnom zračenju pri tlu, posebno tijekom ljeta. Međutim, u usporedbi sa satelitskim mjerenjima, ukupna naoblaka *CLD* u RegCM(UW,EI) je poboljšana u odnosu na RegCM(HL,EI): dolazi do povećanja *CLD*-a od 0.4 u RegCM(HL,EI) do 0.5 u RegCM(UW,EI) na području istočne Europe tijekom ljeta.

Najveće pogreške u ukupnom dugovalnom zračenju na površini (*LWR*) u rasponu od 20 do 30 W m$^{-2}$ također nalazimo u toplom dijelu godine na području istočne Europe (Slika 3.8). U hladnom dijelu godine RegCM simulacije su bliže GEWEX/SRB, CLARA-A1 i ERA-Interim godišnjim hodovima, osim iznad Rusije, gdje su prisutne pogreške reda 10 W m$^{-2}$ no približno istog iznosa kao razlike između dva GEWEX/SRB produkta. Na području Sahare nalazimo još veće razlike između dva GEWEX/SRB produkta (iznosa između 20 i 30 W m$^{-2}$), a posljedica toga je ograničena mogućnost procjene točnog iznosa pogreške *LWR*-a u RegCM simulacijama. U RegCM simulacijama, pogreške u ukupnoj naoblaci *CLD* i prizemnoj temperaturi (preciznije, u površinskoj temperaturi kao što je analizirano u npr. Güttler i sur. (2013b)) u toplom dijelu godine mogu imati važnu ulogu u nastanku pogrešaka u *LWR*-u u odnosu prema mjerenjima i ERA-Interim. Na području istočne Europe smanjena ukupna naoblaka (Slika 3.6b) i povećana temperatura (Slika 3.2b) su sukladne s precjenjivanjem *LWR*-a u RegCM simulacijama (u apsolutnom smislu; Slika 3.8b). Ipak, sve tri veličine (*T2m*, *CLD* i *LWR*) u RegCM(UW,EI) simulaciji imaju manje sustavne pogreške u usporedbi s RegCM(HL,EI).

Magnituda turbulentnog toka osjetne topline (eng. *sensible heat flux*; *SHF*) velikim dijelom ovisi o razlici temperatura između površine i najbližih slojeva atmosfere. Pozitivne vrijednosti *SHF*-a na području Rusije i istočne Europe u hladnom dijelu godine ukazuju da je atmosfera toplija od površine te stoga postoji mogućnost nastanka statički stabilnih graničnih slojeva (Slika 3.9a,b). U ostatku godine te na ostala dva analizirana područja, tok *SHF* prenosi energiju od površine prema atmosferi. Na području istočne Europe i Sredozemlja, *SHF* je u apsolutnom smislu veći u RegCM simulacijama nego li u ERA-Interim i to između 20 i 40 W m$^{-2}$ tijekom ljeta (Slika 3.9b,c). Sličan odnos između RegCM simulacija i ERA-Interim prisutan je i iznad Sahare, no s manjim razlikama u *SHF*-u (Slika 3.9d).

Godišnji hod turbulentnog toka latentne topline (eng. *latent heat flux; LHF*) vrlo je izražen na području Rusije i istočne Europe, nešto slabije izražen na području Sredozemlja te gotovo izostaje na području Sahare (Slika 3.10). U smislu amplitude i oblika, godišnji hod *LHF*-a u RegCM simulacijama blisko prati ERA-Interim iznad Rusije i istočne Europe. Uzak raspon *LHF* vrijednosti na području Sahare (između -6 W m$^{-2}$ i -2 W m$^{-2}$) upućuje na gotovo identičan utjecaj tla siromašnog vlagom koja je raspoloživa za isparavanje u obje RegCM simulacije i u ERA-Interim. U obje RegCM simulacije oblik godišnjeg hoda *LHF*-a iznad područja Sredozemlja bitno se razlikuje od ERA-Interim. Ipak, godišnji hod zbroja osjetne i latentne topline (ukupan turbulentan tok topline) ERA-Interim i RegCM simulacija je vrlo blizak te upućuje na neusklađenosti u podijeli ukupnog toka turbulentne topline na pojedine komponente u dva modela.

Turbulentni tokovi topline *SHF* i *LHF* analizirani su za široki interval vrijednosti dostupnih svaka tri sata te koristeći funkcije gustoće vjerojatnosti za pojedinu veličinu. Kao mjera slaganja gustoća vjerojatnosti između RegCM i C-SRNWP, odnosno između RegCM i ERA-Interim, koristio se tzv. *Perkins Skill Score* (Perkins i sur. 2007; Slike 3.11 i 3.12). Ovaj dio analize ukazuje da su poboljšanja u RegCM(UW,EI) u simuliranju *SHF*-a očita i u slučaju usporedbe u odnosu na stanična mjerenja iz C-SRNWP programa i u odnosu na ERA-Interim reanalizu na razini odabranih regija. Ipak, manje pogreške *SHF*-a na području Sahare te veće pogreške *SHF*-a na području Rusije nisu u skladu s većim pogreškama u *T2m* na području Sahare te manjim pogreškama u *T2m* na području Rusije. Ovaj rezultat ukazuje na to da druge veličine koje opisuju stanje atmosferskog graničnog sloja, a nisu analizirane u ovoj disertaciji, mogu imati važnu ulogu u promjenama u temperaturi zraka te kako utjecaj PBL parametrizacije može imati suprotan učinak na različite veličine. Ipak, unatoč ograničenom poboljšanju u simuliranju *SHF* i *LHF* polja, općenito se može zaključiti kako korištenje UW parametrizacije u RegCM poboljšava simuliranje dijela fizike koji je povezan s površinskim turbulentnim tokovima.

### *9.4 Utjecaj PBL parametrizacija na sustavne pogreške*

U trećem poglavlju prikazane su sustavne pogreške u RegCM simulacijama te razlike između RegCM(HL,EI) i RegCM(UW,EI) simulacija koje koriste različite parametrizacije turbulentnog miješanja u atmosferskom graničnom sloju. Jedan od glavnih rezultata je općenito smanjenje temperature zraka u RegCM(UW,EI). U četvrtom poglavlju detaljno su analizirane ove dvije simulacije te su dana moguća objašnjenja razlika između simulacija. Dodatno je ispitana osjetljivost RegCM(UW,EI) simulacije na specifične vrijednosti/formulacije tri ključna elementa u UW parametrizaciji. Konkretno, ispitane su (1) dvije formulacije karakteristične duljine miješanja u statički nestabilnim atmosferskim uvjetima $l_1$ i $l_2$ (Grenier i Bretherton 2001), (2) interval vrijednosti parametra u formulaciji pojačanog turbulentnog uvlačenja na vrhu oblaka uslijed isparavanja $a_2$ (eng. *evaporative enhancement of the cloud-top entrainment*) (Bretherton i Park 2009) te (3) interval vrijednosti parametra u formulaciji karakteristične duljine miješanja u statički stabilnim atmosferskim uvjetima $R_{STBL}$ (Nieuwstadt 1984).

Utjecaj regionalnih geofizičkih svojstava podloge na vertikalne profile temperature zraka $T$ je jasno vidljiv na Slika 4.1a,b: područje Rusije je najhladnije a područje Sahare najtoplije područje zimi i ljeti u čitavom analiziranom pripadnom atmosferskom stupcu. Razlike između dvije PBL parametrizacije (Slika 4.1c,d) su općenito veće ljeti kada se u RegCM(UW,EI) javlja hlađenje u iznosu između 1 °C i 2 °C. Zimi je hlađenje u RegCM(UW,EI) najviše izraženo u najnižim slojevima. Rezultati upućuju na izraženu osjetljivost temperature zraka na izbor PBL parametrizacije u atmosferskim slojevima na kojima je turbulentno miješanje izraženo. Na primjer, tijekom ljeta turbulentno miješanje je posljedica nestabilnosti uslijed izraženog zagrijavanja površine, a hlađenje u RegCM(UW,EI) se javlja u svim područjima osim Rusije (Slika 4.1d).

Razlike tijekom ljeta između RegCM(UW,EI) i RegCM(HL,EI) u omjeru miješanja vodene pare *qv* upućuju na porast na najnižim atmosferskim nivoima i smanjenje na nivoima modela u blizini $\sigma$=0.7 (Fig. 4.2d). Vertikalni profili omjera miješanja vodene pare zimi ukazuju na porast u RegCM(UW,EI) na svim odabranim područjima osim Rusije. Osjetljivost modela na izbor PBL parametrizacije ponovno je najviše izražena ljeti kada porast *qv* na najnižim nivoima može ići do 0.6 g kg$^{-1}$ na području Sredozemlja a pad do 0.4 g kg$^{-1}$ u srednjoj troposferi na području istočne Europe i Sahare. Porast omjera miješanja vodene pare u nižoj atmosferi iznad Rusije, istočne Europe i Sredozemlja je u skladu s povećanom količinom oborine u RegCM(UW,EI) (Slika 3.3b,d i Slika 3.4a,b,c).

Vertikalni profili koeficijenta turbulentnog miješanja za toplinu $K_H$ u osnovnoj simulaciji RegCM(HL,EI) dosežu maksimum u nižoj atmosferi (između površine i $\sigma$=0.9) tijekom ljeta iznad Sahare u iznosu do 160 m$^2$ s$^{-1}$, te postiže vrijednosti između 40 m$^2$ s$^{-1}$ i 90 m$^2$ s$^{-1}$ na ostalim područjima (Slika 4.4b). Srednje zimske maksimalne vrijednosti $K_H$ iznad različitih područja ne prelaze 30 m$^2$ s$^{-1}$ i smanjuju se od juga prema sjeveru. Zimi su vertikalni profili $K_H$ iznad Sredozemlja slični profilima iznad Sahare (Slika 4.4a,c), a ljetni profili $K_H$ iznad Sredozemlja slični su profilima iznad istočne Europe (Slika 4.4b,d). Tijekom zime, ova sličnost je dijelom posljedica utjecaja temperature mora na turbulentno miješanje u obalnoj zoni: više temperature mora od temperature susjednog kopna su povezane sa statički nestabilnijim zrakom iznad mora te je moguć utjecaj mora na susjedno kopno. Tijekom ljeta, površina mora je hladnija od susjednog kopna te su koeficijenti turbulentnog miješanja za toplinu niži nego iznad izraženo toplog područja sjeverne Afrike i Sahare.

U RegCM(UW,EI) nalazimo smanjeno turbulentno miješanje u odnosu na RegCM(HL,EI), s razlikama do 60 m$^2$ s$^{-1}$ na području Sahare tijekom ljeta i između 20 m$^2$ s$^{-1}$ i 40

$m^2\ s^{-1}$ iznad ostalih područja (Slika 4.4d). Smanjenje $K_H$ do 15 $m^2\ s^{-1}$ je prisutno i tijekom zime. Ovaj rezultat je u skladu s Cuxartom i sur. (2006) gdje je za srednje stabilno stratificiran atmosferski granični sloj pokazano općenito smanjenje turbulentnog miješanja u prognostičkim parametrizacijama (kao što je UW parametrizacija) u odnosu na dijagnostičke parametrizacije (kao što je Holtslagova parametrizacija).

Iz jednadžbe (4.1) je vidljivo kako $K_H$ i vertikalni gradijent $\partial K_H/\partial z$ u međudjelovanju s vertikalnim profilima $\partial T/\partial z$ i $\partial^2 T/\partial z^2$ utječu na predznak i iznos promjene temperature dobivene pomoću PBL parametrizacije. S obzirom kako su $K_H$ i $\partial K_H/\partial z$ smanjeni u RegCM(UW,EI), moguće je očekivati i smanjenje temperature u istom eksperimentu. Ipak, konačan vertikalni profil bilo koje prognostičke veličine ovisit će o međudjelovanjima između pojedinačne PBL parametrizacije i svih ostalih komponenti modela.

U obje sezone i iznad većine područja, tendencija temperature u RegCM(UW,EI) je smanjena na većini nivoa u nižoj atmosferi (Slika 4.5c,d). Smanjenje je do $6\times10^{-5}$ K $s^{-1}$ u odnosu na tendenciju temperature zbog PBL parametrizacije u RegCM(HL,EI). Razlike između RegCM(UW,EI) i RegCM(HL,EI) velikim su dijelom posljedica razlika u vertikalnim profilima koeficijenta turbulentnog miješanja za toplinu. Međutim, u RegCM(UW,EI) za neke slučajeve uočava se zatopljenje na najnižim nivoima te su razlike u odnosu na RegCM(HL,EI) pozitivne (Slika 4.5c,d). Ovo je vrlo vjerojatno posljedica prisutnosti protugradijentnog turbulentnog toka u Holtslag parametrizaciji koji dodatno smanjuje ukupnu tendenciju temperature u istoj parametrizaciji (Slika 4.5a,b). Za detaljniju analizu potrebno je daljnje istraživanje doprinosa ostalih nerazlučenih i razlučenih procesa na tendencije temperature i omjera miješanja vodene pare u RegCM modelu (npr. van de Berg i sur. 2007).

U potpoglavlju 4.2 analiziran je ansambl perturbirane fizike (eng. *Perturbed Physics Ensemble;* PPE) u UW parametrizaciji. Analizirana je osjetljivost temperature i specifične vlažnosti na 2 m (*T2m* i *q2m*) te koeficijenta turbulentnog miješanja za toplinu na najnižem nivou modela u ovisnosti o vrijednostima i formulacijama parametara $l$, $a_2$ i $R_{STBL}$ (Tablica 1). U nastavku će RegCM(HL,EI) biti označen kao EXP001 a članovi PPE-a od EXP002 do EXP019, s time da je RegCM(UW,EI) eksperiment EXP002. Duljina integracije u svim eksperimentima bila je tri godine (1989.-1991.).

U usporedbi s EXP001, promjena *T2m* u PPE je gotovo jedinstvena: temperatura zraka je snižena u gotovo svim eksperimentima od EXP002 od EXP019 iznad sve četiri regije i u obje sezone (zima i ljeto). U disertaciji su prikazani rezultati za Rusiju (Slika 4.6a) dok su rezultati za ostale regije dostupni u Güttler i sur. (2013; njihova Slika 9). Amplituda hlađenja dostiže 3 °C u Rusiji tijekom zime, i slično u istočnoj Europi ljeti. Hlađenje je uz korištenje UW parametrizacije u skladu s predznakom promjena u vertikalnom profilu temperature (Slika 4.1c,d). Negativne razlike prisutne na Slici 4.6a mogu se smatrati poboljšanjem RegCM modela prilikom korištenja UW parametrizacije. Utjecaj UW parametrizacije je veći iznad Rusije zimi nego ljeti, što sugerira poboljšanu simulaciju stabilno stratificiranog atmosferskog graničnog sloja.

Jedino očito sustavno grupiranje eksperimenata prikazanih na Slici 4.6a moguće je povezati s vrijednostima $R_{STBL}$=1.00 (EXP 3, 6, 9, 12, 15 i 18). U ovom slučaju javlja se veće hlađenje nego u ostalim eksperimentima, ponekad i dvostruko veće za istu vrijednost parametra $a_2$. Smanjenje $R_{STBL}$ vodi ka smanjenju turbulentne duljine miješanja (jednadžba 2.8) i smanjenom vertikalnom miješanju hladnog zraka pri tlu i nešto toplijeg zraka iznad podloge (Slika 4.1a).

Odgovor modela na promjenu PBL parametrizacije u smislu specifične vlažnosti na 2 m *q2m* je složeniji nego u slučaju *T2m*. Rezultati za područje Rusije su prikazani na Slici 4.6b a za ostale regije su prikazani u radu Güttler i sur. (2013a; njihova Slika 10). Ljeti u većini UW simulacija dolazi do povećanja *q2m* što je u skladu i s porastom količine oborine u RegCM(UW,EI) (Slika 3.3d). Do sustavnog grupiranja u ovisnosti o perturbiranim parametrima ponovno dolazi za eksperimente s $R_{STBL}$=1.00 na području Rusije. U konkretnim eksperimentima dolazi do smanjenja *q2m* što je ponovno u skladu sa smanjenim vertikalnim miješanjem koje se očekuje iz jednadžbe (2.8) i blisko je povezano s vertikalnim profilom omjera miješanja vodene pare zimi iznad područja Rusije (Slika 4.2a).

Amplituda *T2m* i *q2m* u perturbiranim RegCM eksperimentima s aktivnom UW parametrizacijom (eksperimenti od EXP003 do EXP019) ne razlikuju se bitno od osnovne UW simulacije EXP002. Relativno malen do umjeren rasap unutar ansambla UW simulacija te sličnost odziva na različitim geografskim područjima implicira da osnovni skup vrijednosti analiziranih parametara u RegCM(UW,EI) vrlo izgledno može dati sličan odziv na drugim područjima i u drugim vremenskim intervalima. Ipak, osjetljivost pojedinih elemenata modela (npr. vertikalni profili $K_H$) mogu motivirati daljnje istraživanje i uključivanje razvijenijih formulacija karakteristične turbulentne duljine miješanja (Grisogono 2010).

*9.5 Utjecaj PBL parametrizacija na projicirane klimatske promjene*

U petom poglavlju analiziran je utjecaj parametrizacija za turbulentno miješanje u atmosferskom graničnom sloju na projicirani signal klimatskih promjena u RegCM modelu uz rubne uvjete iz HadGEM2-ES za razdoblje 1971.-2098., te uz korištenje IPCC scenarija koncentracije stakleničkih plinova RCP4.5 i RCP8.5 od prosinca 2005. pa do kraja simuliranog perioda. Simulacije su označene kao RegCM(HL,HA) i RegCM(UW,HA), no osim razlike u rubnim uvjetima, simulacije se razlikuju od prethodnih eksperimenata u domeni koja sada pokriva područje južne Europe i šire područje Sredozemlja (Slika 4.1b) te u nekoliko opcija u parametrizacijama nerazlučenih procesa za konvektivno miješanje i procesa na tlu (potpoglavlje 2.1.1). Ipak, razlike između samih eksperimenata RegCM(HL,HA) i RegCM(UW,HA) su samo u odabranoj parametrizaciji turbulentnog miješanja te je stoga moguće odrediti osjetljivost projekcija buduće klime RegCM modelom na taj odabir. Analiza je napravljena za područje Sredozemlja (definirano na isti način kao u trećem i četvrtom poglavlju) s obzirom da se u području Sredozemlja mogu očekivati izraženije klimatske promjene u smislu porasta temperature zraka i smanjenja količine oborine tijekom 21. stoljeća (Giorgi 2006; Christensen i sur. 2007). Poglavlje je strukturirano na način da se nakon analize promjena u godišnjem hodu *T2m* i oborini, različite komponente energetske ravnoteže na površini interpretiraju i povezuju s određenim scenarijem i PBL parametrizacijom. Povijesno razdoblje P0 je definirano za period 1971.-2000. dok su budući periodi definirani za intervale 2011.-2040. (P1), 2041.-2070. (P2) te 2071.-2098. (P3).

U godišnjem hodu *T2m* za razdoblje P0 nalazimo u području Sredozemlja vrijednosti između 6 °C i 25 °C u RegCM(UW,HA) i RegCM(HL,HA) (Slika 5.1a). *T2m* je niži u RegCM(UW,HA) i razlike s obzirom na RegCM(HL,HA) su statistički značajne tijekom godine, osim u zimski mjesecima (Slika 5.1b). Hlađenje u RegCM(UW,HA) je prisutno i u projekcijama za kraj 21. stoljeća u slučaju oba RCP scenarija. Hlađenje se sastoji od najvećih razlika između dvije simulacije u iznosu do 1.2 °C (Slika 5.1b). Ipak, razlike između RegCM(UW,HA) i RegCM(HL,HA) su blago povećane pri usporedbi perioda P0 i P3. Moguće objašnjenje ovog porasta razlika leži u većem smanjenju oborine i vlage u tlu u RegCM(HL,HA) simulaciji (Slika 5.3 i Slika 5.2).

Pri usporedbi projekcija buduće klime, RegCM(UW,HA) i RegCM(HL,HA) blisko simuliraju amplitudu klimatskih promjena *T2m*. Najveće zagrijavanje projicirano je u srpnju i kolovozu (između 6 i 7 °C) za RCP8.5 u razdoblju P3. U RCP4.5 scenariju dolazi do gotovo jednakog porasta temperature na kraju 21. stoljeća kao u RCP8.5 u sredini 21. stoljeća. Može se zaključiti kako korištenje različitih PBL parametrizacija uzrokuje različitu klimatologiju u razdoblju P0, no signal klimatskih promjena u *T2m* na području Sredozemlja ne ovisi bitno o odabiru PBL parametrizacije (usporediti s Jerez i sur. 2013).

U godišnjem hodu ukupne količine oborine u RegCM(HL,HA) i RegCM(UW,HA) minimalne srednje vrijednosti na području Sredozemlja nalazimo u srpnju (~0.5 mm $dan^{-1}$), a maksimalne srednje vrijednosti u jesen i početkom zime (~2.5 mm $dan^{-1}$). U RegCM(UW,HA) nema pojave sustavno veće količine oborine nego u RegCM(HL,HA) kao što je pokazano za slučaj simulacija forsiranih ERA-Interim reanalizom. Ova razlika upućuje na to da neke druge razlike u postavkama eksperimenta mogu isto tako utjecati na ponašanje modela te mogu nadvladati promjenu koja je uzrokovana samo izborom PBL parametrizacije.

U usporedbi s temperaturom zraka *T2m*, simulirani signal promjene srednje mjesečne količine oborine nije često statistički značajan. Ipak, utjecaj izbora pojedine PBL parametrizacije je jasnije prisutan nego u slučaju *T2m*. Iako postoji sklonost smanjenim količinama oborine u budućoj klimi tijekom cijele godine (osim u nekoliko mjeseci na početku godine), razlike između budućih perioda i povijesnog perioda su statistički značajne u većem dijelu godine u RegCM(HL,HA) (Slika 5.3c,d). Smanjenje oborine na području Sredozemlja je također funkcija primijenjenog RCP scenarija (npr. Jacob i sur. 2013). Najveće smanjenje oborine je projicirano za kraj 21. stoljeća tijekom jeseni uz RCP8.5 u simulaciji RegCM(HL,HA) te iznosi -0.5 mm $dan^{-1}$ u odnosu na razdoblje P0 (Slika 5.3c). Moguća objašnjenja smanjenja oborine uključuju utjecaj smanjenog turbulentnog toka latentne topline (npr. Andrews 2009) i utjecaj razlika u zagrijavanju iznad mora i kopna (npr. Rowell i Jones 2006).

Ukupno kratkovalno zračenje na površini *SWR* u razdoblju P0 je značajno različito između dvije RegCM simulacija tijekom cijele godine (Slika 5.4a,b), a amplituda *SWR*-a je značajno veća u RegCM(HL,HA) a *SWR* postiže maksimum u svibnju. Kao što je pokazano u prethodnim poglavljima, *SWR* je velikim dijelom funkcija ukupne naoblake *CLD* i površinskog albeda *ALB*. Veći *SWR* u RegCM(HL,HA) je povezan s nižom ukupnom naoblakom (Slika 5.5a) što rezultira jačim kratkovalnim zračenjem na površini te porasta *T2m* i/ili porasta turbulentnih tokova topline (Andrews i sur. 2009; Tang i sur. 2012).

Razlike u *SWR* između budućih razdoblja i povijesnog razdoblja su u intervalu -2 W m$^{-2}$ i 6 W m$^{-2}$ (Lenderink i sur. 2007). Usporedba P0 i P3 razdoblja za RCP8.5 scenariji pokazuje statistički značajne razlike u *SWR* u većini mjeseci u RegCM(UW,HA). Porast *SWR*-a sukladan je smanjenju ukupne naoblake (Slika 5.5c,d)a ovo smanjenje ukupne naoblake nadvladava tendenciju malom (ali statistički značajnom) porastu površinskog albeda i pripadnom smanjenju *SWR*-a (Slika 5.6c,d). Porast albeda povezan je sa smanjenjem oborine i vlage u tlu (Slike 5.3c,d i 5.2c,d), a ovaj proces je uključen u RegCM parametrizaciji za procese u tlu (Dickinson i sur. 1993; Seneviratne i sur. 2010).

Razlike između dvije RegCM simulacije u ukupnom dugovalnom zračenju na površini *LWR* su između 5 W m$^{-2}$ i 10 W m$^{-2}$ te su statistički značajne tijekom cijele godine (Slika 5.7a,b). Veći *LWR* (u apsolutnom smislu) je u RegCM(HL,HA) nego u RegCM(UW,HA), što je u skladu s višom temperaturom (Slika 5.1a) i manjom ukupnom naoblakom (Slika 5.5). Ovakav odnos između RegCM simulacija je zadržan do kraja 21. stoljeća (Slika 5.7b). Razlike u *LWR* između budućih i povijesnog razdoblja su uglavnom u intervalu -2 W m$^{-2}$ i 6 W m$^{-2}$ (Slika 5.7c,d) te su za scenarij RCP8.5 uglavnom pozitivne. Ipak, porast *LWR* nije u skladu samo s porastom *T2m* i smanjenjem *CLD*. Jednostavni dijagnostički model opisan jednadžbom (2.14) ne može objasniti pozitivne *LWR* promjene, dijelom jer ne uključuje ovisnost *LWR*-a o količini vodene pare u atmosferskom stupcu (Kothe i sur. 2011). Ipak, pozitivne *LWR* promjene su u skladu s npr. Andrews i sur. (2009), gdje na globalnoj skali, različiti globalni klimatski modeli simuliraju smanjenje amplitude *LWR*-a u toplijoj i vlažnijoj atmosferi. Takva promjena u *LWR* jer rezultat porasta u dolaznom dugovalnom zračenju na površini koji nadvladava toplinski odgovor površine i pridruženo odlazno dugovalno zračenje.

Gubitak energije u obliku turbulentnog toka osjetne topline *SHF* u RegCM(UW,HA) i RegCM(HL,HA) je najveći ljeti (Slika 5.9a). Više se topline gubi u RegCM(UW,HA) u povijesnom i budućim razdobljima, a razlike u odnosu na RegCM(HL,HA) su do 5 W m$^{-2}$ i statistički značajne za gotovo svaki mjesec (Slika 5.9b). Projicirane promjene za *SHF* upućuju na povećan gubitak energije i to do 6 W m$^{-2}$ sa scenarijem RCP4.5 te do 10 W m$^{-2}$ sa scenarijem RCP8.5 (Slika 5.9c,d). RegCM simulacije s različitim PBL parametrizacijama daju vrlo slične rezultate za *SHF* za svaki promatrani RCP scenarij.

Projicirani gubitak energije u obliku turbulentnog toka latentne topline *LHF* se povećava u području Sredozemlja u oba RCP scenarija (Slika 5.10c,d). Manje energije u obliku *LHF*-a gubi se u samo u lipnju (ovo je najjasnije prisutno u slučaju RegCM(HL,HA) i RCP8.5), u mjesecu kada inače *LHF* postiže maksimum (u apsolutnom smislu). Ovakva promjena *LHF*-a upućuje na to da uslijed smanjenja oborine (Slika 5.3) i vlage u tlu (Slika 5.2) u ljetnim mjesecima na području Sredozemlja dolazi do manjeg *LHF*-a a time do pojačane uloge *SHF*-a u održavanju površine u energetskoj ravnoteži. Manje evapotranspiracije tijekom ljeta je simulirano i u drugim regionalnim i globalnim klimatskim modelima za područje južne Europe te se promjena vlage u tlu smatra važnom komponentom doprinosa ovakvoj promjeni *LHF*-a (npr. Lenderink i sur. 2007; Boé i Terray 2008).

Smanjenje oborine je moguće dovesti u vezu sa smanjenjem naoblake na području Sredozemlja u kontekstu razlika u zagrijavanju između kopna i mora (npr. Manabe i sur. 1992; Rowell i Jones 2006; Boé i Terray 2014). Ipak, potvrda ove hipoteze te potpuno odvajanje doprinosa različitih procesa (npr. međudjelovanja tla i atmosfere, promjene u strujanju na velikoj skali, međudjelovanje procesa na malim i velikim skalama) traži dodatno istraživanje.

Razlike između projiciranih klimatskih promjena u *LHF* u RegCM(UW,HA) i RegCM(HL,HA) ukazuju na veći gubitak *LHF*-a u RegCM(UW,HA) (Slika 5.10c,d). Ovo je sukladno manjem gubitku oborine (Slika 5.3c,d) i manjem gubitku vlage u tlu (Slika 5.2c,d) u RegCM(UW,HA) simulaciji.

### *9.6 Zaključak*

Razlike u simuliranoj i opaženoj količini naoblake glavni su izvor razlika u konačnom kratkovalnom zračenju na površini što uzrokuje razlike u ostalim komponentama energetske ravnoteže na površini i u konačnici na temperaturu zraka *T2m*. Povećanjem ukupne naoblake u RegCM simulacijama koje koriste UW parametrizaciju za turbulentno miješanje u atmosferskom graničnom sloju dijelom dovodi do smanjenja temperature zraka. Drugi izvor hlađenja u UW simulacijama je smanjenje u prognostičkoj tendenciji temperature zraka zbog PBL parametrizacije (vidjeti jed. (2.1)) u velikom dijelu niže atmosfere, a što proizlazi iz promjena u amplitudi i vertikalnom gradijentu koeficijenta turbulentnog miješanja za toplinu u UW simulacijama u odnosu na simulacije s Holtslagovom parametrizacijom. Pozitivan učinak UW parametrizacije je najjasniji na području Rusije tijekom zime i na području istočne Europe tijekom ljeta gdje dolazi do bitnog poboljšanja u simuliranju temperature zraka. Preostale nedostatke u simuliranju temperature zraka na području sjeverne Afrike potrebno je dodatno istražiti. Metodologiju je potrebno proširiti uključivanjem toka topline u tlo u jednadžbu energetske ravnoteže na površini.

Analiza ansambla eksperimenata s perturbiranom fizikom u simulacijama s UW parametrizacijom upućuje na njenu robusnost. U ispitanom intervalu parametara i formulacija karakteristične duljine miješanja u nestabilno i stabilno stratificiranim uvjetima te u pojačanju turbulentnog uvlačenja na vrhu oblaka uslijed isparavanja, dolazi do sličnog odgovora u gotovo svim članovima ansambla: smanjenje ljetnih i zimski temperatura u simulacijama s UW parametrizacijom u odnosu na osnovnu simulaciju s Holtslagovom parametrizacijom i do 3 °C.

U simulacijama prošle i buduće klime u drugom skupu eksperimenata također su detektirane statistički značajne razlike u klimatologiji modela uslijed promjene parametrizacije za turbulentno miješanja u atmosferskom graničnom sloju. Iako je pokazan važan utjecaj PBL parametrizacije na klimatologiju raznih prizemnih veličina, nije uočen bitno različit signal u projiciranim promjenama u području Sredozemlja. Ne može se isključiti mogućnost drugačijeg rezultata ovisno o parametrizaciji drugih nerazlučenih procesa te je za stjecanje potpunijeg uvida potrebno obaviti analizu promjena većeg broja parametrizacija nerazlučenih procesa u modelu. Ipak, projicirani porast temperature zraka i smanjenje količine oborine na području Sredozemlja u analiziranim simulacijama za 21. stoljeće su sukladani ranijim istraživanjima.

# 10. LIST OF ABBREVIATIONS

*ALB* surface albedo

*CLD* total cloud cover

GCM global climate model

*GHF* ground heat flux

GHG greenhouse gases

IPCC Intergovernmental Panel on Climate Change

$K_H$ eddy heat diffusivity

*l* master turbulent mixing length

*LHF* latent heat flux

*LWD* downward surface longwave radiative flux

*LWR* net surface longwave radiative flux

PBL planetary boundary layer

PDF probability density function

PPE perturbed physics ensemble

PPS Perkins Skill Score

*q2m* near-surface specific humidity (i.e. specific humidity at 2 m)

*qv* water vapour mixing ratio

*R* total precipitation

RCM regional climate model

SEB surface energy budget

*SHF* sensible heat flux

*SWR* net surface shortwave radiation flux

*T2m* near-surface air temperature (i.e. air temperature at 2 m)

*T* air temperature

## 11. CURRICULUM VITAE

### General information

| | |
|---|---|
| Name and surname | Ivan Güttler |
| Academic title | dipl. ing. phy.-geophy. |
| Home address | Ivana Meštrovića 79, 31511 Đurđenovac, Croatia |
| Office address | Grič 3, 10000 Zagreb, Croatia |
| E-mail | ivan.guettler@gmail.com<br>ivan.guettler@cirus.dhz.hr |
| Personal web page | https://sites.google.com/site/ivanguettler |
| Citizenship | Croatian |
| Date and place of birth | 13.02.1985., Našice, Croatia |
| Work experience | 01.03.2009.-<br>Meteorological and Hydrological Service of Croatia (DHMZ)<br>Graduate research assistant |

### Formal Education

University

2003-2008
University of Zagreb
- Faculty of Science
  - Department of Physics
  - Department of Geophysics
    - Physics of the Atmosphere and Sea

PhD

2009-
University of Zagreb
- Faculty of Science
  - Department of Geophysics
    - Physics of the Atmosphere and Sea

**Conferences and workshops participation**

| Date | Place | Activity |
|---|---|---|
| 27.04. -08.05. 2009. | ICTP, Trieste, Italy | Water Resources in Developing Countries: Planning and Management in a Climate Change Scenario |
| 22.-31. 05. 2009. | Split, Croatia | Split Workshop in Atmospheric Physics and Oceanography |
| 24.-25.02. 2010. | GFZ, Zagreb, Croatia | Atmospheric Boundary Layers - Current Problems & Advancements |
| 31.05.-11.06. 2010. | ICTP, Trieste, Italy | Fifth ICTP Workshop on the Theory and Use of Regional Climate Models |
| 06.-09.09. 2010. | ECMWF, Reading, UK | Seminar on Predictability in the European and Atlantic regions from days to years |
| 09.-10.11. 2010. | Zagreb, Croatia | Meteorološki izazovi 1. "Meteorologija u fokusu javnosti" |
| 21.-26.04. 2011. | ICTP, Trieste, Italy | International Conference on the CORDEX |
| 18.-21.05. 2011. | Opatija, Croatia | 5. Hrvatska konferencija o vodama s međunarodnim sudjelovanjem: Hrvatske vode pred izazovom klimatskih promjena |
| 06.-09.06. 2011. | Lecce, Italy | MedCLIVAR Final Conference Mediterranean Climate: From Past to Future |
| 15.06. 2011. | UNDP&DHMZ, Zagreb, Croatia | CLIM-RUN: Klimatske informacije, klimatske promjene i proizvodnja energije iz obnovljivih izvora |
| 12.-16.09. 2011. | Berlin, Germany | 11. EMS Annual Meeting / 10. ECAM: Forecasting the weather - ensemble techniques in probabilistic weather prediction |
| 02.12.2011. | Zagreb, Croatia | Geophysical Challenges of the 21$^{st}$ century |

| | | |
|---|---|---|
| 06.-07.03. 2012. | HMD, Zagreb, Croatia | Meteorološki izazovi 2. “Meteorologija u fokusu javnosti” |
| 22.-27.04. 2012. | Vienna, Austria | European Geosciences Union General Assembly |
| 07.-18.05. 2012. | ICTP, Trieste, Italy | Sixth ICTP Workshop on the Theory and Use of Regional Climate Models |
| 01.-11.06. 2012. | Kos, Greece | European Earth System and Climate Modelling School |
| 25.02. 2013. | SRCE, Zagreb, Croatia | Korištenje računalnih klastera |
| 04.06. 2013. | UNDP&DHMZ, Zagreb, RH | CLIM-RUN radionica: Potencijal klimatskih informacija za planiranje u turizmu |
| 06.06. 2013. | UNDP&DHMZ, Zagreb, Croatia | CLIM-RUN radionica: Klimatske informacije i obnovljivi izvori energije |
| 24.-27.09. 2013. | Pržno/Budva, Montenegro | Regional Workshop on Hydrological Forecasting and Impact of Climate Change on Water Resources |
| 16.-17.10. 2013. | Beograd, Serbia | Climate Change Impact on Water Resources |
| 04.-07.11. 2013. | Brussels, Belgium | International Conference on Regional Climate - CORDEX 2013 |
| 21.-22.11. 2013. | Zagreb, Croatia | Meteorološki izazovi 3. “Ekstremne vremenske prilike i utjecaj na društvo” |

**Specialisations enrolled**

| Date | Place | Activity |
|---|---|---|
| 15.10.-15.12. 2009. | ICTP, Trieste, Italy | Use and development of regional climate model RegCM3. |
| 25.04.-17.05. 2011. | ICTP, Trieste, Italy | Use and development of regional |

| | | |
|---|---|---|
| | | climate model RegCM4. |
| 21.09.-13.10. 2011. | SMHI, Norrköping, Sweden | Analysis of high resolution simulations of regional climate model RCA3. |
| 15.11.-18.11. 2011. | ICTP, Trieste, Italy | Use and development of regional climate model RegCM4 and CORDEX experiments specifications. |

**Projects**

1. 2007-2008 Rossby2050, University of Zagreb grant for the study of the climate change of atmosphere stability measures
2. 2009-2013 Climate variations and change and responses in affected systems (004-1193086-3035), Marjana Gajić-Čapka, Ministry of Science, Education and Sport of the Republic of Croatia
3. 2011-2014 CLIM-RUN (Climate Local Information in the Mediterranean region Responding to User Needs), EU FP7 project

**Awards**

1. 2007: University of Zagreb, Faculty of Science laud for high grades accomplishment
2. 2010: WMO Professor Mariolopoulos Trust Fund Award, together with dr.sc. Danijel Belušić for the paper entitled "Can mesoscale models reproduce meandering motions?"
3. 2010: EMS Young Scientist Travel Award for ECMWF 2010 Annual Seminar
4. 2014: HMD Young Scientist Award

**Teaching**

1. 2010 – present: Teaching Assistant at Department of Geophysics, Faculty of Science, University of Zagreb. Course: "Računarstvo i numerička matematika" (2+1, winter semester)

**Other professional activities**

1. Member of the Croatian Meteorological Society (HMD)
2. 2013: Member of the HMD MI3 Organizing committee

# 12. LIST OF PUBLICATIONS


1. Güttler, I., Branković, Č., O'Brien, T.A., Coppola, E., Grisogono, B., Giorgi, F., (2013) Sensitivity of the regional climate model RegCM4.2 to planetary boundary layer parameterisation. *Clim. Dyn.*, doi: 10.1007/s00382-013-2003-6
2. Güttler, I., Branković, Č., Srnec, L., Patarčić, M. (2013) The impact of boundary forcing on RegCM4.2 surface energy budget. *Climatic Change*, doi: 10.1007/s10584-013-0995-x
3. Vautard, R., Gobiet, A., Jacob, D., Belda, M., Colette, A., Déqué, M., Fernández, J., Garica-Díez, M., Goergen, K., Güttler, I., Halenka, T., Karakostas, T., Katragkou, E., Keuler, K., Kotlarski, S., Mayer, S., Nikulin, G., Patarčić, M., Scinocca, J., Sobolowski, S., Suklitsch, M., Teichmann, C., van Meijgaard, E., Warrach-Sagi, K., Wulfmeyer, V., Yiou, P. (2013) The simulation of European heat waves from an ensemble of regional climate models within the EURO-CORDEX project. *Clim. Dyn*., 41:2555–2575
4. Branković, Č., Güttler, I., Gajić-Čapka, M. (2013) Evaluating climate change at the Croatian Adriatic from observations and regional climate models' simulations. *Clim. Dyn.*, 41: 2353–2373
5. Güttler, I., Belušić, D. (2012) The nature of small-scale non-turbulent variability in a mesoscale model. *Atmospheric Science Letters*, 13:163–173
6. Giorgi, F., Coppola, E., Solmon, F., Mariotti, L., Sylla, M. B., Bi, X., Elguindi, N., Diro, G. T., Nair, V., Giuliani, G., Cozzini, S., Güttler, I., O'Brien, T. A., Tawfik, A. B., Shalaby, A., Zakey, A. S., Steiner, A. L., Stordal, F., Sloan, L. C., Brankovic, C. (2012) RegCM4: Model description and preliminary tests over multiple CORDEX domains. *Clim. Res.,* 52:7–29
7. Branković, Č., Patarčić, M., Güttler, I., Srnec, L. (2012) Near-future climate change over Europe and Croatia in an ensemble of regional climate model simulations. *Climate Research,* 52:227–251
8. Güttler, I. (2011) Reducing warm bias over the north-eastern Europe in a regional climate model. *Hrvatski Meteorološki Časopis*/*Croatian Meteorological Journal*, 44/45:19–29
9. Belušić, D., Güttler, I. (2010): Can mesoscale models reproduce meandering motions? *Quart. J. Roy. Meteor. Soc.*, 136, 553–565